

ALMA MATER STUDIORUM · UNIVERSITY OF BOLOGNA

School of Science
Department of Physics and Astronomy
Master Degree in Physics

Primordial Black Holes from Multi-Field Inflation

Supervisor:

Prof. Francisco G. Pedro

Submitted by:

Dario Libero Lorenzoni

Academic Year 2021/2022

Abstract

In this master's thesis, the formation of Primordial Black Holes (PBHs) in the context of multi-field inflation is studied. In these models, the interaction of isocurvature and curvature perturbations can lead to a significant enhancement of the latter, and to the subsequent production of PBHs. Depending on their mass, these can account for a significant fraction (or, in some cases, the entirety) of the universe's Dark Matter content.

After studying the theoretical framework of generic \mathcal{N} -field inflationary models, the focus is restricted to the two-field case, for which a few concrete realisations are analysed. A numerical code (written in *Wolfram Mathematica*) is developed to make quantitative predictions for the main inflationary observables, notably the scalar power spectra. Parallely, the production of PBHs due to the dynamics of 2-field inflation is examined: their mass, as well as the fraction of Dark Matter they represent, is calculated for the models considered previously.

Contents

1	Introduction	1
1.1	Historical Overview	2
1.1.1	The Standard Model of Cosmology	2
1.1.2	Shortcomings of Λ CDM Cosmology	5
1.1.3	Inflation	6
1.1.4	Primordial Black Holes	7
1.2	Notation	8
2	Cosmology and Inflation	9
2.1	The Λ CDM Model	9
2.1.1	Dynamics of an Expanding Universe	11
2.1.2	Composition and History of the Universe	12
2.1.3	Towards Inflation	16
2.2	Single-Field Inflation	19
2.2.1	Background Dynamics	20
2.2.2	Slow-Roll	21
2.2.3	Simple Example: Quadratic Inflation	24
3	Multi-Field Inflation	26
3.1	Theoretical Framework	26
3.2	Background Dynamics	28
3.3	Cosmological Perturbation Theory	33
3.3.1	Metric Perturbations	34
3.3.2	Matter Perturbations	35
3.3.3	Adiabatic and Entropy Perturbations	36
3.3.4	Field Equations	37
3.3.5	Scalar Field Perturbations	38
3.3.6	Quantising the Perturbations	40
3.3.7	Power Spectra and Observables	41
4	Primordial Black Holes	43
4.1	PBH Formation	43
4.2	PBHs as Dark Matter	46
4.3	Constraints	48

CONTENTS

5	PBHs from 2-Field Inflation	52
5.1	Reducing to $\mathcal{N} = 2$ Fields	52
5.2	Double Quadratic model	54
5.3	Achúcarro's model	60
5.4	Braglia's model	65
6	Closing Remarks	72
6.1	Summary	72
6.2	Conclusions	73
6.3	Future Outlook	73
	Bibliography	76
A	Key Elements of General Relativity	85
A.1	Basic Definitions	85
A.2	Deriving the Friedmann Equations	87
B	\mathcal{N}-Field Equations of Motion	90
B.1	Single-Field Case	91
B.2	Multi-Field Case	93

Chapter 1

Introduction

One of the greatest achievements of 20th century cosmology is the formulation of a self-consistent model that accurately describes the universe around us, providing an explanation for most of the revolutionary observations made over the last hundred years. A number of shortcomings of the model nevertheless persist; in order to solve them, the idea of *cosmic inflation* was introduced [1]. This is a short period of extremely rapid expansion of space, taking place during the very early universe. Furthermore, high energy physics considerations are shifting the attention from “standard” inflation to models with multiple interacting fields driving the expansion.

Additional open questions relate to the nature of Dark Matter and Dark Energy, which are included in the standard model of cosmology without having a fundamental description. Interesting candidates for the former are *Primordial Black Holes* (PBHs), which could in some models account for a significant fraction or even the totality of Dark Matter [2, 3]. These are the result of the collapse of local energy overdensities generated during inflation.

The work presented in this thesis focuses on these two aspects of great scientific interest within the world of theoretical physics and cosmology. Joining the two topics, we show how (and in what amount) PBHs could have formed in models of multi-field inflation, and what impact these results may have on our understanding of the universe.

* * *

In the present Chapter, we introduce the subject by looking at its historical context and by highlighting its new-found scientific interest. We also comment on the notation that will be used throughout this work. In Chapter 2, the standard model of cosmology – the Λ CDM model – is briefly reviewed before moving to the discussion of single-field inflation. Multi-field inflation is the topic of Chapter 3, in which we detail its theoretical framework from both the background and the perturbation theory points of view.

Switching gears, we study the theory and interest of Primordial Black Holes in Chapter 4, focusing on their significance as a candidate for Dark Matter. PBHs are then discussed within the framework of 2-field inflation in Chapter 5, where we explain how

we analytically and numerically reproduced the 2-field models of Huston & Christopher-son [4], Achúcarro *et al.* [5], and Braglia *et al.* [6, 7].

Chapter 6 summarises our work and formulates its main conclusions. A discussion on its interest and future legacy concludes this thesis.

1.1 Historical Overview

Understanding the universe around us – and our place within it – has been a key question in humanity’s search for understanding since the dawn of time. Significant progress in this regard was made in the 16th century during the Copernican revolution, and with the subsequent invention of the telescope. These theoretical and observational advances relegated the Earth to the outskirts of (or rather, to an insignificant place in) the known universe, giving rise to what is now called the *cosmological principle*:

The universe on the largest scales is homogeneous (it looks the same every-where) and isotropic (there exist no special directions).

This approximation, which clearly only holds for scales greater than those of galaxy clusters, i.e. $\gtrsim 100 \text{ Mpc}^1$, is the foundation of modern cosmology [8, 9]. It has now been proven by deep galaxy surveys such as the Sloan Digital Sky Survey [10].

1.1.1 The Standard Model of Cosmology

At the beginning of the past century, Einstein’s theory of General Relativity revolutionised our way of thinking about the universe, relating the geometry of spacetime with the distribution of mass (or energy) within it [11]. Einstein was philosophically in favour of a static universe (infinite in time but finite and constant in space), notably pushing him to add (and later remove) the cosmological constant Λ to his field equations as an attempt to counterbalance gravity [8, 12]. Nevertheless, solutions to his equations – notably those by Friedmann [13] – suggested that the universe is expanding spatially in time.

Eventually, Hubble’s observations [14] showed that the recessional radial velocity, v , of remote galaxies (their velocity in our line-of-sight direction) is proportional to their distance from us, d ; this relation takes the name of Hubble’s law, the proportionality being given by the omonymous constant, H_0 [15]:

$$v = H_0 d \quad . \quad (1.1)$$

The quantities appearing in this relation are not directly measured. The distance to remote objects is often calculated by measuring the flux of incoming photons from a source of known luminosity, i.e. a “standard candle”, such as type IA supernovae [16]. The velocity of distant galaxies is instead inferred from their observed redshift, z , such

¹Megaparsecs are the typical cosmological units of length: $1 \text{ Mpc} = 3.086 \times 10^{22} \text{ m}$.

CHAPTER 1. INTRODUCTION

that $z = v/c$ in the limit $v/c \ll 1$ ². Cosmological redshift can be thought of as a Doppler effect of light waves with respect to the galaxy's known absorption and emission spectra, and is defined as

$$z \equiv \frac{\lambda_o - \lambda_e}{\lambda_e} .$$

Here λ_e and λ_o are the emitted and observed photon wavelengths respectively, the latter having been stretched by travelling across an expanding universe [8, §2.4]. Redshift can be used to describe the temporal evolution of the universe: high- z events took place in early epochs of the universe.

Hubble's law, often rewritten as $z = Hd$ [17, §2.1], tells us that the further away a galaxy is (in any direction on the sky), the faster it moves away from us. As argued by Lemaître [18], the cosmological principle then implies that the universe itself is expanding. This expansion is characterised by the dimensionless scale factor $a = a(t)$, which is related to cosmological redshift by

$$a = \frac{1}{1 + z}$$

and grows in time, such that the distance between any two distant objects is $\propto a(t)$. The Hubble parameter – itself a function of time – is then defined as

$$H \equiv \frac{\dot{a}}{a} , \tag{1.2}$$

such that it describes the rate of the expansion, and it is positive in an expanding universe. The present-day value of H , denoted by the subscript 0, is nonetheless than the Hubble constant of Equation (1.1) and is measured to be³ $H_0 = 67.7 \text{ km s}^{-1}\text{Mpc}^{-1}$. The present-day value of a , denoted as a_0 , is usually set to unity, and $a \rightarrow 0$ as $t \rightarrow 0$. Since H has units of inverse time, the *Hubble time* $t_H = H^{-1}$ sets the scale for the age of the universe, while the *Hubble radius* $d_H = c H^{-1}$ defines the size of the *observable universe*, i.e. a sphere of radius d_H centred around the observer, which delimits the portion of the universe that can be directly observed.

* * *

Tracing this cosmological expansion back in time leads to the appearance of an initial singularity, when all matter is concentrated in a single point of extreme temperature [23]. This paved the way to the Hot Big Bang (HBB) scenario in the 1930s, although consensus on this theory was not reached until much later. The age of the present universe (i.e. the time that passed since the initial singularity) is related to H_0^{-1} , today's Hubble time.

Formalising this model, the decrease of temperature and energy density as the universe expands was studied. This led to estimates for the production of nuclei in the early

²Notice that Hubble's linear law is only valid in the limit $z \ll 1$, while the relation is more complicated at higher z [9, §I.1.2.2].

³It is important to note that a tension between the measured values of H_0 coming from different observations (*Planck* [19] on one side, SH0ES [20] on the other) is one of the hot topics of modern cosmology, as it questions the validity of the Λ CDM model [21]. A study by Blanchard *et al.* [22] that just appeared on the arXiv nevertheless opposes this claim, finding that the tension vanishes when considering a unknown bias in the distance calibration of Cepheid variables.

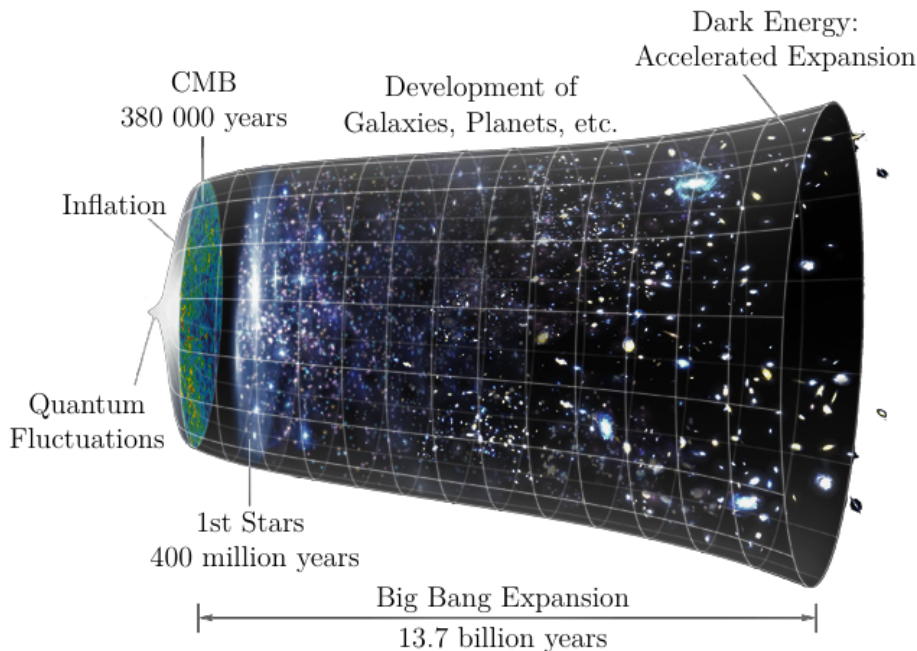


Figure 1.1: Diagram of the evolution of the universe in Λ CDM cosmology, highlighting its key features. The Big Bang singularity is represented on the left, and time flows rightwards. Image adapted from NASA/WMAP Science Team [30]

universe (the Big Bang Nucleosynthesis) [24] and to the prediction of the Cosmic Microwave Background (CMB) [25], the relic radiation from the epoch when photons began propagating freely. The CMB was first observed in 1965 by Penzias and Wilson [26], and currently represents the richest available source of cosmological data.

Further progress was achieved in the following decades, partly due to the technological advances that allowed for more precise observations. Galaxy rotation curves [27] and gravitational lensing events provided new evidence for the existence of Dark Matter (DM), a concept first introduced in the late 19th century [28], while observations of an acceleration in the present-day expansion of the universe [29] indicated the presence of a new unknown energy density opposing gravity, denominated Dark Energy (DE).

These last ingredients led to the formulation of the current Standard Model of Hot Big Bang cosmology, the Λ CDM model [9]. The reinstated cosmological constant Λ is the simplest way to represent Dark Energy, in the form of a vacuum energy permeating all of space. CDM, on the other hand, stand for Cold Dark Matter, “cold” meaning that it is considered to be non-relativistic. The Λ CDM model is the simplest theory that fits even the most recent observations, notably those from the *Planck* satellite [19]; these have shown that the universe is almost flat (see §2.1), and is composed by around 5% ordinary baryonic matter, 26% DM, and 69% DE (Λ) [19, Table 2]. Its principal features are shown in Figure 1.1, together with the initial inflationary phase introduced hereafter.

1.1.2 Shortcomings of Λ CDM Cosmology

While the Λ CDM model has proven to be successful at making accurate predictions, some observations cannot be explained within this framework without requiring extreme and unnatural fine-tuning of initial conditions [31, §II.11.1]. As argued in [32, §5.1], a complete cosmological theory should explain how a particular universe evolved from generic initial conditions, and Hot Big Bang cosmology does not provide this answer. The most notable drawbacks of the theory are illustrated below.

Horizon problem. The CMB temperature has been observed to be homogeneous to $\delta T/T_0 \sim 10^{-5}$ (where $T_0 \sim 2.7$ K is its monopole temperature) [33], even across regions of the universe that should have never been in causal contact. Because of the finite age of the universe, a CMB photon (emitted shortly after the Big Bang) can only have travelled a finite distance $d_H(t_0) \sim H_0^{-1}c$, accounting for the expansion of space. Since information cannot travel faster than light, regions separated by a distance greater than this horizon have never been causally connected. No known physical process can thus be used to explain the observed homogeneity across diametrically-opposite regions of the observable universe.

Flatness problem. As will be explained in Chapter 2, an expanding universe that satisfies the Cosmological Principle can have one of three spatial geometries, differing in their spatial curvature. Observations show that the present-day universe is very close to being flat (it has *almost* no curvature): since this quantity increases during the evolution of the universe, we would need to require an unnaturally small initial value for the curvature. In fact, the quantity accounting for the curvature is inversely proportional to the combination aH , which decreases in time during HBB cosmology [17, §3.1].

Primordial perturbations problem. Clearly, the universe is not homogeneous on small scales, cosmologically speaking: there are structures such as galaxies and voids. Tracing their evolution backwards in time leads to the presence of small-scale primordial density perturbations; however, no suitable mechanism for their generation exists within the Hot Big Bang model, and their initial power spectrum needs to be inserted *ad hoc* as an initial condition of the theory.

* * *

There furthermore exist a number of open questions in Λ CDM cosmology, such as the observed matter-antimatter asymmetry of the universe [34] or those regarding the fundamental nature of Dark Matter and Dark Energy. The latter fluids are included in the model, but a definitive explanation of what they are composed of is still missing, and a variety of hypotheses have been postulated to this regard. It cannot be excluded that the whole of Λ CDM cosmology, or even General Relativity on some scales, may be incorrect; an alternative approach is that of modified gravity theories, such as $f(R)$ theories [35], MOND [36], or teleparallel gravity [37]. In some of these theories, for example, DM and DE could arise naturally. These considerations nevertheless exceed the scope of this thesis.

1.1.3 Inflation

As a solution to the horizon and flatness problems, Alan Guth postulated in 1981 the existence of an *inflationary* epoch of accelerated expansion of space taking place during the very early universe, before the Hot Big Bang stage [1]. During inflation, causally-connected regions were expanded to encompass many of what would now seem to be causally-disconnected areas, and could thus explain the observed CMB homogeneity. That is, the entire present-day observable universe would have expanded from a small region that was within the particle horizon at early times. Meanwhile, the spatial curvature of the universe would decrease during an accelerated expansion, allowing for its present-day value to be small. This is because, during an accelerated expansion of space (i.e. $\ddot{a} > 0$), the combination aH would increase in time. Since the fields of conventional matter (i.e. those described by the Standard Model of particle physics) do not allow for $\ddot{a} > 0$, inflation introduces a new hypothetical field – or, as we will see later, a set of fields – called *inflaton*, which drives the accelerated expansion of space [9, §1.7].

Inflation in its current formulation also includes a built-in *reheating* mechanism for particle creation, providing a transition from the inflationary epoch to standard Hot Big Bang cosmology. When at some point the conditions for inflation get violated, the inflaton’s energy gets transferred to conventional matter. This process also gives rise to primordial density perturbations coming from vacuum fluctuations of the inflaton field, and thus explains structure formation [9, §1.7]. An inflationary era would solve additional outstanding problems, such as the absence of magnetic monopoles and other unwanted relics that were predicted to form in Grand Unified Theories: these would be spread apart by inflation, so much so as to be presently undetectable [38, §1.5].

* * *

Guth initially suggested the inflationary phase to correspond to a de Sitter (dS) universe, the expansion being driven by a vacuum energy with equation of state $\rho = -p$, where ρ is the fluid’s energy density and p its pressure. Starting from a state of very high temperature, the universe inflates as it supercools to temperatures below that of some phase transition, with the potential that drives inflation reaching an unstable false vacuum state. Eventually, the inflaton decays to true vacuum by quantum tunneling (the phase transition happens), albeit it does so gradually, at random points in space: this creates “bubbles” of true vacuum that expand in an (itself expanding) false vacuum background. The energy density of the false vacuum is contained in the bubble domain walls, and is released under the form of particles when bubbles collide [39, Chapter 11]. This process nevertheless concentrates most of the universe’s energy in large expanding bubbles, thus not allowing for an homogeneous universe. This is called the problem of *graceful exit* from the inflationary phase of what is known as the *old* inflation model.

Shortly after Guth’s work, Linde [40] and Albrecht & Steinhardt [41] postulated inflation to take place in a deformed dS universe, lasting for a finite time and being followed by a built-in reheating mechanism to produce particles and allow for usual HBB cosmology. As opposed to the old model in which the field driving inflation would need to tunnel from a false vacuum of the potential to a true vacuum, abruptly terminating the inflationary phase, in this *new* inflation the field rolls slowly down the potential slope, eventually

oscillating around its minimum and allowing for particle creation [39, Chapter 12]. In this scenario, the energy density of the false vacuum is gradually released within a true vacuum bubble, which expands generating an homogeneous universe. This theory took the name of *Slow-Roll* (SR) inflation, and solved Guth’s graceful exit problem. Slow-roll is nowadays the most common paradigm of inflation, and is the one we will consider in later Chapters. Note that alternative mechanisms for inflation exist, such as Dirac–Born–Infeld inflation [42] or k-Inflation [43]; these go beyond our scope and will not be considered further.

In its simplest form, the SR paradigm requires flat inflaton potentials, and models are divided between *small* and *large* field depending on the “distance” traveled by the field, ϕ , during inflation. Various models of SR have been suggested, notably Linde’s *chaotic* inflation [44], which was the first not to depend on early universe high-temperature phase transitions; a chaotic set of initial conditions (ϕ ’s value is randomly distributed throughout space) can be shown to always reach SR in any region in which the field is large enough [44].

1.1.4 Primordial Black Holes

Let us focus on the subject of Dark Matter. This has been indirectly detected: it behaves as ordinary baryonic matter except that it does not interact with light, and is estimated to account for $\sim 85\%$ of the matter content of the universe [19]. Nevertheless, different particle physics and cosmological theories exist as to what it is composed of. From the particle physics point of view, one such hypothesis is that of Weakly Interacting Massive Particles (WIMPs) [45]; this has received a lot of interest, and experiments are being carried out to try to constrain it. In this work, however, we are interested in another candidate for Dark Matter: Primordial Black Holes. These have received renewed attention in recent years, ever since the first Gravitational Wave events were observed at LIGO/Virgo in 2016 [46].

* * *

The theory of General Relativity predicts that if a mass M is contained within a spherical region of radius smaller than its Schwarzschild radius $R_S = 2G_N M$, the curvature of spacetime will be so extreme that not even light will be able to escape it. Such an object takes the name of Black Hole (BH), since it cannot be directly observed. Black Holes can exist over a wide mass range. Those of order several solar masses (denoted in what follows by M_\odot) are produced by stars which cease to be able to sustain nuclear fusion at their core (or rather, where this is not sufficient to counterbalance the gravitational collapse of the star on itself), and are expected to be quite common. Supermassive BHs, of masses $10^6 M_\odot \lesssim M \lesssim 10^{10} M_\odot$, are instead found at the centre of galaxies, the first (indirect) image of one causing quite some excitement not long ago [47]⁴.

Another possibility is that BHs formed in the early universe – thus dubbed *Primordial* Black Holes (PBHs). These were first considered by Zel’dovich & Novikov [49] and Hawking [50], and were found to have an initial mass close to that of the cosmological

⁴The first results of the Event Horizon Telescope’s new imaging of the supermassive BH at the centre of our own galaxy have just been published: see [48].

horizon [51]. PBHs would have been formed from the gravitational collapse of the primordial fluctuations generated during inflation. No decisive proof exists yet regarding the existence of PBHs (as is in fact the case for WIMPs and other candidates as well), but they are thought to be able to account for either a fraction or, in some models, the entirety of DM [51]; in either case, their study would prove beneficial. An additional interesting aspect of PBHs is that they neither require physics beyond the Standard Model of particle physics, nor modified theories of gravity. These considerations make them an interesting candidate for DM, and a natural one in the context of inflation. We will detail the theory of their formation and evolution in Chapter 4, after having studied the theory of cosmological perturbations in §3.3.

1.2 Notation

Below are listed a few noteworthy details regarding the notation used throughout this report. These are given here for ease of reference, and will become clear in later Chapters.

Units. Natural units $c = \hbar = 1$ are adopted. Unless otherwise stated, the Planck mass $M_{\text{Pl}} = 1/\sqrt{8\pi G_{\text{N}}}$ (where as usual G_{N} is Newton’s gravitational constant) will be written explicitly. Notice that H has dimensions of mass in these units.

Spacetime metric. We will adopt the $(-+++)$ signature for the spacetime metric, as is done *e.g.* in [17, 52, 53]. Furthermore, we will usually work in a flat universe in which the curvature parameter, k , and the Ricci scalar, R , are both equally zero.

Indices. The greek indices $(\mu, \nu, \dots = 0, 1, 2, 3)$ will refer to spacetime coordinates, while the latin indices $(i, j, \dots = 1, 2, 3)$ indicate spatial coordinates. A different set of latin indices $(a, b, \dots = 1, 2, \dots, \mathcal{N})$ will instead refer to field-space coordinates.

Derivatives. The dot notation will refer to time derivatives, $\dot{} \equiv \partial/\partial t \equiv \partial_t$. The prime notation will instead indicate derivatives with respect to the number of e -foldings, $N_e \equiv \ln a$, a being the scale factor: $' \equiv \partial/\partial N_e \equiv \partial_{N_e} \equiv H^{-1}\partial_t$. Here $H \equiv \dot{a}/a$ is the Hubble parameter. Conformal time derivatives will be used in a couple of occasion, but will be written explicitly as $\partial_\tau \equiv a\partial_0$ to avoid polluting the notation.

* * *

Closing this Chapter, let us mention a few aspects regarding the format of this thesis. The document was typeset in L^AT_EX from a class file prepared by the author, based on the `memoir` document class. The title page matches the University’s required house style, the characteristic double line being then used in the Chapter headings. Overall, the focus of the page layout was set on allowing for the best possible readability. Various tweaks and tools were introduced for ease of writing. The class file – `almathesis.cls` – is well-documented and can be used as-is: contact the author for a copy.

All the Figures in this thesis are the author’s own production, unless otherwise stated (such as the case of Figure 1.1). Most of them were produced using Wolfram Mathematica.

Chapter 2

Cosmology and Inflation

After the qualitative introduction to the topic given in the previous Chapter, we review here the fundamental elements of Λ CDM cosmology: the spacetime geometry, its dynamics, and the content of the universe. We then present the theoretical framework of standard single-field inflation, describing its background dynamics, Slow-Roll limit, and providing a simple example.

2.1 The Λ CDM Model

An homogeneous and isotropic universe, as required by the cosmological principle discussed in §1.1, can have one of three possible spatial geometries: 3-sphere, 3-plane (Euclidean space), and 3-hyperboloid. Note that homogeneous and isotropic spaces are respectively translation- and rotation-invariant [53, §3.1]. The 3-sphere and 3-hyperboloid manifolds can be understood by embedding them in hypothetical 4-dimensional Euclidean and Minkowski spaces (see [9, §I.2.1] for a detailed description), and have positive and negative spatial curvature, respectively. The curvature is labelled by the parameter κ , such that

$$\kappa = \begin{cases} +1 & \text{3-sphere, positive curvature, } \textit{closed} \text{ universe} \\ 0 & \text{3-plane, zero curvature, } \textit{flat} \text{ universe} \\ -1 & \text{3-hyperboloid, negative curvature, } \textit{open} \text{ universe} \end{cases} ,$$

and has an associated radius of curvature of space, R . In polar coordinates (χ, θ, φ) , the $\kappa = \pm 1$ metrics include terms $\sin(\chi/R)$ and $\sinh(\chi/R)$, respectively. Unifying the three possible spatial metrics, one finds the line element

$$ds_{\text{III}}^2 = d\chi^2 + S_{\kappa}^2(\chi) \left(d\theta^2 + \sin^2 \theta d\varphi^2 \right) ,$$

where

$$S_\kappa(\chi) = \begin{cases} R \sin(\chi/R) & \text{if } \kappa = +1 \\ \chi & \text{if } \kappa = 0 \\ R \sinh(\chi/R) & \text{if } \kappa = -1 \end{cases} .$$

Embedding this line element in a 4-dimensional spacetime manifold, $ds^2 = -dt^2 + ds_{\text{III}}^2$, and accounting for the expansion of space as well (i.e. including the scale factor introduced in §1.1, $ds_{\text{III}}^2 \rightarrow a^2(t) ds_{\text{III}}^2$), we obtain the Friedmann–Lemaître–Robertson–Walker (FLRW) metric:

$$ds^2 = -dt^2 + a^2(t) \left[\frac{dr^2}{1 - kr^2} + r^2 d\Omega^2 \right] . \quad (2.1)$$

To reach this form, known as the Astronomer’s metric, the substitution $r = S_\kappa(\chi)$ was made, together with the rescaling $k = \kappa/R^2$. It is common to consider unit 3-sphere and 3-hyperboloid in the above, such that $R = 1$ and $k = \kappa$ [9, §I.2.2]. The term $d\Omega^2 = d\theta^2 + \sin^2 \theta d\varphi^2$ is the element solid angle. From the metric (2.1), one can compute the Christoffel symbols, $\Gamma_{\mu\nu}^\lambda$, the Riemann tensor, $R_{\mu\nu\sigma}^\lambda$, the Ricci tensor, $R_{\mu\nu}$, and the Ricci (curvature) scalar, R : refer to Appendix A.1 for their definitions.

The coordinates (r, θ, φ) are called *comoving coordinates*: an observer who is only subject to the expansion of the universe (said to move with the *Hubble flow*) is at rest in these coordinates. This can be seen by solving the geodesic equation for this metric for the worldline $x^i = \text{const}$ [54, §1.1]. Distances expressed in these coordinates are fixed with respect to the expansion of the universe, and should be multiplied by a to obtain the corresponding “physical” distance [55, §2.1]. The time coordinate t is called *cosmological* (or *cosmic*) *time*, and is the one measured by a comoving observer. For such an observer at constant (r, θ, φ) , in fact, $ds^2 = dt^2$.

To understand the causal structure of a FLRW universe, we consider the propagation of massless photons, which follow null geodesics ($ds^2 = 0$). In terms of the *conformal time*

$$\tau \equiv \int \frac{dt}{a(t)} , \quad (2.2)$$

which can be understood as a time coordinate which slows down as the universe expands [53, §3.2], the FLRW metric can be written as

$$ds^2 = a^2(\tau) \left(-d\tau^2 + d\chi^2 + S_\kappa^2(\chi) d\Omega \right) .$$

Radial ($d\Omega^2 = 0$) null ($ds^2 = 0$) geodesics then satisfy $d\tau^2 = d\chi^2$, such that

$$\chi(\tau) = \pm\tau + \text{const} .$$

These are straight lines at $\pm 45^\circ$ in the plane $\tau - \chi$, which define the FLRW light cones; in terms of cosmological time t , the light cones would be curved [53, §3.2].

For a flat universe, i.e. when the curvature constant $k = 0$, the FLRW metric in conformal-time coordinates reduces to the Minkowski one multiplied by the scale factor,

$$ds^2 = a^2(\tau) \left(-dt^2 + d\mathbf{x}^2 \right) \equiv a^2(\tau) g_{\mu\nu}^{(M)} dx^\mu dx^\nu , \quad (2.3)$$

where $d\mathbf{x}$ is the 3-dimensional spatial line element and $g_{\mu\nu}^{(M)} = \text{diag}(-1, +1, +1, +1)$ is the Minkowski metric tensor (see Appendix A.1).

2.1.1 Dynamics of an Expanding Universe

The time evolution of a FLRW universe is implicitly embedded in the time dependence of the scale factor $a(t)$. To make this dependence explicit, one needs to solve the Einstein Field Equations,

$$R_{\mu\nu} - \frac{1}{2}R g_{\mu\nu} \equiv G_{\mu\nu} = 8\pi G_{\text{N}} T_{\mu\nu} \quad , \quad (2.4)$$

for $a(t)$ [9, §I.3.1]. Here $G_{\mu\nu}$ is defined to be the Einstein tensor, and $T_{\mu\nu}$ is the energy-momentum tensor, which describes the matter content of the universe.

The left-hand side of the Einstein equations can be calculated directly from the FLRW metric (2.1). As carefully shown in Appendix A.2, the only non-vanishing components of the Ricci tensor are

$$R_{00} = -3 \frac{\ddot{a}}{a}$$

and

$$R_{ij} = \left(\frac{\ddot{a}}{a} + 2 \frac{\dot{a}^2}{a^2} + 2 \frac{k}{a^2} \right) g_{ij} \quad ,$$

the Ricci scalar then being

$$R = 6 \left(\frac{\ddot{a}}{a} + \frac{\dot{a}^2}{a^2} + \frac{k}{a^2} \right) \quad .$$

To calculate the left-hand side of the Einstein equations (2.4), we consider the matter content of the universe to be a homogeneous perfect fluid, with energy density $\rho = \rho(t)$ and pressure $p = p(t)$. The energy-momentum tensor for such a fluid is given by [56, §5.4]

$$T_{\mu\nu} = (p + \rho) u_{\mu} u_{\nu} + p g_{\mu\nu} \quad . \quad (2.5)$$

Since this fluid is comoving with the Hubble flow, i.e. it is at rest in the comoving coordinates, its only non-vanishing 4-velocity component is $u^0 = 1$, subject to $g_{\mu\nu} u^{\mu} u^{\nu} = -1$. The energy-momentum tensor thus reduces to $T_{00} = \rho$ and $T_{ij} = p g_{ij}$.

The (00) component of the Einstein equations then gives

$$\frac{\dot{a}^2}{a^2} \equiv H^2 = \frac{8\pi G_{\text{N}}}{3} \rho - \frac{k}{a^2} \quad , \quad (2.6)$$

which is known as the *Friedmann equation*, while the (ii) components give the so-called Raychaudhuri equation [9, §I.3.1],

$$2 \frac{\ddot{a}}{a} + \frac{\dot{a}^2}{a^2} = -8\pi G_{\text{N}} p - \frac{k}{a^2} \quad . \quad (2.7)$$

The difference of the two above equations gives a relation for the acceleration \ddot{a} , that is [55, §3.1]

$$\frac{\ddot{a}}{a} \equiv \dot{H} + H^2 = -\frac{4\pi G_{\text{N}}}{3} (\rho + 3p) \quad , \quad (2.8)$$

sometimes called the *second Friedmann equation*.

The Friedmann equation is supplemented by the covariant conservation of $T_{\mu\nu}$,

$$\nabla_{\nu} T^{\mu\nu} = 0 \quad .$$

Its $\mu = 0$ component gives the First Law of Thermodynamics $d(\rho a^3) = -pd(a^3)$ or, more conveniently,

$$\dot{\rho} + 3\frac{\dot{a}}{a}(\rho + p) = 0 \quad , \quad (2.9)$$

known as the fluid equation or the *energy conservation equation*. Notice that only two of the three equations (2.6), (2.8), and (2.9) are independent, as they are related by the Bianchi identities [55, §3.1].

The dynamical equations (the two Friedmann equations (2.6) and (2.8), as well as the energy conservation equation (2.9)) are complemented by the *equation of state* for the perfect fluid,

$$p = \omega\rho \quad , \quad (2.10)$$

with ω a dimensionless, time-independent parameter (the equation of state parameter) whose value depends on the characteristics of the fluid considered [55, §3.1]. Before moving on to discussing ω and the composition of the universe, we point out that the Friedmann equation (2.6) can be rewritten as

$$1 = \frac{\rho}{3H^2/8\pi G_N} - \frac{k}{H^2 a^2} \equiv \Omega + \Omega_\kappa \quad , \quad (2.11)$$

where the density parameter $\Omega \equiv \rho/\rho_{\text{crit}}$ was defined, as well as the curvature density parameter $\Omega_\kappa \equiv -k/H^2 a^2$. The critical density, that is the density of matter for which the universe is exactly flat, is defined to be

$$\rho_{\text{crit}} \equiv \frac{3H^2}{8\pi G_N} \quad ,$$

found by evaluating the Friedmann equation with $k = 0$. For $\rho_0 > \rho_{\text{crit},0}$ we would be living in a closed universe, while $\rho_0 < \rho_{\text{crit},0}$ would indicate a closed universe; here and throughout this Section, the subscript 0 indicates present time, such that $\rho_0 \equiv \rho(t_0)$. Note that ρ_{crit} , Ω , and Ω_κ are all functions of time, and Equation (2.11) holds for any t .

2.1.2 Composition and History of the Universe

So far, the matter content of the universe was considered to be a perfect fluid. We know in reality that various components of matter exist, which can be modelled as independent perfect fluids satisfying separate energy conservation equations and equations of state. The assumption here is that the components are decoupled, so that they do not interact with one another [9, §I.3.1]. The energy density ρ appearing in the Friedmann equation (2.6) then represents the sum of the components' energy densities; similarly, the density parameter Ω of Equation (2.11) is the sum of the single density parameters.

For a generic fluid with parameter of state ω (for which we use the label ρ_ω), Equation (2.9) can be solved by substituting the equation of state for p and rewriting $\dot{\rho}_\omega$ as $d\rho_\omega/dt$ and similarly for a :

$$\frac{d\rho_\omega}{\rho_\omega} = -3(1 + \omega)\frac{da}{a} \quad .$$

CHAPTER 2. COSMOLOGY AND INFLATION

Integrating this, we obtain a relation for the evolution of the energy density [55, §3.1],

$$\rho_\omega(a) = \rho_{\omega,0} \left(\frac{a}{a_0} \right)^{-3(1+\omega)}, \quad (2.12)$$

where a_0 is the present-day value of the scale factor, which is usually set to unity; we will adopt the convention $a_0 = 1$ from here onwards, unless otherwise stated. Furthermore, substituting the above result in the Friedmann equation, we get the a -dependence of \dot{a} , which is nonetheless than the quantity aH that will be introduced in Figure 2.1 below:

$$\dot{a} \equiv aH = \sqrt{\Omega_{\omega,0} H_0^2} a^{-\frac{1}{2}(1+3\omega)}. \quad (2.13)$$

Integrating this, we can find the explicit time-dependence of the scale factor,

$$a \propto \begin{cases} t^{\frac{2}{3(1+\omega)}} & \text{if } \omega \neq -1 \\ e^{Ht} & \text{if } \omega = -1 \end{cases}, \quad (2.14)$$

where the constant of proportionality in the first case depends on $\Omega_{\omega,0}$ – the present-day value of the density parameter for the fluid with state parameter ω –, H_0 , and ω . For the $\omega = -1$ case introduced hereafter and corresponding to the constant density ρ_Λ of Equation (2.15), we used the fact that $\Omega_{\omega,0} H_0^2 = H^2 = \Lambda/3$; note that H is constant in this scenario.

* * *

The principal matter components of our universe – a Λ CDM universe – are non-relativistic matter (commonly referred to as *dust* in cosmology¹), radiation, and dark energy. The former includes ordinary baryonic matter as well as dark matter, while radiation refers to massless relativistic particles (photons and neutrinos). As mentioned in §1.1, the simplest model of dark energy – and the one considered by the Λ CDM model – is that of a vacuum energy permeating all of space, in the form of a cosmological constant Λ . We use the self-descriptive subscripts m , r , and Λ for the dust, radiation, and cosmological constant components, respectively; below, the subscript κ will refer to curvature.

We consider dust to be pressureless ($p_m = 0$ and thus $\omega_m = 0$) since the particles it is composed of are well separated and rarely interact [8, §5.3]. Photons and other relativistic particles have a radiation pressure due to their kinetic energy, which can be found to result in $p_r = \rho_r/3$, or $\omega_r = 1/3$ [8, §5.3]. Lastly, the cosmological constant has equation of state $p_\Lambda = -\rho_\Lambda$, i.e. $\omega_\Lambda = -1$. This can be seen by solving the Einstein equations (2.4) with the addition of the Λ term, that is $R_{\mu\nu} - \frac{1}{2}R g_{\mu\nu} = 8\pi G_N T_{\mu\nu} + \Lambda g_{\mu\nu}$. In this case, the Friedmann equations (2.6) and (2.8) have an additional additive term $\Lambda/3$ on their right hand sides, which can be recast as a component of the total energy density ρ by defining

$$\rho_\Lambda \equiv \frac{\Lambda}{8\pi G_N}. \quad (2.15)$$

¹The term “matter” is often used as a synonym for “dust”, as well as to represent the whole matter content of the universe (i.e. dust + radiation + Λ). While we will try to avoid using the former meaning of the word to avoid possible confusion, note that *matter-dominated epoch* (see below) refers to dust-dominance.

CHAPTER 2. COSMOLOGY AND INFLATION

This density is constant, and the energy conservation equation (2.9) thus gives the above-mentioned result [8, §7.2]. Note that a generic dark matter component needs to have $\omega_{\text{de}} < -1/3$ in order to cause an accelerated expansion of the universe, $\ddot{a} > 0$ (this can be seen by substituting Equation (2.12) into the acceleration equation (2.8)).

* * *

The evolution of these single components is found by solving Equations (2.12), (2.13), and (2.14) for the different values of ω , i.e. by solving for a universe dominated by that component of matter (meaning that other components, including curvature, are negligible). The results summarised in Table 2.1 are thus obtained. The Λ -dominated case is called a *de Sitter* (dS) universe and is often considered in the context of inflation [54,57].

Table 2.1: Temporal evolution of the matter components of a Λ CDM universe.

Dust	$\omega_{\text{m}} = 0$	$\rho_{\text{m}} = \rho_{\text{m},0} a^{-3}$	$\dot{a} \propto a^{-1/2}$	$a \propto t^{2/3}$
Radiation	$\omega_{\text{r}} = \frac{1}{3}$	$\rho_{\text{r}} = \rho_{\text{r},0} a^{-4}$	$\dot{a} \propto a^{-1}$	$a \propto t^{1/2}$
Λ	$\omega_{\Lambda} = -1$	$\rho_{\Lambda} = \rho_{\Lambda,0}$	$\dot{a} \propto a$	$a \propto e^{Ht}$

In a generic universe containing all of the above fluids, the total energy density would be $\rho = \rho_{\text{m}} + \rho_{\text{r}} + \rho_{\text{de}} + \rho_{\kappa}$, where we also defined the energy density for curvature, albeit this is not a proper cosmological fluid; from Equation (2.11) we see that $\rho_{\kappa} = \rho_{\kappa,0} a^{-2}$. Considering the a -dependence of each component, we can then write the Friedmann equation (2.6) as

$$H^2(a) = H_0^2 \left(\frac{\Omega_{\text{m},0}}{a^3} + \frac{\Omega_{\text{r},0}}{a^4} + \frac{\Omega_{\text{de},0}}{a^{3(1+\omega)}} + \frac{\Omega_{\kappa,0}}{a^2} \right) . \quad (2.16)$$

We see that when the dark energy component corresponds to the cosmological constant ($\omega = -1$), the denominator of Ω_{Λ} goes to unity: its density is constant in time.

* * *

Since the densities of the matter components evolve differently in time, and we assumed that these do not interact with one another, they will tend to separate from within a mixture of the various fluids. A universe containing several matter components will therefore evolve through different phases, each dominated by a particular fluid. During every phase, the evolution of the scale factor will be influenced by that of the dominating fluid. The time – or a value – of a transition between two epochs is calculated by requiring that the densities of the two fluids at that time be equal. For instance, the matter-radiation transition happens when $\rho_{\text{r}}(a_{\text{rm}}^{\text{eq}}) = \rho_{\text{m}}(a_{\text{rm}}^{\text{eq}})$.

The evolution of the energy density in a Λ CDM universe containing dust, radiation, and a cosmological constant is shown in the left panel of Figure 2.1. We see here that at early times (low a values, $a < a_{\text{rm}}^{\text{eq}}$) the radiation component is dominating, defining a radiation-dominated epoch. This is followed by a matter-dominated stage ($a_{\text{rm}}^{\text{eq}} < a < a_{\text{m}\Lambda}^{\text{eq}}$), and eventually a Λ -dominated one at recent times ($a > a_{\text{m}\Lambda}^{\text{eq}}$). If a non-negligible

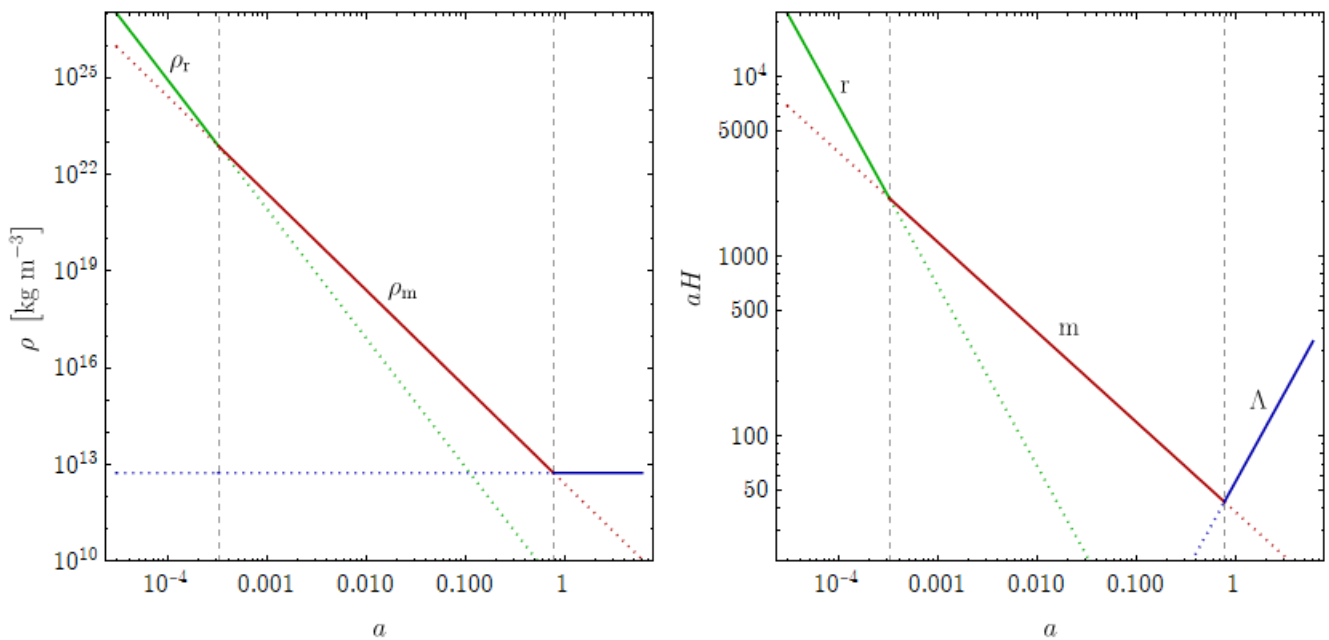


Figure 2.1: *Left panel:* Evolution of the energy density for the matter components of a Λ CDM universe. Radiation ($\rho_r \propto a^{-4}$) dominates at early times ($a < a_{\text{rm}}^{\text{eq}}$), dust ($\rho_m \propto a^{-3}$) at intermediate times ($a_{\text{rm}}^{\text{eq}} < a < a_{\text{m}\Lambda}^{\text{eq}}$), and Λ ($\rho_\Lambda \propto \text{const}$) at late times ($a > a_{\text{m}\Lambda}^{\text{eq}}$). *Right panel:* Evolution of the quantity aH for the matter components of a Λ CDM universe. The same epochs as in the left panel can be seen, where here radiation corresponds to $aH \propto a^{-1}$, dust to $aH \propto a^{-1/2}$, and Λ to $aH \propto a$. *Both panels:* The solid lines indicate the dominating behaviour in each epoch, with the dotted lines of the same colour being their (subleading) contributions in other epochs. Green, red, and blue represent radiation, dust, and Λ , respectively. The vertical dashed lines indicate the transitions between epochs, at $a_{\text{rm}}^{\text{eq}}$ and $a_{\text{m}\Lambda}^{\text{eq}}$. The cosmological parameters were taken from the latest *Planck* results [19], and are reported in Table 2.2. The behaviour of ρ and aH was extrapolated to $a > 1$ (i.e. to the future) for clearer readability.

curvature component² were present (its observed value gives a subleading contribution on all scales, not shown in the Figure), a curvature-dominated epoch would take place between the matter- and Λ -dominated ones. In the right panel of Figure 2.1, we see the corresponding evolution of the quantity aH , which we introduce here as it will be useful when discussing inflation. This follows from Equation (2.13), and determines the rate of expansion of the universe during each epoch.

Note that we extrapolated the behaviour of ρ and aH to $a > 1$ (i.e. to the future) in both panels of this Figure for clearer readability. The parameters used in Figure 2.1 are those of the latest *Planck* results [19, Table 2, *Planck* TT,TE,EE+lowE+lensing+BAO], from which we inferred a radiation component $\Omega_{r,0} = 10^{-4}$. The parameters used are reported in Table 2.2.

²Recent studies [58] based on the latest *Planck* results have shown evidence of a closed universe with $-0.095 < \Omega_\kappa, 0 < -0.007$. If confirmed, these results could strongly affect our understanding of the universe, requiring modifications of the Λ CDM model.

Table 2.2: The values for the parameters used in Figure 2.1. These are taken from the latest *Planck* results [19, Table 2, *Planck* TT,TE,EE+lowE+lensing+BAO]. The approximate $\Omega_{r,0}$ value was calculated through the use of $\Omega_{m,0}$ and $z_{\text{rm}}^{\text{eq}}$ reported there, as $\Omega_{r,0} = \Omega_{m,0}/(1 + z_{\text{rm}}^{\text{eq}})$. We also give the values for the present baryon and Cold Dark Matter density parameters for future reference. These parameters are given here without their associated errors.

H_0 [km s $^{-1}$ Mpc $^{-1}$]	$\Omega_{\Lambda,0}$	$\Omega_{m,0}$	$\Omega_{r,0}$	$\Omega_{b,0}$	$\Omega_{\text{CDM},0}$
67.66	0.6889	0.3111	10^{-4}	0.0490	0.2607

2.1.3 Towards Inflation

It is important to notice from the right panel of Figure 2.1 that the combination aH is a decreasing function of time during the radiation- and matter-dominated epochs. This is an important property of the horizon and flatness problems qualitatively introduced in §1.1.2 (and discussed in more detailed in *e.g.* [31, §II.11.1] and [17, §3.1]). By introducing an inflationary epoch preceding HBB cosmology during which aH *increases* with time (similarly to what happens in the late-time Λ -dominated epoch seen in Figure 2.1), these problems can therefore be solved. This behaviour is shown in Figure 2.2.

The need for an increasing aH is evident in the case of the flatness problem: from Equation (2.11), $\Omega_{\kappa} \propto (aH)^{-2}$ and thus increases with time, requiring an unnaturally small initial value $\Omega_{\kappa,i}$ to explain the current $\Omega_{\kappa,0} \sim 0$. The inflationary phase would instead minimise a more realistic $\Omega_{\kappa,i} \sim \mathcal{O}(1)$ before it starts increasing. The discussion of the horizon problem requires additional care.

The idea of (*physical*) *Hubble radius* was introduced in §1.1 as $d_{\text{H}} = H^{-1}$, setting the size of the observable universe at time t [9, §I.3.2.1]. The *comoving Hubble radius* is then defined to be

$$\chi_{\text{H}} = \frac{d_{\text{H}}}{a} = (aH)^{-1} \quad , \quad (2.17)$$

and therefore increases in time during HBB cosmology. We can furthermore introduce the concept of *comoving particle* (or *cosmological*) *horizon* to be the greatest comoving distance that photons can propagate between an initial time t_i and a time t : in terms of the conformal time defined in Equation (2.2),

$$\chi_{\text{p}} = \tau - \tau_i = \int_{t_i}^t \frac{dt'}{a(t')} \quad .$$

Correspondingly, the *physical particle horizon* will be $d_{\text{p}} = a\chi_{\text{p}}$. The initial time is usually taken to be $t_i = 0$, when $a(0) = 0$ and – for HBB cosmology – $\tau_i = 0$. The comoving particle horizon can then be rewritten as (dropping the prime label for simplicity) [53, §4.1]

$$\chi_{\text{p}}(\tau) = \tau = \int_0^t \frac{dt}{a(t)} = \int_0^a \frac{da}{a^2 H} = \int_0^a d \ln a (aH)^{-1} \quad . \quad (2.18)$$

A subtle yet important distinction between χ_{H} and χ_{p} , described in [52, §6.3.1], is to be noted: the comoving Hubble radius sets the scale for causality at a given time (two particles separated by a distance greater than χ_{H} are not in causal contact *now*), while

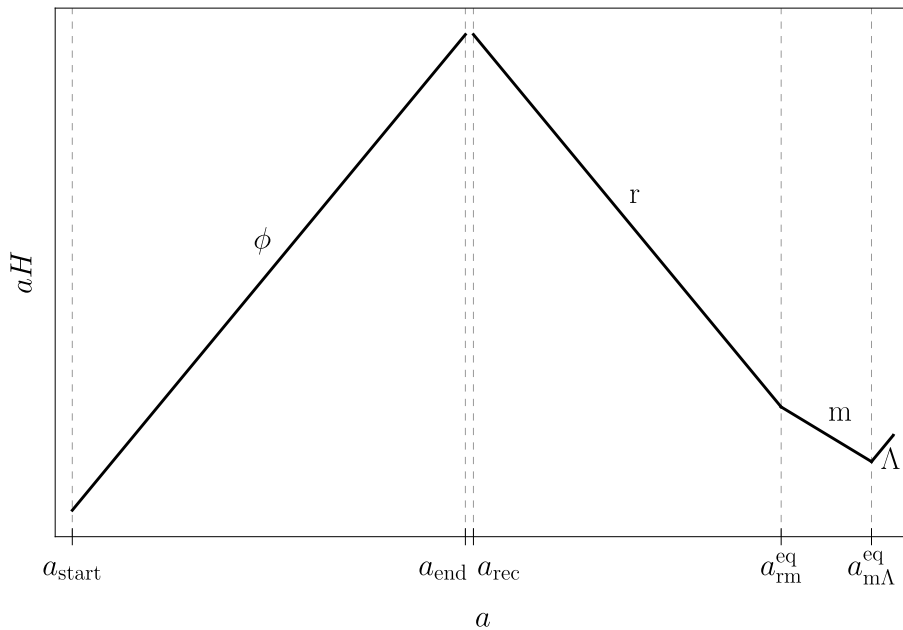


Figure 2.2: Sketch of the evolution of the quantity (aH) throughout the history of the universe. The left-hand side shows how aH increases during inflation – denoted by the field ϕ that drives this expansion, see §2.2 –, while in the right-hand side we see how it behaves during HBB cosmology (i.e. what is shown in the right panel of Figure 2.1). The evolution of aH during inflation was calculated by considering the results of Equations (2.38) and (2.39) of the next Section. The vertical dashed lines indicate the start and end values of inflation, a_{start} and a_{end} , as well as the radiation-matter and matter- Λ equalities, $a_{\text{rm}}^{\text{eq}}$ and $a_{\text{m}\Lambda}^{\text{eq}}$. The present time a_0 is not shown explicitly, as it would overlap with $a_{\text{m}\Lambda}^{\text{eq}}$ in this sketch. We also indicate the time of recombination, a_{rec} , i.e. when the CMB was formed. The period between the end of the exponential expansion and recombination is called *reheating*, and is an important aspect of inflationary cosmology as it explains the origin of elementary particles and provides the link with HBB theory; reheating will nevertheless not be considered in this work: see *e.g.* [59, 60] for reviews. The scales for HBB match those of Figure 2.1, as we used the parameters of Table 2.2, while those on the left-hand side of the plot – including a_{end} – are arbitrary. The plot is in log – log scale.

the comoving particle horizon sets the total scale for causality (two particles separated by a distance greater than χ_p *never* were in causal contact). At present time, the latter distance could thus possibly be greater than the former. As illustrated by the logarithmic integral over the comoving Hubble radius of Equation (2.18), χ_p could have received most of its contribution from some hypothetical early epoch during which χ_H was much larger than it is today. At that time, the comoving Hubble horizon would have encompassed all of today’s cosmologically-relevant scales. This would mean that particles that are not in causal contact *now* could have been connected at early times, solving the core of the horizon problem. This early epoch would have preceded inflation, the condition of an increasing aH translating to a decreasing χ_H .

Looking back at Equation (2.18), we point out that including the inflation stage (which as we will show below drives an exponential expansion of space) the initial conformal time

is pushed back to $\tau_i = -\infty$. Now $\tau = 0$ corresponds to the time of reheating, i.e. the end of inflation.

* * *

On top of solving the horizon and flatness problems of HBB cosmology, the fact that χ_H decreases during inflation also leads to understanding the formation of primordial density perturbations. Cosmological objects with comoving wavelengths that enter the comoving Hubble radius today were outside it at the time of CMB decoupling, but within it during inflation: see Figure 2.3 (or equivalently [52, Figure 6.4]). From now on, we will often call the comoving Hubble radius “horizon” as done in the literature (we talk of *subhorizon* and *superhorizon* evolution).

During inflation, quantum perturbations are generated; in physical coordinates, these are stretched to distances greater than d_H , which remains roughly constant during inflation. In comoving coordinates, this means that the perturbations are generated on subhorizon scales (i.e. their time-independent comoving wavelengths are smaller than the comoving Hubble radius at that time) and exit the horizon when χ_H becomes smaller than their comoving wavelength. They then evolve as classical superhorizon (density) perturbations, their amplitude remaining constant (they are “frozen” [61, 62]), and re-enter the horizon during HBB cosmology forming large-scale structures by gravitationally collapsing [52, §6.3.1].

* * *

From Equation (2.14) (in the $\omega \neq 1$ case³), $a \propto t^\alpha$ so that $aH = \dot{a} \propto \alpha t^{\alpha-1}$. An increasing aH therefore requires $\alpha > 1$ (the scale factor growing faster than time) or, from Equation (2.14), $\omega < -1/3$. This is the same condition that was found below Equation (2.15) when requiring that $\ddot{a} > 0$: inflation in fact corresponds to a phase of accelerating expansion of the universe (which was already understood when requiring that $aH = \dot{a}$ be an increasing function of time).

Three equivalent conditions for inflation can therefore be formulated: an increasing aH (or decreasing comoving Hubble radius), an accelerated expansion, or a negative pressure [53, §5.2]. In equations,

$$\frac{d}{dt}(aH)^{-1} < 0 \quad \Leftrightarrow \quad \ddot{a} > 0 \quad \Leftrightarrow \quad \omega < -\frac{1}{3} . \quad (2.19)$$

The latter corresponds to a violation of the Strong Energy Condition [53, §5.2].

As discussed in §2.1.2 and reported in Table 2.1, baryonic matter and radiation do not satisfy the negative pressure requirement $\omega < -1/3$; a different energy component is therefore needed to drive inflation. It turns out that such a component can be easily and efficiently described in terms of a scalar field (the inflaton). This description will be the matter of the following Section. In Chapter 3 we will instead see how inflation can be described by a *number of* scalar fields. Alternatively, from the particle physics point of view (which motivated the use of a scalar field in the first place), one can use a vector field to drive inflation; this not only complicates things, but does not seem to work better either [52, §6.3].

³In the $\omega = -1$ case, $H = \text{const}$ and $a \propto e^{Ht}$, thus $aH \propto He^{Ht}$, increasing for any $H > 0$.

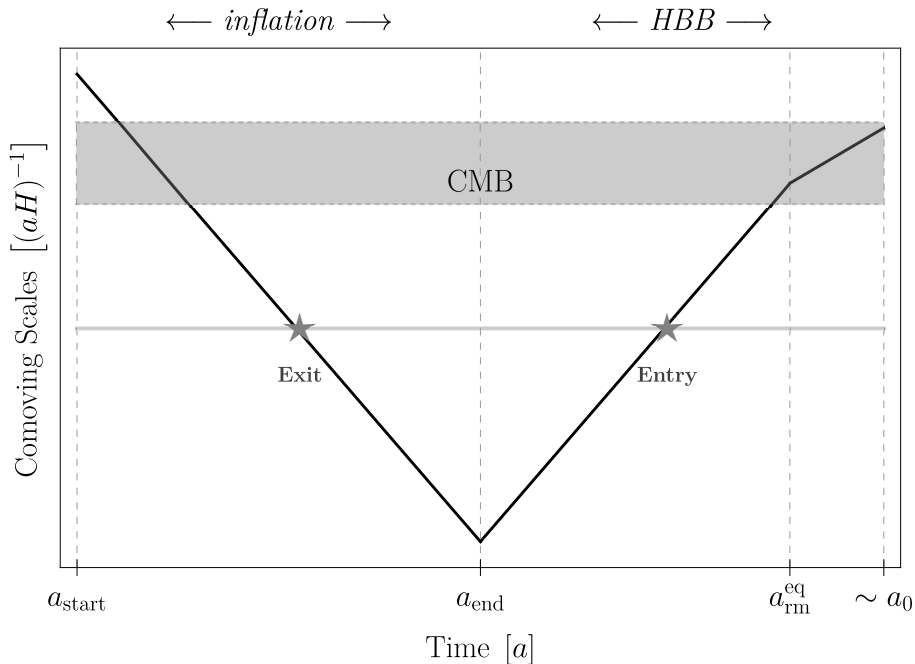


Figure 2.3: Sketch of the evolution of the Hubble radius $(aH)^{-1}$ (the opposite of the quantity aH shown in Figure 2.2) throughout the history of the universe; notice that reheating and Λ -domination are ignored here. The left-hand side shows the decreasing Hubble radius of inflation, while in the right-hand side we see how it increases during HBB cosmology. The evolution of aH during inflation was calculated by considering the results of Equations (2.38) and (2.39) of the next Section. The vertical dashed lines indicate the starting and ending values of inflation, a_{start} and a_{end} , as well as the radiation-matter equality $a_{\text{rm}}^{\text{eq}}$ and the pseudo-present-time a_0 (we extend matter-domination to a_0). The evolution of an arbitrary perturbation is also shown as a straight grey line: we highlight with a grey star the moments where it exits and re-enters the horizon, during inflation and radiation-domination respectively. This perturbation could correspond to Primordial Black Holes (see Chapter 4). Furthermore, the grey band shows CMB-scale perturbations: just like the grey line, these are within the horizon at the beginning of the inflationary epoch, then become superhorizon. These perturbations re-enter the horizon around present-time, and are thus the ones we observe nowadays [52, §6.3.1]. The scales for HBB match those of Figure 2.1, as we used the parameters of Table 2.2, while those on the left-hand side of the plot – including a_{end} – are arbitrary. The plot is in log – log scale.

2.2 Single-Field Inflation

In order to build a model of single-field slow-roll inflation, one needs only consider a generic scalar field ϕ that is minimally coupled to Einstein gravity through the canonical Einstein-Hilbert action [9, §I.4.8.1],

$$S = \int d^4x \sqrt{-g} \left[-\frac{1}{2} g^{\mu\nu} \partial_\mu \phi \partial_\nu \phi - V(\phi) + \frac{M_{\text{Pl}}^2}{2} R \right] , \quad (2.20)$$

where $g \equiv \det g_{\mu\nu}$ is the determinant of the FLRW metric tensor (2.1) and R is its associated Ricci scalar. The field-dependent potential, $V(\phi)$, is specified by the particular

model considered; it describes the field's self-interactions. The field's Energy-Momentum tensor (EMt), as determined in Appendix B, is given by

$$T_{\mu\nu} = \partial_\mu\phi\partial_\nu\phi - g_{\mu\nu}\left(\frac{1}{2}\partial^\alpha\phi\partial_\alpha\phi + V(\phi)\right) , \quad (2.21)$$

while its Equations of Motion (EoM) are found through the use of the Euler–Lagrange equations to be (c.f. Equation (B.14))

$$D_\mu\partial^\mu\phi = V_{,\phi} , \quad (2.22)$$

where $V_{,\phi} = \partial V/\partial\phi$ and the covariant spacetime derivative satisfies $D_\mu A^\nu = \partial_\mu A^\nu + \Gamma_{\mu\lambda}^\nu A^\lambda$, with $\Gamma_{\mu\lambda}^\nu$ the Christoffel symbols associated to the FLRW metric.

We now consider the standard splitting of our fields (clearly the inflaton, but also the metric and the EMt) into classical homogeneous backgrounds and sets of perturbations around the background, which will then be quantised (semiclassical approach). For a generic field,

$$X(t, \mathbf{x}) = X_0(t) + \delta X(t, \mathbf{x}) .$$

Let us begin by focusing on the background fields. The study of cosmological perturbations is quite involved, and is postponed to §3.3, where it will be tackled in the multi-field framework.

2.2.1 Background Dynamics

In the present Section and for the rest of this Chapter, we focus on the homogeneous universe for which all perturbations can be set to zero. We therefore have that $\phi = \phi_0(t)$ here: we will drop the 0 subscript notation for the remainder of this Chapter and will make it explicit when we reintroduce it later.

The background metric in a flat FLRW universe is the Minkowski one multiplied by the scale factor, as was encountered in Equation (2.3). In cosmic time coordinates, this reads

$$ds^2 = -dt^2 + a^2(t)d\mathbf{x}^2 , \quad (2.23)$$

such that $g_{\mu\nu} = \text{diag}(-1, a^2, a^2, a^2)$, for which $g = -a^6$. For this homogeneous universe we have $\partial_i\phi = 0$, and Equation (2.22) then gives us the *background* Equation of Motion

$$\ddot{\phi} + 3H\dot{\phi} + V_{,\phi} = 0 , \quad (2.24)$$

that is, a Klein–Gordon equation for ϕ [63, Chapter 8]. Here we noticed that $\Gamma_{00}^0 = 3H$ from the property $\Gamma_{\mu\nu}^\mu = \partial_\nu \ln \sqrt{-g}$ of the Christoffel symbols [9, Equation (I.A.24)]. Notice that the background EoM can equivalently be obtained by varying the action (2.20) for $\phi = \phi_0(t)$ and $g_{\mu\nu} = g_{\mu\nu,0}$:

$$\begin{aligned} \delta S &= \int d^4x a^3 (\dot{\phi}\delta\dot{\phi} - V_{,\phi}\delta\phi) \\ &= \int d^4x \left(-\frac{d}{dt}(a^3\dot{\phi}) - a^3V_{,\phi} \right) \delta\phi , \end{aligned}$$

where we integrated by parts the first term and noticed that $\delta\phi$ vanishes at the boundaries. The EoM (2.24) then correspond to $\delta S/\delta\phi$.

We point out that the background EoM (2.24) is the same equation as that for the motion of a classical particle of coordinates ϕ rolling a potential well $V(\phi)$, for which $H\dot{\phi}$ is a time-dependent friction term, called the *Hubble friction* [31, §II.12.1].

Assuming the background field ϕ to be a perfect fluid [64], the Energy-Momentum tensor takes the form introduced in (2.5), such that $T_{00} = \rho_\phi$ and $T_{ii} = a^2 p_\phi$. Equating this to the inflaton EMt (2.21), we find that

$$\rho_\phi = \frac{1}{2}\dot{\phi}^2 + V(\phi) \quad , \quad (2.25)$$

$$p_\phi = \frac{1}{2}\dot{\phi}^2 - V(\phi) \quad . \quad (2.26)$$

Inserting these results into the Friedmann equations (2.6) and (2.8) allows to find expressions for the evolution of H and \dot{H} in terms of the inflaton field:

$$H^2 = \frac{1}{3M_{\text{Pl}}^2} \left(\frac{1}{2}\dot{\phi}^2 + V(\phi) \right) \quad , \quad (2.27)$$

$$\dot{H} = -\frac{1}{2M_{\text{Pl}}^2} \dot{\phi}^2 \quad , \quad (2.28)$$

written in terms of the Planck mass $M_{\text{Pl}} = 1/\sqrt{8\pi G_N}$. These equations, together with the EoM (2.24), determine the dynamics of the system of background fields when no other matter components are present [31, §II.12.1].

Furthermore, the Equation of State (2.10) for the inflaton component described by Equations (2.25) and (2.26) gives

$$\omega_\phi = \frac{\frac{1}{2}\dot{\phi}^2 - V(\phi)}{\frac{1}{2}\dot{\phi}^2 + V(\phi)} \quad . \quad (2.29)$$

2.2.2 Slow-Roll

The scalar field's Equation of State (2.29) allows for negative pressure and especially for the condition $\omega_\phi < -1/3$ of (2.19) to be satisfied if the potential energy dominates over the kinetic energy,

$$\frac{1}{2}\dot{\phi}^2 \ll V(\phi) \quad .$$

In the extreme case where $\dot{\phi}^2/2 \sim 0$, a quasi-de Sitter expansion $\omega_\phi \sim -1$ would take place. In general, for $\dot{\phi}^2/2 \ll V$ we have that $H^2 \propto V$ from Equation (2.27), which becomes very large for large V . This leads to a significant Hubble friction term $H\dot{\phi}$ in the background EoM (2.24) [53, §6.1]: the field ϕ is therefore *slowly rolling* down the potential well $V(\phi)$.

CHAPTER 2. COSMOLOGY AND INFLATION

The *first Hubble Slow-Roll (SR) parameter*⁴ is defined as

$$\epsilon \equiv -\frac{\dot{H}}{H^2} = -\frac{d \ln H}{dN_e} = \frac{1}{2M_{\text{Pl}}^2} \frac{\dot{\phi}^2}{H^2} \quad , \quad (2.30)$$

where the second equality requires the introduction of the number of e -foldings (or e -folds) of inflationary expansion, $dN_e = H dt = d \ln a$, and the third equality comes from using Equation (2.28). The physical meaning of N_e is that during an e -folding, the universe expands by a factor e : over N_e e -folds, it expands by e^{N_e} . Rewriting the second Friedmann equation (2.8) in terms of ϵ , one finds that

$$\frac{\ddot{a}}{a} = \dot{H} + H^2 = H^2(1 - \epsilon) \quad .$$

The inflation acceleration condition $\ddot{a} > 0$ of Equation (2.19) therefore translates to requiring that $\epsilon < 1$. This can be read as the fractional change of H per e -folding (i.e. per Hubble time) being small – the Hubble parameter varies slowly, and is therefore roughly constant during inflation [53].

In the case that $\dot{\phi}^2/2 \ll V$, we have from Equations (2.27) and (2.28) that $H^2 \propto V$ and $\dot{H} \propto -\dot{\phi}^2$, such that $\epsilon \sim \dot{\phi}^2/V$ and therefore

$$\epsilon \ll 1 \quad .$$

While $\epsilon < 1$ is the generic requirement for inflation, $\epsilon \ll 1$ is the first Slow-Roll condition. The de Sitter case corresponds to the limit $\epsilon \rightarrow 0$.

* * *

In order to sustain a sufficiently long inflation period, the acceleration of the scalar field must be much smaller than the friction and potential terms of the EoM (2.24),

$$|\ddot{\phi}| \ll |3H\dot{\phi}|, |V_{,\phi}| \quad .$$

Introducing the *second Hubble Slow-Roll parameter*,

$$\eta \equiv -\frac{\ddot{\phi}}{H\dot{\phi}} = -\frac{d \ln \dot{\phi}}{dN_e} = \epsilon - \frac{1}{2} \frac{\dot{\epsilon}}{H\epsilon} = \epsilon - \frac{1}{2} \frac{d \ln \epsilon}{dN_e} \quad , \quad (2.31)$$

the above requirement translates to

$$|\eta| \ll 1 \quad ,$$

i.e. that the fractional change of ϵ per Hubble time (or per e -folding) is small.

Note that different definitions of η exist in the literature. We choose to follow the notation of Baumann [53] for consistency with the multi-field generalisation of this parameter as used by Achúcarro *et al.* [5] and (differing by a minus sign) Groot Nibbelink

⁴As pointed out in [65, §2.4], the parameter ϵ describes the deviation of the inflationary spacetime from perfect de Sitter. Being finite (although small), the universe never is perfectly de Sitter; in such a universe, in fact, inflation would never end.

CHAPTER 2. COSMOLOGY AND INFLATION

& van Tent [66, 67] – see Equation (3.22) in §3.2. Other choices are that of Gorbunov & Rubakov [31], $\eta_{(\text{GR})} = \epsilon - \ddot{\phi}/H\dot{\phi} = \epsilon + \eta$, or that of Braglia *et al.* [6, 7],

$$\eta_{(\text{B})} = \frac{\dot{\epsilon}}{H\epsilon} = \frac{d \ln \epsilon}{dN_e} = 2\epsilon - 2\eta \quad , \quad (2.32)$$

which will also be considered in the multi-field case: see Equation (3.28). Importantly, all of these choices equivalently satisfy $|\eta| \ll 1$.

The SR conditions can be shown to be equivalent to requiring a flat enough potential, such that it can behave as an effective cosmological constant driving near-exponential expansion. Following the reasoning of [31, §II.12.1], the *potential Slow-Roll parameters*

$$\epsilon_V \equiv \frac{M_{\text{Pl}}^2}{2} \frac{V_{,\phi}^2}{V^2} \quad (2.33)$$

and

$$\eta_V \equiv M_{\text{Pl}}^2 \frac{V_{,\phi\phi}}{V} \quad (2.34)$$

are introduced, where $V_{,\phi\phi} = \partial^2 V / \partial \phi^2$. Using the Friedmann equations and the EoM, the SR conditions translate to

$$\epsilon_V, \eta_V \ll 1 \quad \Leftrightarrow \quad \frac{V_{,\phi}}{V}, \frac{V_{,\phi\phi}}{V} \ll 1 \quad . \quad (2.35)$$

The precise relation between the Hubble and potential SR parameters is discussed in [53, Appendix D]. For our concerns, we can write that $\epsilon \approx \epsilon_V$ and $\eta \approx \eta_V - \epsilon_V$. For the other definitions of η introduced above, $\eta_{(\text{B})} \approx 4\epsilon_V - 2\eta_V$ while $\eta_{(\text{GR})} \approx \eta_V$: see [31, §II.12.1].

* * *

We showed that Slow-Roll inflation is allowed to take place while the Slow-Roll conditions,

$$\epsilon, |\eta| \ll 1 \quad , \quad (2.36)$$

are satisfied. Inflation ends when at least one of ϵ or η reach unity: usually, the end of inflation is defined to satisfy $\epsilon(\phi_{\text{end}}) = 1$.

During Slow-Roll, the evolution of the background fields is simplified: the EoM (2.24) and Friedmann equation (2.27) in fact reduce to

$$\dot{\phi} \approx -\frac{V_{,\phi}}{3H} \quad (2.37)$$

and

$$H^2 \approx \frac{1}{3M_{\text{Pl}}^2} V(\phi) \approx \text{const} \quad . \quad (2.38)$$

Integrating the latter equation, we see that the time evolution of the scale factor in the SR regime is near-exponential [31, §II.12.1],

$$a(t) \approx a_{\text{start}} \exp\left(\int_{t_{\text{start}}}^t H(t') dt'\right) \sim e^{Ht} \quad , \quad (2.39)$$

where t_{start} is the time at which inflation begins. In other words, spacetime is approximately de Sitter during Slow-Roll inflation.

Considering the discussion of §2.1.2, we see from Equations (2.39) and (2.38) that $aH \sim He^{Ht}$, similarly to the Λ case of the late-time universe. aH is therefore an increasing function of time, as advertised.

* * *

The duration of inflation is determined by the *total* number of e -foldings, N_e^{tot} . First, the number of e -folds between a time t within inflation and the end of that epoch at t_{end} is given as

$$N_e(\phi) = \ln \frac{a_{\text{end}}}{a} = \int_t^{t_{\text{end}}} H dt = \int_{\phi_{\text{end}}}^{\phi} \frac{H}{\dot{\phi}} d\phi = \int_{\phi_{\text{end}}}^{\phi} \frac{1}{\sqrt{2M_{\text{Pl}}^2 \epsilon}} d\phi \quad , \quad (2.40)$$

where the definition of ϵ , Equation (2.30), was used in the last equality.

A minimum number of e -folds of around 60 is needed in order to solve the flatness and horizon problems (see *e.g.* [31, §II.11.2] for a discussion). Regarding the flatness problem, this can be found by requiring that the curvature parameter of Equation (2.11) at the end of inflation be $|\Omega_\kappa| \lesssim 10^{-60}$ (as found by working backwards from its present-day value), and of order unity at the start of the expansion (the most natural assumption): since $\Omega_\kappa \propto a^{-2}$ [68],

$$\frac{|\Omega_\kappa^{\text{end}}|}{|\Omega_\kappa^{\text{start}}|} \approx \frac{a_{\text{start}}^2}{a_{\text{end}}^2} = e^{-2N_e^{\text{tot}}} \quad .$$

The commonly quoted value for N_e^{tot} (although this value is model-dependent) is

$$N_e^{\text{tot}} = \ln \frac{a_{\text{end}}}{a_{\text{start}}} \gtrsim 60 \quad .$$

The fluctuations on CMB scales are produced at $N_e^{\text{CMB}} \sim 40 - 60$ e -folds before inflation ends: this is required for perturbations to grow to reach the observed amplitude, and depends on post-inflationary thermal processes [69]. From the definition of $N_e(\phi)$, we can then calculate ϕ_{CMB} , the field value corresponding to N_e^{CMB} :

$$\int_{\phi_{\text{end}}}^{\phi_{\text{CMB}}} \frac{1}{\sqrt{2M_{\text{Pl}}^2 \epsilon}} d\phi = N_e^{\text{CMB}} \quad .$$

2.2.3 Simple Example: Quadratic Inflation

Before introducing multi-field inflation, which will be the main topic of this work, let us have a look at the simplest concrete model of inflation. In this case, the potential takes the quadratic form

$$V(\phi) = \frac{1}{2} m^2 \phi^2 \quad , \quad (2.41)$$

with $m \ll M_{\text{Pl}}$ the mass of the scalar field. The potential is shown in Figure 2.4.

The dynamical equations for the background (EoM and Friedmann equation) can be solved for $\phi(N_e)$ to determine the evolution of the field given the appropriate initial conditions. This will be done explicitly in Chapter 5 for 2-field models.

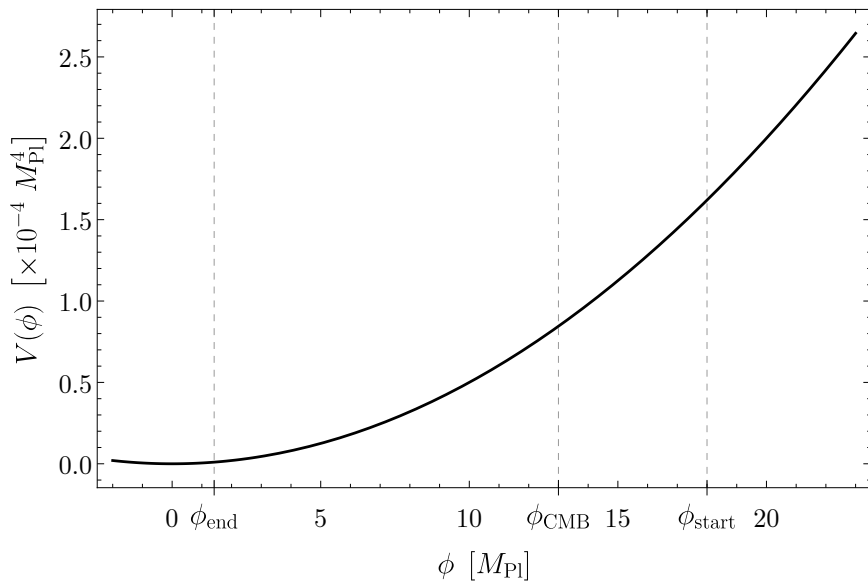


Figure 2.4: Sketch of the single field quadratic inflaton potential, $V(\phi) = \frac{1}{2}m^2\phi^2$. The dashed vertical lines represent the field values corresponding to the start and end of inflation, and to perturbations on CMB scales. The field rolls down the potential from left to right towards the minimum of $V(\phi)$, to then oscillate around it. The value $N_e^{\text{tot}} = N_e(\phi_{\text{start}}) \approx 80$ e -folds was taken here, so that $\phi_{\text{start}} \approx 18$ from Equation (2.40). An arbitrary mass $m = 10^{-3} M_{\text{Pl}}$ was chosen.

The potential Slow-Roll parameters (2.33) and (2.34) are thus found to be [53, §6.3]

$$\epsilon_V = \eta_V = 2 \frac{M_{\text{Pl}}^2}{\phi^2} \quad ,$$

such that, for the SR conditions $\epsilon_V, \eta_V < 1$ to be satisfied, we need the field to take values

$$\phi > \sqrt{2}M_{\text{Pl}} \equiv \phi_{\text{end}} \quad .$$

With this ϕ_{end} , the number of e -foldings before the end of inflation found in Equation (2.40) gives

$$N(\phi) = \int_{\phi_{\text{end}}}^{\phi} \frac{\phi}{2M_{\text{Pl}}^2} d\phi = \frac{\phi^2}{4M_{\text{Pl}}^2} - \frac{1}{2} \quad .$$

The field value corresponding to fluctuations on CMB scales is then found from $N_e^{\text{CMB}} = N(\phi_{\text{CMB}})$,

$$\phi_{\text{CMB}} = 2M_{\text{Pl}}\sqrt{N_e^{\text{CMB}}} \approx (12 - 15) M_{\text{Pl}} \quad .$$

Chapter 3

Multi-Field Inflation

While the most natural assumption, considered thus far, is to account for a single scalar field driving inflation, this is not the only possibility: starting from the mid 1980s, different hypotheses of multiple field inflation were brought forward (see for example [70, 71]). Using multiple fields induces new phenomenology, increasing the amount of physics that can be explained by the theory. For example, multi-field inflation predicts isocurvature fluctuations [72] and allows for new consistency relations to be defined [73]. These, as well as other effects such as significant non-Gaussianity, increase the observational prospects of inflation [53]. Furthermore, realistic models of high energy physics comprise multiple interacting scalar fields: a model that takes them into account is therefore expected to be more reliable from this point of view.

3.1 Theoretical Framework

As an extension to single-field inflation, one substitutes the field ϕ by a set of \mathcal{N} scalar fields ϕ^a , with $a = 1, \dots, \mathcal{N}$. The \mathcal{N} -field action is then given by a generalisation of Equation (2.20).

In its canonical form, the kinetic term of the Lagrangian would look like $g^{\mu\nu} \partial_\mu \phi^a \partial_\nu \phi_a$. We are nevertheless interested in a more general case, in which the fields ϕ^a span an abstract \mathcal{N} -dimensional real manifold \mathcal{M}_ϕ endowed with a metric γ_{ab} . This allows for non-trivial couplings between the fields to be due not only to the fields potential $V(\phi)$ (where from now on ϕ denotes the set of all ϕ^a), but also to this metric¹. The \mathcal{N} -field action therefore takes the form

$$S = \int d^4x \sqrt{-g} \left[-\frac{1}{2} \gamma_{ab} g^{\mu\nu} \partial_\mu \phi^a \partial_\nu \phi^b - V(\phi) + \frac{M_{\text{Pl}}^2}{2} R \right] . \quad (3.1)$$

¹Note that the non-minimal kinetic coupling between the fields appears naturally in supergravity models: see [66] and references therein.

CHAPTER 3. MULTI-FIELD INFLATION

The Christoffel symbols of the field-space manifold \mathcal{M}_ϕ , upon which the fields ϕ^a act as coordinates, are given by²

$$\Gamma_{bc}^a = \frac{1}{2}\gamma^{ad}(\partial_b\gamma_{dc} + \partial_c\gamma_{bd} - \partial_d\gamma_{bc}) \quad , \quad (3.2)$$

where we defined the partial derivatives with respect to the scalar fields, $\partial_a \equiv \partial/\partial\phi^a$. The corresponding Riemann tensor is

$$\mathbb{R}_{bcd}^a = \partial_c\Gamma_{bd}^a - \partial_d\Gamma_{bc}^a + \Gamma_{ce}^a\Gamma_{db}^e - \Gamma_{de}^a\Gamma_{cb}^e \quad , \quad (3.3)$$

and the field-space Ricci tensor and Ricci scalar are respectively defined as $\mathbb{R}_{ab} = \mathbb{R}_{acb}^c$ and $\mathbb{R} = \gamma^{ab}\mathbb{R}_{ab}$. In correspondence with Equation (A.6), the field-space Ricci tensor can be written as

$$\mathbb{R}_{ab} = \partial_c\Gamma_{ab}^c - \partial_a\Gamma_{bc}^c + \Gamma_{ab}^c\Gamma_{cd}^d - \Gamma_{ad}^c\Gamma_{cb}^d \quad . \quad (3.4)$$

For a detailed discussion of the geometry of the field-space manifold \mathcal{M}_ϕ , see References [66, 67].

The metric γ_{ab} as well as the scalar potential $V(\phi)$ appearing in Equation (3.1) are given a concrete form by the choice of the \mathcal{N} -field model one chooses to study. Specific examples will be considered in Chapter 5, where different 2-field models will be analysed.

* * *

The action (3.1) leads to the following equations of motion (EoM), as detailed in Appendix B:

$$\square\phi^a + \Gamma_{bc}^a g^{\mu\nu}\partial_\mu\phi^b\partial_\nu\phi^c = V^{,a} \quad . \quad (3.5)$$

We defined here the covariant spacetime d'Alembert operator $\square\phi \equiv D_\mu\partial^\mu\phi$ acting on a scalar, where $D_\mu A^\nu \equiv \partial_\mu A^\nu + \Gamma_{\mu\lambda}^\nu A^\lambda$ is the covariant spacetime derivative acting on a (spacetime) vector. The potential's derivative $V^{,a} \equiv \gamma^{ab}\partial_b V$ was also used. Notice that it is visible in the EoM how the fields are coupled through both the potential and the field-space metric (i.e. through the Γ_{bc}^a term), as mentioned earlier.

The action also leads to the definition of the multi-field Energy-Momentum tensor,

$$T_\nu^\mu = \gamma_{ac}\partial^\mu\phi^a\partial_\nu\phi^c - \delta_\nu^\mu\left(\frac{1}{2}\gamma_{ac}\partial^\alpha\phi^a\partial_\alpha\phi^c + V(\phi)\right) \quad , \quad (3.6)$$

as shown again in Appendix B.

The semiclassical approximation is now considered. All of our fields are separated in the sum of a background value, assumed to be homogeneous, and a perturbative term. The former is taken to be classical, while the latter will be quantised. For a generic field, X , this means that

$$X(t, \mathbf{x}) \equiv X_0(t) + \delta X(t, \mathbf{x}) \quad . \quad (3.7)$$

The background dynamics will be analysed first; this will allow the definition of the various quantities that describe our system. The evolution of the perturbations, which

²The notation we introduced for the geometrical quantities of the \mathcal{N} -dimensional field-space (Γ_{bc}^a , \mathbb{R} , ...) is defined such as to avoid confusion with the corresponding geometrical quantities of the four-dimensional spacetime. The latter are the spacetime Christoffel symbols, $\Gamma_{\mu\nu}^\lambda$, Riemann tensor, $R_{\mu\nu\sigma}^\lambda$, Ricci tensor, $R_{\mu\nu}$, and Ricci scalar, R , as defined in Appendix A.1.

will then lead us to the subsequent study of PBH formation, will be discussed in §3.3. This separation also matches the chronological development of our numerical work.

We note that we will work here in terms of comoving time, t , for consistency with the literature; our code is nevertheless written in terms of the number of e -foldings, $N_e = \ln a$, for ease of numerical calculations. These are related through $\dot{X} = HX'$ for any time-dependent quantity X , where the prime notation indicates derivatives with respect to N_e . The principal results will therefore be presented in both fashions.

3.2 Background Dynamics

We analyse here the case in which all the perturbations are considered to be null, i.e. $\delta X = 0$ in Equation (3.7). We therefore study the dynamics of the background fields $\phi_0^a(t)$ in this Section.

The background metric in a flat FLRW universe is that of (2.23). The background Equations of Motion are derived from Equation (3.5) by noticing that the space derivatives of the homogeneous background fields all vanish, $\partial_i \phi_0^a = 0$. Using the property $\Gamma_{\mu\nu}^\mu = \partial_\nu \ln \sqrt{-g}$ of the Christoffel symbols [9, Equation (I.A.24)] to show that $\Gamma_{tt}^t = 3H$, we find the Klein–Gordon equation [63, §8.2]

$$\mathcal{D}_t \dot{\phi}_0^a + 3H \dot{\phi}_0^a + V^{,a} = 0 \quad . \quad (3.8)$$

The covariant spacetime derivative acting on a field-space vector was defined here as $\mathcal{D}_\mu A^a \equiv \partial_\mu A^a + \Gamma_{bc}^a \partial_\mu \phi_0^b A^c$, and the usual dot notation $\dot{\phi}_0^a \equiv \partial_t \phi_0^a$ was used for time derivatives. Since \mathcal{D}_μ is equal to the partial derivative ∂_μ when acting on a field-space scalar, this result clearly reduces to Equation (2.24) when only considering a single scalar field. Notice the use of the subscript t rather than 0 to indicate time derivatives, to avoid polluting the latter, already in use for the background quantities.

In terms of N_e , the background EoM read

$$\mathcal{D}_{N_e} \phi_0^{\prime a} + (3 - \epsilon) \phi_0^{\prime a} + \frac{1}{H^2} V^{,a} = 0 \quad , \quad (3.9)$$

where the substitution $\epsilon = -H'/H$ was used. As a shorthand, we will sometimes write the field derivatives as $\pi_0^a \equiv \phi_0^{\prime a}$.

Since the multi-field Energy-Momentum tensor (3.6) has no additional terms with respect to its single-field equivalent (2.21), the considerations of the previous Chapter still hold. The (00) Friedmann equation (2.6) takes the same form as in Equation (2.27), that is

$$H^2 = \frac{1}{3M_{\text{Pl}}^2} \left(\frac{1}{2} \dot{\phi}_0^2 + V(\phi) \right) \quad , \quad (3.10)$$

and similarly the second Friedmann equation (2.8) gives the variation of H ,

$$\dot{H} = -\frac{1}{2M_{\text{Pl}}^2} \dot{\phi}_0^2 \quad , \quad (3.11)$$

CHAPTER 3. MULTI-FIELD INFLATION

with $\dot{\phi}_0^2 \equiv \gamma_{ab} \dot{\phi}_0^a \dot{\phi}_0^b$. The latter can be used to rewrite the *first slow-roll parameter* ϵ from its definition (2.30) as

$$\epsilon = -\frac{\dot{H}}{H^2} = \frac{1}{2M_{\text{Pl}}^2} \frac{\dot{\phi}_0^2}{H^2} \quad , \quad (3.12)$$

which then allows to rewrite (3.10) as a function of ϵ and $V(\phi)$:

$$H^2 = \frac{1}{M_{\text{Pl}}^2} \frac{V(\phi)}{3 - \epsilon} \quad , \quad (3.13)$$

which is the form we used in our numerical calculations.

In terms of N_e , Equation (3.11) is trivially rewritten as

$$H' = -\frac{1}{2M_{\text{Pl}}^2} H \sigma^2 \quad , \quad (3.14)$$

where we defined the shorthand $\sigma^2 \equiv \dot{\phi}_0^2 = H^2 \dot{\phi}_0^2$. Writing $\epsilon = -H'/H = \sigma^2/2M_{\text{Pl}}^2$ as in (3.12) then leads to rewriting Equation (3.10) in terms of N_e as

$$H^2 = \frac{1}{M_{\text{Pl}}^2} \frac{V}{3 - \sigma} \quad . \quad (3.15)$$

These equations can be solved for a particular realisation of γ_{ab} and $V(\phi)$ to determine the trajectory $\phi_0^a(t)$ (or $\phi_0^a(N_e)$) of the background fields on the manifold \mathcal{M}_ϕ . This will be shown in Chapter 5 for the case of $\mathcal{N} = 2$ fields.

* * *

It is important to notice that in (3.10) and (3.11), the “field velocity” $\dot{\phi}_0^2 \equiv \gamma_{ab} \dot{\phi}_0^a \dot{\phi}_0^b$ is the (square of the) rate of change of ϕ_0 along the trajectory followed by the background fields, ϕ_0 being the fields’ vacuum expectation value [5]. The “field acceleration” $\mathcal{D}_t \dot{\phi}_0$ then represents the (covariant) rate of change of $\dot{\phi}_0$ with respect to the field-space manifold \mathcal{M}_ϕ , and will generally not point in the same direction as $\dot{\phi}_0$. This motivates the introduction of unit vectors parallel and perpendicular to the trajectory of the fields, respectively e_{\parallel}^a and e_{\perp}^a , which satisfy $e_{\parallel a} e_{\perp}^a = 0$. Their derivation through the Gram-Schmidt orthogonalisation process is carefully explained by Groot Nibbelink & van Tent [66,67], the main takeaway being that e_{\parallel}^a points in the direction of $\dot{\phi}_0^a$, while e_{\perp}^a is determined by the part of $\mathcal{D}_t \dot{\phi}_0^a$ normal to e_{\perp}^a . We can then write

$$e_{\parallel}^a \equiv \frac{\dot{\phi}_0^a}{\dot{\phi}_0} \quad , \quad (3.16)$$

$$\mathcal{D}_t e_{\parallel}^a \equiv -\Omega e_{\perp}^a \quad , \quad (3.17)$$

CHAPTER 3. MULTI-FIELD INFLATION

where Ω is an angular velocity which parametrises the rate of bending of the background trajectory [74]. Projecting Equation (3.17) along e_{\parallel}^a and e_{\perp}^a ,

$$\begin{aligned} \mathcal{D}_t e_{\parallel}^a &= \frac{1}{\dot{\phi}_0} \mathcal{D}_t \dot{\phi}_0^a - \frac{\dot{\phi}_0^a}{\dot{\phi}_0^2} \mathcal{D}_t \dot{\phi}_0 \\ &= -\frac{1}{\dot{\phi}_0} \left(3H \dot{\phi}_0^a + V^{,a} \right) - \frac{\ddot{\phi}_0}{\dot{\phi}_0} e_{\parallel}^a \\ &= -3H e_{\parallel}^a + \frac{1}{\dot{\phi}_0} \left(V_{\phi} e_{\parallel}^a + V_N e_{\perp}^a \right) - \frac{\ddot{\phi}_0}{\dot{\phi}_0} e_{\parallel}^a \ , \end{aligned}$$

where we substituted the EoM (3.8) in the second row, and have expanded $V^{,a} = V_{\phi} e_{\parallel}^a + V_N e_{\perp}^a$ in terms of its projections along the two orthogonal directions, $V_{\phi} \equiv e_{\parallel}^a V_{,a}$ and $V_N \equiv e_{\perp}^a V_{,a}$. One obtains

$$\ddot{\phi}_0 + 3H \dot{\phi}_0 + V_{\phi} = 0 \ , \quad (3.18)$$

$$\Omega = \frac{V_N}{\dot{\phi}_0} \ . \quad (3.19)$$

The first equation specifies the evolution of the background fields along their trajectory, while the second one completes Equation (3.17) by showing that Ω equals the slope of V_N in the direction perpendicular to the trajectory [74].

Note that the angle-formalism first introduced by Gordon *et al.* [72] and often found in the literature for two-field models (and expanded upon in [75], then used by Braglia *et al.* [6]) is a special limit of this basis. While this will not be used further, we briefly mention it here for completeness, as it provides a helpful visual representation; we temporarily ignore the field-space metric (set it to the identity matrix, $\gamma = \mathbf{1}_2$) for simplicity. The “path-length-elements” along- and orthogonal to the trajectory of two fields $\phi^1 = \varphi$ and $\phi^2 = \chi$ are given by

$$d\sigma = \cos \theta d\varphi + \sin \theta d\chi \ , \quad (3.20)$$

$$ds = -\sin \theta d\varphi + \cos \theta d\chi \ , \quad (3.21)$$

where in these authors’ formalism σ is the “adiabatic field” (not to be confused with our $\sigma = \phi_0^!$) and s is the “entropy field”, and

$$\begin{aligned} \cos \theta &= \frac{\dot{\varphi}}{\sqrt{\dot{\varphi}^2 + \dot{\chi}^2}} \ , \\ \sin \theta &= \frac{\dot{\chi}}{\sqrt{\dot{\varphi}^2 + \dot{\chi}^2}} \ . \end{aligned}$$

We refer the reader to [72, Figure 1] for a clear visualisation of this directional system.

* * *

Following the reasoning of Achúcarro *et al.* [5], we define the *second slow-roll parameter* vector as a generalisation of the single-field η of Equation (2.31):

$$\eta^a \equiv -\frac{\mathcal{D}_t \dot{\phi}_0^a}{H \dot{\phi}_0} \ . \quad (3.22)$$

CHAPTER 3. MULTI-FIELD INFLATION

This comes from the multi-field slow-roll vector $\tilde{\eta}^{(n)}$ introduced by Groot Nibbelink & van Tent [66,67], which in our notation reads

$$\tilde{\eta}^{a,(n)} \equiv \frac{\mathcal{D}_t^{n-1} \dot{\phi}_0^a}{H^{n-1} \dot{\phi}_0} , \quad (3.23)$$

and we identify $\eta^a = -\tilde{\eta}^{a,(2)}$. We will continue using the simpler notation of Achúcarro *et al.* for the remainder of this discussion, but refer the reader to References [66,67] for the generalisation of these parameters.

When projected along e_{\parallel}^a and e_{\perp}^a , the parameter η^a can be decomposed as

$$\eta^a = \eta_{\parallel} e_{\parallel}^a + \eta_{\perp} e_{\perp}^a ,$$

where, using again the EoM (3.8),

$$\eta_{\parallel} \equiv -\frac{\ddot{\phi}_0}{H \dot{\phi}_0} , \quad (3.24)$$

$$\eta_{\perp} \equiv \frac{V_N}{H \dot{\phi}_0} . \quad (3.25)$$

Notice that, by comparing Equations (3.19) and (3.25), the angular velocity of (3.17) becomes $\Omega = H \eta_{\perp}$: this hints at the fact that η_{\perp} is strictly related to the rate of change of e_{\parallel}^a , i.e. to the presence of curves in the trajectory of the background fields. As detailed in [5], this can be seen by introducing the radius of curvature, \mathbb{k} , of a trajectory of the fields on the field-space manifold \mathcal{M}_{ϕ} . Quoting only the results, this radius – which has units of mass – can be shown to satisfy

$$|\eta_{\perp}| = \frac{\dot{\phi}_0}{H} \frac{1}{\mathbb{k}} = \sqrt{2\epsilon} \frac{M_{\text{Pl}}}{\mathbb{k}} .$$

A geodesic on \mathcal{M}_{ϕ} would have no curvature, i.e. infinite radius of curvature or equivalently $\mathbb{k}^{-1} = 0$: such a curve therefore has $\eta_{\perp} = 0$. This parameter thus describes the bending of the trajectory of the system of fields with respect to a geodesic on the field-space manifold.

Closing this discussion, we point out that Peterson & Tegmark [73,76], in their geometric approach to the matter, use a parameter $\eta_{(\text{PT})}^a \equiv \mathcal{D}_{N_e} \phi_0^a$ that is related (but not equal) to our η^a of Equation (3.22). They then call the quantity $\eta_{(\text{PT})\perp} / \dot{\phi}_0$, which matches our η_{\perp} , the *turn rate*, since it determines how quickly the trajectory of the fields changes direction with respect to \mathcal{M}_{ϕ} .

In terms of N_e , the components of η^a read

$$\eta_{\parallel} = \frac{H' \sigma + H \sigma'}{H \sigma} , \quad (3.26)$$

$$\eta_{\perp} = \frac{V_N}{H^2 \sigma} . \quad (3.27)$$

We also define the η parameter used by Braglia *et al.* [6], which we introduced in Equation (2.31). It is slightly different from the above definitions while being closely related to η_{\parallel} ,

$$\eta_{(\text{B})} \equiv \frac{d \ln \epsilon}{d N_e} = \frac{\epsilon'}{\epsilon} = 2 \frac{\sigma'}{\sigma} = 2\epsilon - 2\eta_{\parallel} . \quad (3.28)$$

* * *

Lastly, we introduce here the *third slow-roll parameter* vector,

$$\xi^a = \frac{\mathcal{D}_t^2 \dot{\phi}_0^a}{H^2 \dot{\phi}_0} , \quad (3.29)$$

which was identified as $\xi^a = -\tilde{\eta}^{a,(3)}$ from Groot Nibbelink & van Tent's multi-field slow-roll vector of Equation (3.23) [66,67]. This parameter decomposes into ξ_{\parallel} and ξ_{\perp} just like η^a does:

$$\xi^a = \xi_{\parallel} e_{\parallel}^a + \xi_{\perp} e_{\perp}^a ,$$

its components being, following again the notation of Achúcarro *et al.* [5, Equations (2.28) and (4.13)],

$$\xi_{\parallel} \equiv -\frac{\ddot{\phi}_0}{H \ddot{\phi}_0} , \quad (3.30)$$

$$\xi_{\perp} \equiv -\frac{\dot{\eta}_{\perp}}{H \eta_{\perp}} , \quad (3.31)$$

or equivalently, in terms of N_e ,

$$\xi_{\parallel} \equiv -\frac{(H'^2 + HH'')\sigma + 3HH'\sigma' + H^2\sigma''}{HH'\sigma + H^2\sigma'} , \quad (3.32)$$

$$\xi_{\perp} \equiv -\frac{\eta'_{\perp}}{H \eta_{\perp}} . \quad (3.33)$$

The relation for ξ_{\perp} will be useful in the following Section.

Rewriting Equation (3.13) as follows, and substituting (3.24) in the relation (3.18), one finds

$$3 - \epsilon = \frac{V}{M_{\text{Pl}}^2 H^2} ,$$

$$3 - \eta_{\parallel} = -\frac{V_{\phi}}{H \dot{\phi}} .$$

Squaring the ratio of these equations, and substituting the definition of ϵ , Equation (3.12), we get

$$\epsilon = \frac{M_{\text{Pl}}^2}{2} \left(\frac{V_{\phi}}{V} \right)^2 \left(\frac{3 - \epsilon}{3 - \eta_{\parallel}} \right)^2 .$$

On the other hand, by differentiating the relation (3.18) with respect to time, dividing by $H^2 \dot{\phi}_0$, and identifying ϵ , η_{\parallel} , and ξ_{\parallel} as well as using (3.13), we see that

$$3(\epsilon + \eta_{\parallel}) = \eta_{\parallel} \eta_{\parallel} + M_{\text{Pl}}^2 \frac{\partial_{\phi} V_{\phi}}{V} (3 - \epsilon) .$$

Finally, in the regime where $\epsilon, \eta_{\parallel}, \xi_{\parallel} \ll 1$, we recover from the above relations the potential Slow-Roll parameters (2.33) and (2.34):

$$\begin{aligned}\epsilon &\approx \frac{M_{\text{Pl}}^2}{2} \frac{V_{\phi}^2}{V^2} = \epsilon_V \quad , \\ \epsilon + \eta_{\parallel} &\approx M_{\text{Pl}}^2 \frac{\partial_{\phi} V_{\phi}}{V} = \eta_V \quad .\end{aligned}$$

As a related side note, we mention that Peterson & Tegmark [73, 76] identify the condition for which the turn rate $\eta_{(\text{PT})\perp}/\phi'_0 \ll 1$ to be a *slow-turn* behaviour: in this regime, the trajectory of the fields curves slowly. These authors also show that the turn rate is related to the amount of multi-field behaviour. We will ourselves principally not be interested in the slow-turn behaviour, as we shall see that drastic turns in the field trajectory greatly enhance the scalar power spectrum – which we shall shortly introduce –, and could thus lead to significant production of Primordial Black Holes.

3.3 Cosmological Perturbation Theory

Having carefully analysed the dynamics of the background fields, and having introduced the $e_{\parallel}^a - e_{\perp}^a$ basis, we are now ready to tackle the second term of (3.7): the perturbations $\delta X(t, \mathbf{x})$ about the homogeneous background $X_0(t)$. In the semiclassical approximation, X_0 is a classical field, and the perturbations will be quantised. We consider the perturbations to be small, $\delta X \ll X_0$, thus only keeping first-order terms in the δ quantities.

With this approach, the matter fields (i.e. the scalar fields ϕ^a and the density and pressure) are written as

$$\begin{aligned}\phi^a &= \phi_0^a + \delta\phi^a \quad , \\ \rho &= \rho_0 + \delta\rho \quad , \\ p &= p_0 + \delta p \quad .\end{aligned}\tag{3.34}$$

Consequently, the Energy-Momentum tensor becomes (where we write the index 0 as a superscript for clarity)

$$T_{\mu\nu} = T_{\mu\nu}^0 + \delta T_{\mu\nu} \quad .$$

Through the Einstein field equations (2.4), we then understand that the Einstein tensor needs to be perturbed as well,

$$G_{\mu\nu} = G_{\mu\nu}^0 + \delta G_{\mu\nu} \quad ,$$

which leads us to realise that perturbations of the spacetime geometry – i.e. of the metric – must also be considered:

$$g_{\mu\nu} = g_{\mu\nu}^0 + \delta g_{\mu\nu} \quad .$$

We will mostly follow the treatment of Bassett *et al.* [68] in the following review.

3.3.1 Metric Perturbations

In its most generic form, the perturbed FLRW metric (2.1) can be written as [77]

$$\begin{aligned}
 ds^2 = & -(1 + 2A)dt^2 + 2a(B_{;i} - S_i) dx^i dt \\
 & + a^2 [(1 - 2\psi)\gamma_{ij} + 2E_{;ij} + 2(F_{i;j} + F_{j;i}) + h_{ij}] dx^i dx^j \quad , \quad (3.35)
 \end{aligned}$$

the semicolon $_{;i}$ indicating covariant derivatives with respect to the background metric γ_{ij} of constant-time hypersurfaces, which accounts for non-flat universes. In the $\kappa = 0$ case, which will be considered in the following discussion³, these reduce to partial derivatives $_{,i}$, and $\gamma_{ij} = \delta_{ij}$. The different perturbations are separated between scalars (A , ψ , B , and E)⁴, transverse three-vectors (S_i and F_i), and a transverse traceless symmetric three-tensor (h_{ij}) based on how they transform on spatial hypersurfaces. Notice there are exactly 10 perturbation components, matching the 10 degrees of freedom of $\delta g_{\mu\nu}$ [77].

The Scalar, Vector, and Tensor modes decouple to first order in the perturbations (SVT decomposition), and can thus be studied independently [64, 78]. Tensor perturbations lead to the production of gravitational waves – a fascinating and related subject which is nevertheless beyond the scope of this work – while vector perturbations vanish in a universe filled with only scalar fields, which we consider to be the case during inflation [68]. Scalar perturbations, on the other hand, show instabilities and could eventually seed (large-scale) structure formation [77]. We will therefore focus on these modes (i.e. set $S_i = F_i = H_{ij} = 0$ in Equation (3.35)).

The four scalar quantities A, B, ψ, E are functions of space and time coordinates, and the corresponding perturbations are constructed from their spatial derivatives and the background metric δ_{ij} (or γ_{ij} in the generic case) of constant time hypersurfaces. Using the spatial Laplacian $\nabla^2 = \delta^{ij}\partial_i\partial_j$, the corresponding Ricci (curvature) scalar can be found to be

$$\tilde{R} = \frac{4}{a^2} \nabla^2 \psi \quad .$$

This is the reason why ψ is called the *curvature perturbation*.

A generic gauge (or coordinate) transformation for the perturbed metric (3.35) is given by the temporal and spatial gauge parameters $\delta t, \delta x$,

$$\begin{aligned}
 t & \rightarrow t + \delta t \quad , \\
 x^i & \rightarrow x^i + \delta^{ij}\partial_j \delta x \quad . \quad (3.36)
 \end{aligned}$$

The perturbed metric tensor will transform accordingly, and the perturbations will satisfy [68]

$$\begin{aligned}
 A & \rightarrow A - \dot{\delta}t \quad , \\
 B & \rightarrow B + a^{-1}\delta t - a\dot{\delta}x \quad , \\
 \psi & \rightarrow \psi + H\delta t \quad , \\
 E & \rightarrow E - \delta x \quad .
 \end{aligned}$$

³This is to avoid considering the anisotropic stress, which vanishes in a spatially flat background such as our universe seems to be. Notice that this γ_{ij} has nothing to do with the field-space metric γ_{ab} .

⁴We call the perturbation of the lapse function A rather than ϕ as it is denoted in [77] to avoid confusion with the homonymous scalar field, as done in [68].

These are clearly not gauge-invariant quantities (they take different values for different choices of δt and δx). As explained in [77], one can take two approaches to calculating the perturbations. The first option is to work with a particular choice of gauge, such as the conformal Newtonian (or longitudinal) gauge $B = E = 0$, making sure that the derived quantities are gauge invariant [32, Sec. 7.3.1]. Alternatively, it is possible to *construct* gauge invariant variables, such as those first introduced by Bardeen [64], from the perturbations of the metric tensor. Both of these methods are possible because only two out of A, B, ψ, E correspond to physical scalar perturbations.

In particular, we notice that the combination $\dot{E} - B/a$ is independent of the spatial gauge. This motivates the choice of the gauge-invariant variables [79, 80]

$$\Phi \equiv A - \frac{d}{dt} \left[a^2 \left(\dot{E} - \frac{B}{a} \right) \right] , \quad (3.37)$$

$$\Psi \equiv \psi + a^2 H \left(\dot{E} - \frac{B}{a} \right) . \quad (3.38)$$

The physical interpretation of these quantities is evident in the Newtonian gauge, $B = E = 0$. The perturbed metric becomes

$$ds^2 = -(1 + 2\Psi)dt^2 + a^2 [(1 - 2\Psi)\delta_{ij}] dx^i dx^j ,$$

such that Φ and Ψ correspond to the metric perturbations [79]. These are in fact called longitudinal gauge metric perturbations (or Bardeen potentials [64]).

3.3.2 Matter Perturbations

The matter perturbations ($\delta\phi^a, \delta\rho, \delta p$) are not gauge-invariant either: under the transformation (3.36), they obey

$$\begin{aligned} \delta\phi^a &\rightarrow \delta\phi^a - \dot{\phi}_0^a \delta t , \\ \delta\rho &\rightarrow \delta\rho - \dot{\rho}_0 \delta t , \\ \delta p &\rightarrow \delta p - \dot{p}_0 \delta t . \end{aligned}$$

As a side note, in the single-field case a simple gauge-invariant variable can be defined for the scalar field as [79]

$$\delta\bar{\phi} \equiv \delta\phi + \frac{\dot{\phi}_0}{H} \psi .$$

For future reference, we introduce the adiabatic and non-adiabatic (or entropy) pressure perturbations,

$$\delta p_{\text{ad}} \equiv \frac{\dot{p}_0}{\rho_0} \delta\rho , \quad (3.39)$$

$$\delta p_{\text{nad}} \equiv \delta p - \frac{\dot{p}_0}{\rho_0} \delta\rho , \quad (3.40)$$

the latter being a gauge-invariant quantity. Another gauge-invariant quantity is the co-moving density perturbation

$$\delta\rho_{\text{m}} = \delta\rho - 3H\delta q , \quad (3.41)$$

with $\delta q = \partial_i \delta u^i$ the three-momentum potential (δu^i being the perturbation of the three-velocity), which satisfies

$$\delta q \rightarrow \delta q + (\rho_0 + p_0) \delta t \quad .$$

Finally, and most importantly, the curvature perturbation on uniform-density hypersurfaces and the comoving curvature perturbation are defined as

$$-\zeta \equiv \psi + \frac{H}{\dot{\rho}_0} \delta \rho \quad , \quad (3.42)$$

$$\mathcal{R} \equiv \psi - \frac{H}{\rho_0 + p_0} \delta q \quad , \quad (3.43)$$

such that these gauge-invariant variables are related through

$$-\zeta = \mathcal{R} + \frac{H}{\dot{\rho}_0} \delta \rho_m \quad .$$

3.3.3 Adiabatic and Entropy Perturbations

Before continuing with our discussion, a digression on the significance of the curvature and isocurvature perturbations is in order. In single-field inflation, perturbations can clearly only occur along the trajectory of the field, e_{\parallel}^a . They affect the total density (thus curvature) of different regions of the universe once inflation ends, keeping the number ratios of particle species (baryons, dark matter, photons, and neutrinos) spatially constant ($\delta(n_i/n_\gamma) = 0$). For this reason, these perturbations are called *adiabatic*, and are characterised by the comoving curvature perturbation \mathcal{R} of Equation (3.43), which is common to all cosmological fluids [53, 72]. \mathcal{R} can be recast in terms of the Bardeen potentials as

$$\mathcal{R} = \Psi - \frac{H}{\dot{H}} (\dot{\Psi} + H\Phi) \quad ,$$

such that its relation to the curvature density on uniform-density hypersurfaces ζ becomes (borrowing the result (3.49) from below)

$$-\zeta = \mathcal{R} + \frac{2\rho}{3(\rho + p)} \left(\frac{k}{aH} \right)^2 \Psi \quad .$$

The two curvature perturbations thus coincide in the large-scale limit $k \ll aH$

In multi-field inflation, we have additional perturbations which allow n_i/n_γ to vary, but leave the total energy density unperturbed [81]. These take the name of *entropy* or *isocurvature* perturbations, and are characterised by the automatically-gauge-invariant total entropy perturbation [72]

$$\mathcal{S} = H \left(\frac{\delta p}{\dot{p}_0} - \frac{\delta \rho}{\dot{\rho}_0} \right) \quad . \quad (3.44)$$

We expect $\mathcal{N} - 1$ entropy perturbation modes in addition to the adiabatic one, corresponding to the directions perpendicular to the trajectory of the fields, e_{\perp}^a . Entropy

perturbations are strongly dependent on the physics of reheating, that is, the conditions inflation ends with. In particular cases, such as too strong interaction between the particles to which the different fields decay, can cause the entropy perturbations to be short-lived; this increases the difficulty of their observation [66].

Curvature and isocurvature modes are orthogonal, so that any other perturbation can be described as a linear combination of these. Importantly, the two can be correlated and may in some contexts source one another, giving distinctive observational signatures.

3.3.4 Field Equations

The Einstein field equations (2.4) can be decomposed in background and perturbation parts,

$$\begin{aligned} G_{\mu\nu}^0 &= 8\pi G_{\text{N}} T_{\mu\nu}^0 \quad , \\ \delta G_{\mu\nu} &= 8\pi G_{\text{N}} \delta T_{\mu\nu} \quad . \end{aligned}$$

We thus have the linearised Einstein equations, as well as the linearised covariant conservation of the Energy-Momentum tensor,

$$\nabla_{\mu} \delta T_{\nu}^{\mu} = 0 \quad .$$

The derivation of the perfect fluid δT_{ν}^{μ} and of δG_{ν}^{μ} in the conformal Newtonian gauge can be found in [31, §II.2.3], while the gauge-invariant approach is taken in [32, §7.3].

The components of the perturbed Einstein tensor are derived in [82, Equation (D.7)] or equivalently in [77, Equations (4.6)–(4.8)]. The components of the perturbed EMt are instead calculated in [77, Equation (5.10)] for the perfect fluid approximation. Moving to Fourier space⁵, such that $\nabla^2 \phi = -k^2 \phi$, we can then write the (00), (0*i*), and (*i**j*) components of the linearised Einstein field equations (EFE) as

$$3H \left(\dot{\psi} + HA \right) + \frac{k^2}{a^2} \left[\psi + H \left(a^2 \dot{E} - aB \right) \right] = 4\pi G_{\text{N}} \delta \rho \quad , \quad (3.45)$$

$$\dot{\psi} + HA = -4\pi G_{\text{N}} \delta q \quad , \quad (3.46)$$

$$\ddot{\psi} + 3H\dot{\psi} + H\dot{A} + A \left(3H^2 + 2\dot{H} \right) = 4\pi G_{\text{N}} \delta p \quad , \quad (3.47)$$

$$\partial_i \left(\dot{E} - \frac{B}{a} \right) + 3H \left(\dot{E} - \frac{B}{a} \right) + \frac{\psi - A}{a^2} = 0 \quad . \quad (3.48)$$

The last two equations both come from the (*ij*) component, and we have ignored the anisotropic stress, which vanishes to linear order for \mathcal{N} scalar fields minimally coupled to gravity [72], which is our case. Equations (3.45)–(3.48) can be easily rewritten in terms of the Bardeen potentials Ψ and Φ from their definitions (3.38) and (3.37); from the last one, we will find that $\Psi = \Phi$. This means that there is only one dynamical degree of

⁵We decompose a perturbation ψ with respect to the complete set of eigenvectors of the Laplacian, such that the comoving wavenumber $k = 2\pi/\lambda$ indicates the eigenvalues corresponding to a mode of physical wavelength λ [68, 72].

freedom in the linearised EFE. Notice also that the first two of the above equations give the generalised Poisson equation, relating Ψ and the comoving density perturbation:

$$\frac{k^2}{a^2}\Psi = -4\pi G_N \delta\rho_m . \quad (3.49)$$

On the other hand, the conservation of the Energy-Momentum tensor gives

$$\dot{\delta\rho} + 3H(\delta\rho + \delta p) = \frac{k^2}{a^2}\delta q + (\rho_0 + p_0) \left[3\dot{\psi} + k^2 \left(\dot{E} + \frac{B}{a} \right) \right] , \quad (3.50)$$

$$\dot{\delta q} + 3H\delta q = -\delta p - (\rho_0 + p_0)A . \quad (3.51)$$

The first relation can be rewritten in terms of ζ of Equation (3.42), giving

$$\dot{\zeta} = -H \frac{\delta p_{\text{nad}}}{\rho_0 + p_0} - \Sigma , \quad (3.52)$$

where the scalar shear $\Sigma/H \propto (k^2/a^2 H^2)(\zeta + \Psi)$. This means that, for a finite Ψ , the curvature perturbation ζ remains constant for adiabatic perturbations on super-horizon scales, that is scales for which $k/aH \ll 1$. This is what was previously mentioned when talking of super-horizon modes being frozen.

3.3.5 Scalar Field Perturbations

The \mathcal{N} -field Equations of Motion (3.5) can be expanded by considering that $\phi^a = \phi_0^a + \delta\phi_0^a$ and simultaneously $g_{\mu\nu} = g_{\mu\nu}^0 + \delta g_{\mu\nu}$. Working in the $\psi = B = 0$ (flat) gauge and taking into account the linearised EFE (3.45) and (3.46), Nakamura & Stewart [83, Appendix B] determine the Fourier-space EoM for the perturbations $\delta\phi_k^a$ for the most general \mathcal{N} -field case. We report it here in coordinate space,

$$\mathcal{D}_t^2 \delta\phi^a + 3H\mathcal{D}_t \delta\phi^a + \mathbb{R}^a{}_{cbd} \dot{\phi}_0^c \dot{\phi}_0^d \delta\phi^b - \frac{\nabla^2}{a^2} \delta\phi^a + \delta\phi_b V^{;ab} = \frac{\delta\phi_b}{a^3} \mathcal{D}_t \left(\frac{a^3}{H} \dot{\phi}_0^a \dot{\phi}_0^b \right) . \quad (3.53)$$

This result is often quoted in the literature (see *e.g.* [5, 73, 84]) and reduces to the commonly-found equations of [68, 72] in the flat field-space case, $\gamma_{ab} = \mathbb{1}_{\mathcal{N}}$.

We now introduce another gauge-invariant combination, the field perturbations in the spatially-flat gauge $\psi = 0$. These take the name of Mukhanov–Sasaki (MS) variables [79, 80] and were found by comparing the perturbed metric (3.35) with the ADM (Arnowitt–Deser–Misner [85]) formalism:

$$Q^a \equiv \delta\phi^a + \frac{\dot{\phi}^a}{H} \psi . \quad (3.54)$$

These variables allow for the field perturbations to decouple from the metric perturbations [73]. Furthermore, in terms of the Mukhanov–Sasaki variables the comoving curvature perturbation (3.43) can be written as

$$\mathcal{R} = \gamma_{ab} \frac{\dot{\phi}_0^a}{\dot{\phi}_0^2} Q^b . \quad (3.55)$$

CHAPTER 3. MULTI-FIELD INFLATION

Substituting these variables in the EoM (3.53), Achúcarro *et al.* [5] rewrite it in terms of the basis vectors e_{\parallel}^a and e_{\perp}^a of the previous Section (see Equations (3.16) and (3.17)):

$$\mathcal{D}_t^2 Q^a + 3H\mathcal{D}_t Q^a - \frac{\nabla^2}{a^2} Q^a + C_b^a Q^b = 0 \quad , \quad (3.56)$$

with the tensor C_b^a , which satisfies the symmetry relation $C_{ab} = \gamma_{ac} C_b^c = C_{ba}$, being defined as

$$C_b^a \equiv \nabla_b V^{,a} - \dot{\phi}_0^2 \mathbb{R}^a_{\quad cbd} e_{\parallel}^c e_{\parallel}^d + 2\epsilon \frac{H}{\dot{\phi}_0} \left(e_{\parallel}^a V_{,b} + e_{\parallel,b} V^{,a} \right) + 2\epsilon (3 - \epsilon) H^2 e_{\parallel}^a e_{\parallel,b} \quad .$$

Following the steps of these authors (see [5, §3] for a more detailed discussion), we recast the Mukhanov–Sasaki variables in a local orthogonal frame that is parallel-transported along the background inflationary trajectory $\phi_0^a(t)$ [83]. By introducing a complete set of vielbeins $e_a^I(t)$, where the new I index indicates this local frame while the a index is that of the field-space manifold M_{ϕ} , we define $Q^I(t, \mathbf{x}) \equiv e_a^I(t) Q^a(t, \mathbf{x})$. Considering the properties of the vielbeins and introducing the antisymmetric matrix $Y_J^I = e_a^I \mathcal{D}_t e_J^a$, a new covariant derivative acting on the I indices is introduced, such that

$$\mathcal{D}_t Q^I \equiv \dot{Q}^I + Y_J^I Q^J \quad . \quad (3.57)$$

This allows to rewrite the perturbations' EoM (3.56), with $C^I_J = e_{Ia} e_J^b C_b^a$, as

$$\mathcal{D}_t^2 Q^I + 3H\mathcal{D}_t Q^I - \frac{\nabla^2}{a^2} Q^I + C^I_J Q^J = 0 \quad . \quad (3.58)$$

Finally, we rescale the MS variables by introducing a new set of perturbations $v^I \equiv aQ^I$, and rewrite the EoM in terms of conformal time ($d\tau = dt/a$, as defined in Equation (2.2)), such that $\mathcal{D}_\tau = a\mathcal{D}_t$. By defining the symmetric mass matrix as $\Omega_{IJ} = -a^2 H^2 (2 - \epsilon) \delta_{IJ} + a^2 C_{IJ}$, Equation (3.58) becomes

$$\mathcal{D}_\tau^2 v^I - \nabla^2 v^I + \Omega^I_J v^J = 0 \quad . \quad (3.59)$$

In Fourier space, this reads

$$\mathcal{D}_\tau^2 v_k^I + k^2 v_k^I + \Omega^I_J v_k^J = 0 \quad , \quad (3.60)$$

i.e. a generalised Mukhanov–Sasaki equation [79, 80], which can now be quantised. In fact, the Fourier space solution of the MS equation allows for the calculation of the power spectrum of the curvature perturbations \mathcal{R} [84]. Before moving on, we mention the considerations of [83], who reach a similar MS equation with a variable corresponding to our v^I . It is shown there that in the limit of small-scale perturbations ($-k\tau \rightarrow \infty$, such that the effective mass term in (3.60) vanishes with respect to the k^2 term), the v^I behave like real massless Klein–Gordon fields. On the other hand, it can be seen that perturbations become classical on super-horizon scales ($-k\tau \rightarrow 0$).

We also point out that the EoM (3.59) can be directly derived from the \mathcal{N} -field action (3.1) by performing the substitutions illustrated above. This would lead to the action

$$S = \frac{1}{2} \int d\tau d^3 \mathbf{x} \left[\sum_I (\mathcal{D}_\tau v^I)^2 - \sum_I (\nabla v^I)^2 - \Omega_{IJ} v^I v^J \right] \quad ,$$

which is a generalisation of the action considered in the original paper deriving the MS equations [79].

3.3.6 Quantising the Perturbations

The system is quantised by demanding the standard equal-time canonical commutation relations⁶ between the fields v^I and their associated momenta, $\Pi^I \equiv \mathcal{D}_\tau v^I$:

$$\left[v^I(\tau, \mathbf{x}), \Pi^J(\tau, \mathbf{y}) \right] = \delta^{IJ} \delta^3(\mathbf{x} - \mathbf{y}) . \quad (3.61)$$

The v^I fields can then be written in terms of \mathcal{N} linearly-independent creation and annihilation operators $a_\alpha^\dagger(\mathbf{k})$ and $a_\alpha(\mathbf{k})$ ($\alpha = 1, \dots, \mathcal{N}$), where the α label indicates scalar quantum modes (one for each field), and *not* directions in field space (various α modes can contribute to the same perturbation along some direction I^7), by considering the Fourier decomposition

$$\begin{aligned} v^i(\tau, \mathbf{x}) &= \int \frac{d^3\mathbf{k}}{(2\pi)^{3/2}} e^{i\mathbf{k}\cdot\mathbf{x}} v^I(\mathbf{k}, \tau) \\ &= \int \frac{d^3\mathbf{k}}{(2\pi)^{3/2}} e^{i\mathbf{k}\cdot\mathbf{x}} \sum_\alpha \left[v_\alpha^I(k, \tau) a_\alpha(\mathbf{k}) + v_\alpha^{I*}(k, \tau) a_\alpha^\dagger(-\mathbf{k}) \right] . \end{aligned} \quad (3.62)$$

The creation and annihilation operators naturally need to satisfy the commutation relations

$$\left[a_\alpha(\mathbf{k}), a_\beta^\dagger(\mathbf{q}) \right] = \delta_{\alpha\beta} \delta^{(3)}(\mathbf{k} - \mathbf{q}) , \quad (3.63)$$

with the other commutators vanishing, such that they define a (non-unique) vacuum state $a_\alpha(\mathbf{k})|0\rangle = 0$. The mode functions then need to satisfy the previously anticipated generalised Mukhanov–Sasaki equation,

$$\mathcal{D}_\tau^2 v_\alpha^I(k, \tau) + k^2 v_\alpha^I(k, \tau) + \Omega_{IJ}^I v_\alpha^J(k, \tau) = 0 . \quad (3.64)$$

The last step is to impose the initial conditions for the system. Inflation exhibits the limit $a \rightarrow 0$ as $\tau \rightarrow -\infty$ (i.e. at the start of inflation), in which case the mass matrix is subleading, $\Omega_{IJ} \rightarrow 0$ in (3.60), and the EoM reduce to

$$\left(\mathcal{D}_\tau^2 + k^2 \right) v_\alpha^I(k, \tau) = 0 ,$$

where no α -mode mixing occurs. On these grounds, we choose the Bunch–Davies vacuum as an initial condition, imposing the (Minkowski) initial conditions,

$$v_\alpha^I(k, \tau) = \delta_\alpha^I \frac{1}{\sqrt{2k}} e^{-ik\tau} , \quad (3.65)$$

to our Mukhanov–Sasaki equations. Equation (3.65) is a solution to (3.64) that indeed satisfies the commutation relations (3.61). Furthermore, a condition on the momentum is also imposed by taking the \mathcal{D}_τ derivative of (3.65):

$$\Pi_\alpha^I(k, \tau) = -i\delta_\alpha^I \sqrt{\frac{k}{2}} e^{-ik\tau} + a\delta_\alpha^I Y_J^I \frac{1}{\sqrt{2k}} e^{-ik\tau} . \quad (3.66)$$

This will be necessary for our numerical considerations. The Bunch–Davies initial conditions (3.65)–(3.66) are imposed at early times, before perturbations exit the horizon.

⁶We point out that, as discussed in [5], this quantisation prescription is justified by considering a transformation to an alternative set of canonical fields, u^I .

⁷While α runs over field labels (1, 2, ...), I could be the direction of the inflation trajectory, or one of those perpendicular to it.

3.3.7 Power Spectra and Observables

The (physical) power spectrum is the Fourier transform of the two-point correlation function:

$$\langle 0|v^I(\mathbf{k}, \tau)v^{J*}(\mathbf{q}, \tau)|0\rangle \equiv \delta^{(3)}(\mathbf{k} - \mathbf{q}) \frac{2\pi^2}{k^3} \mathcal{P}_v^{IJ}(k, \tau) .$$

Therefore, in terms of the mode functions, \mathcal{P}_v^{IJ} becomes

$$\mathcal{P}_v^{IJ}(k, \tau) = \frac{k^3}{2\pi^2} \sum_{\alpha} v_{\alpha}^I(\tau, k)v_{\alpha}^{J*}(k, \tau) .$$

The spectrum in terms of the $Q^I = v^I/a$ variables is instead given by

$$\mathcal{P}_Q^{IJ}(k, \tau) = \frac{k^3}{2\pi^2} \sum_{\alpha} Q_{\alpha}^I(\tau, k)Q_{\alpha}^{J*}(k, \tau) = \frac{1}{a^2} \mathcal{P}_v^{IJ}(k, \tau) . \quad (3.67)$$

The single-field curvature power spectrum is also introduced, following the reasoning of [65, §2.4], as it will be useful for comparison with our results. The two-point correlation function in that case similarly gives us that

$$\langle 0|v(\mathbf{k}, \tau)v^*(\mathbf{q}, \tau)|0\rangle = |v_k|^2 \delta(\mathbf{k} + \mathbf{q}) \equiv \delta(\mathbf{k} - \mathbf{q}) \frac{2\pi^2}{k^3} \mathcal{P}_v^{\text{1-field}}(k, \tau) ,$$

and it can be found from the decomposition considerations that on super-horizon scales,

$$|v_k|^2 = \frac{1}{2k^3} \frac{1}{\tau} = \frac{a^2 H^2}{2k^3} .$$

Looking back at (3.55), and remembering that $v = aQ$, we find that $\mathcal{R} = \frac{H}{\phi_{0a}}v$ and therefore

$$\begin{aligned} \mathcal{P}_{\mathcal{R}}^{\text{1-field}} &= \frac{H^2}{a^2 \dot{\phi}_0^2} \mathcal{P}_v^{\text{1-field}} \\ &= \frac{1}{2a^2 \epsilon} \frac{k^3}{2\pi^2} |v_k|^2 \\ &= \frac{H^2}{8\pi^2 \epsilon} \Big|_{k=aH} , \end{aligned} \quad (3.68)$$

where we evaluate the right-hand side at horizon crossing, since \mathcal{R} is frozen on super-horizon scales.

* * *

Since H and ϵ are time-dependent, the power spectrum $\mathcal{P}_{\mathcal{R}}(k)$ is not scale invariant. Nevertheless, as these quantities vary slowly with time, the departure from perfect scale invariance is small; it is described by the *spectral index*, defined as

$$n_s - 1 \equiv \frac{d\mathcal{P}_{\mathcal{R}}(k)}{d \ln k} \Big|_{k=aH} . \quad (3.69)$$

This is also valid in the multi-field case.

The spectral index is related to the curvature power spectrum by observational constraints [19]: at the reference (pivot) scale $a_0 H_0 \equiv k_* = 0.005 \text{ Mpc}^{-1}$, the power spectrum is normalised to a value $A_s = 2.1 \times 10^{-9}$, such that

$$\mathcal{P}_{\mathcal{R}}(k) = A_s \left(\frac{k}{k_*} \right)^{n_s - 1} .$$

The latest observations (*Planck* 2018 TT,TE,EE+lowE+lensing+BAO) constrain $n_s = 0.9665 \pm 0.0038$ [19, Table 2]. Further related measured quantities are the *running* and the *running of the running* of the scalar index,

$$\begin{aligned} \frac{dn_s}{d \ln k} &= -0.0041 \pm 0.0067 \quad , \\ \frac{d^2 n_s}{d \ln k^2} &= 0.009 \pm 0.012, \end{aligned}$$

respectively.

* * *

Although this is beyond the present scope, we mention another important topic that is related to our discussion. In this Section's considerations, we only worked to linear order in the perturbations, and looked solely at the two-point function at the beginning of 3.3.7; arbitrary higher-order perturbation theory is quite involved, but some results may be obtained, notably the three-point correlation function. This approach leads to calculating the bispectrum of perturbations, which describes the departure from the Gaussian distribution of perturbations. This non-Gaussianity (NG) is characterised by a model-dependent *non-linearity* parameter, f_{NL} , and is a powerful test of inflation. Without dwelling deeper into the subject, which can be found in *e.g.* [86, 87], we mention that significant NG could be an important indicator of multi-field inflation. So far, this is not ruled out by observations, although no significant evidence of NG was found [88]; see also the recent review by Acúcarro *et al.* [89].

Finally, Gravitational Waves (GWs) are produced during inflation both directly, by fluctuations of the perturbed spacetime metric (*primordial* GWs, i.e. the tensor modes of (3.35)), and by PBHs, which induce the Stochastic Gravitational Wave Background (the Energy-Momentum tensor of scalar perturbations behaves like a source term when computing the GW Equations of Motion). These GWs could be observed by current and upcoming experiments, and provide important insight into inflationary physics. This topic is discussed *e.g.* in [90], and by Braglia *et al.* [6] in the context of the model we will consider in §5.4.

Chapter 4

Primordial Black Holes

Having studied the framework of \mathcal{N} -field inflation in some detail, acquiring familiarity with the theory of cosmological perturbations, we are now interested in determining how inflation models could lead to a production of Primordial Black Holes (PBHs). If an overdensity in the early Universe is large enough, it may in fact collapse to form a PBH when it re-enters the Hubble radius during the radiation dominated era. The main reason we are interested in this study is that these objects could account for a significant fraction of the Dark Matter component of the universe. We begin by explaining how PBHs are formed and how they may account for Dark Matter, then review the current theoretical and observational constraints on their abundance.

4.1 PBH Formation

The theory of General Relativity predicts that Black Holes form when a mass M is contained within the Schwarzschild radius $R_S = 2G_N M$. This is true for BHs of order a few solar masses (which we denote by M_\odot) that form at the end of the life cycle of massive stars, but can also happen in the early universe. In the latter case, we talk of *Primordial* Black Holes [50]. Contrarily to late-universe BHs, which require masses of order M_\odot to be able to form, these can be as small as $10^{-18} M_\odot$, the lower limit being set by BH evaporation as shown by Hawking [91].

While different approaches have been taken to explaining how PBHs are generated (see [51] for a discussion), we will follow the most natural one in the context of inflation, i.e. that they form from primordial inhomogeneities. The curvature perturbations introduced in the previous Chapter re-enter the horizon¹ during the radiation-dominated era after having been frozen super-horizon: see the grey line in Figure 2.3 on page 19. If their mass is larger than the Jeans mass, $M_J \sim \rho/k^3$ [31, §II.1.1], they undergo gravitational collapse. That is, a whole Hubble region (of physical radius H^{-1}) collapses. Naturally,

¹As a reminder, by “horizon” we are talking of the comoving Hubble radius, $(aH)^{-1}$.

CHAPTER 4. PRIMORDIAL BLACK HOLES

not all fluctuations will form PBHs; the collapse fraction for a region of mass M is given by the initial abundance (i.e. that at the time of horizon re-entry or PBH formation, denoted by the subscript f from here onwards),

$$\beta_f(M) \equiv \left. \frac{\rho_{\text{PBH}}(M)}{\rho_{\text{tot}}} \right|_f, \quad (4.1)$$

which is calculated as follows.

Consider the comoving density contrast of perturbations, that is, the fractional overdensity $\delta\rho$ with respect to the average density ρ of the universe: $\delta \equiv \delta\rho/\rho$. PBHs will form if δ_f at horizon re-entry is larger than a critical value δ_c , which was found to be $\delta_c = 0.45$ [92, 93]². PBHs will have a mass comparable to the horizon mass at that time [49, 51],

$$M_f = \frac{4}{3}\pi \left(\frac{1}{H}\right)^3 \rho_{\text{tot}} \Big|_f = \frac{1}{2G_N H_f} \sim \frac{t_f}{G_N} \sim 5 \times 10^5 \frac{t_f}{\text{s}} M_\odot, \quad (4.2)$$

where in the first equality we consider H_f^{-1} to be the (physical) Hubble radius at re-entry, and in the third one we take it to be the corresponding Hubble time. In the second equality, we used $\rho_{\text{tot}} = \rho_{\text{crit}}\Omega$ with $\Omega = 1$ (see Equation (2.11) on page 12). The PBH mass is defined as

$$M_{\text{PBH}} \equiv \gamma M_f,$$

where $0 \leq \gamma \leq 1$ is a correction factor described in References [94] which accounts for the efficiency of collapse, and is sometimes assumed to correspond to unity³. Equation (4.2) also shows that the earlier in radiation-domination the PBHs form, the smaller their mass will be.

Using the Press–Schechter formalism [95], Carr [96] first calculated the fraction of the universe’s total energy density that is contained within regions where $\delta > \delta_c$, i.e. that can sustain PBH formation:

$$\beta_f(M) = 2 \int_{\delta_c}^{\infty} \frac{M_{\text{PBH}}}{M} P(\delta(R)) d\delta(R).$$

Here the factor two is a bookkeeping that accounts for locally underdense regions collapsing into globally overdense ones [97], and $\delta(R)$ is the smoothed (over a comoving scale R) density contrast at horizon re-entry, which we assume to be Gaussian with a mass variance $\sigma(R)$:

$$P(\delta(R)) = \frac{1}{\sqrt{2\pi}\sigma(R)} e^{-\delta^2(R)/2\sigma^2(R)}.$$

Assuming also that all PBHs form contemporarily, such that M is the same, and they all have a common dependency on M (i.e. γ), we find that the mass function of PBHs is

²An approximate but immediate result is given by considering $\delta_c = c_s^2$ where $c_s = 1/\sqrt{3}$ is the speed of sound for the radiation-dominated epoch.

³Other authors, such as Braglia *et al.* [7], consider the efficiency factor to be $\gamma = 0.2$.

monochromatic. Therefore,

$$\begin{aligned}\beta_f(M) &= \sqrt{\frac{2}{\pi}} \frac{\gamma}{\sigma(R)} \int_{\delta_c}^{\infty} e^{-\delta^2(R)/2\sigma^2(R)} d\delta(R) \\ &= \gamma \operatorname{Erfc} \left(\frac{\delta_c}{\sqrt{2}\sigma(R)} \right) \ ,\end{aligned}\tag{4.3}$$

where we introduced the complementary error function from its definition (and rescaled our variable). The variance is given by [94]

$$\sigma^2(R) = \frac{16}{81} \int_0^{\infty} (kR)^4 \widetilde{W}^2(kR) \mathcal{P}_{\mathcal{R}}(k) T^2(kR/\sqrt{3}) \frac{dk}{k} \ ,$$

with the Fourier transform of the window function, $\widetilde{W}(kR)$, being usually taken to be a top-hat or Gaussian function⁴, and the transfer function,

$$T(y) = 3 \frac{\sin y - y \cos y}{y^3} \ ,$$

modelling the sub-horizon evolution of fluctuations [94].

For a Gaussian distribution of curvature perturbations on horizon scales, as considered here⁵, Motohashi & Hu [97] compare the result (4.3) to the analogous probability of finding perturbations above a threshold \mathcal{R}_c :

$$\begin{aligned}\beta_f(M) &= 2 \int_{\mathcal{R}_c}^{\infty} \frac{1}{\sqrt{2\pi}\Delta_{\mathcal{R}}} e^{-\mathcal{R}^2/2\Delta_{\mathcal{R}}^2} d\mathcal{R} \\ &= \operatorname{Erfc} \left(\frac{\mathcal{R}_c}{\sqrt{2}\Delta_{\mathcal{R}}} \right) \\ &\approx \frac{1}{\sqrt{2\pi}} \frac{\Delta_{\mathcal{R}}}{\mathcal{R}_c} e^{-\mathcal{R}_c^2/2\Delta_{\mathcal{R}}^2} \ ,\end{aligned}\tag{4.4}$$

where $\Delta_{\mathcal{R}}(k)^2 \equiv \mathcal{P}_{\mathcal{R}}(k)$. The last approximation comes from assuming $\mathcal{R}_c \gg \Delta_{\mathcal{R}}$, i.e. that PBH formation is due to rare peaks in the spectrum. This allows to directly relate $\beta_f(M)$ to the curvature power spectrum. Assuming a near-scale invariant $\mathcal{P}_{\mathcal{R}}$ around the time of horizon re-entry, the density contrast and curvature thresholds can be related by [99, 100]

$$\mathcal{R}_c = \frac{9}{4} \delta_c \ .\tag{4.5}$$

Notice from Equation (4.4) that, in order for $\beta(M)$ to be significant, we need $\mathcal{P}_{\mathcal{R}}$ to be much greater than its CMB normalisation $A_s \approx 2.1 \times 10^{-9}$ at $k_* = 0.05 \text{ Mpc}^{-1}$ (see §3.3.7). We will soon come back to this observation.

⁴The value of $\sigma(R)$, and thus of $\beta_f(M)$, strongly depends on the choice of the window function: a study of its consequences can be found in [98].

⁵As explained in [51, §2.12], the abundance of Primordial Black Holes strongly depends on the departure from Gaussianity of the perturbations' density profile. This is because PBHs are generated by extreme-density perturbations, which populate the tail of the distribution.

4.2 PBHs as Dark Matter

Since PBHs form during radiation-domination, by considering the Friedmann equation (2.11) one sees that the Hubble parameter at that time evolves as [101]

$$H_f^2 = H_0^2 \frac{\Omega_{r,0}}{a_f^4} \left(\frac{g_{*f}}{g_{*0}} \right)^{-\frac{1}{3}}, \quad (4.6)$$

where the g_* indicate the number of relativistic degrees of freedom at formation and present time. Substituting this in Equation (4.2), we find the PBH mass in terms of the horizon crossing time (or rather, a):

$$M_{\text{PBH}} = 4\pi\gamma \frac{a_f^2}{H_0 \sqrt{\Omega_{r,0}}} \left(\frac{g_{*f}}{g_{*0}} \right)^{\frac{1}{6}} M_{\text{Pl}}. \quad (4.7)$$

PBHs will behave as matter, and their density will therefore evolve as $\rho_{\text{PBH}}(M) \propto a^{-3}$; noticing that ρ_{PBH} depends on the PBH mass, we define their density parameter as (where as usual the lack of subscript refers to a general time t)

$$\Omega_{\text{PBH}}(M) = \frac{\rho_{\text{PBH}}(M)}{\rho_{\text{crit}}} = \frac{\Omega_{\text{PBH},0}(M)}{a^3}. \quad (4.8)$$

The PBH energy density fraction at formation can then be related to the present one by [101]

$$\beta_f(M) = \frac{\Omega_{\text{PBH},0}(M)}{a_f^3} \left(\frac{H_0}{H_f} \right)^2.$$

Introducing the fraction of PBHs against (Cold) Dark Matter (CDM) – i.e. the fraction of CDM that is composed by PBHs – for a given mass M ,

$$f_{\text{PBH}}(M) \equiv \frac{\Omega_{\text{PBH}}(M)}{\Omega_{\text{CDM}}}, \quad (4.9)$$

where $\Omega_{\text{CDM}} = \Omega_{\text{CDM},0} a^{-3}$ is the Dark Matter density parameter⁶, we can rewrite the above expression as

$$\beta_f(M) = \frac{\Omega_{\text{CDM},0}}{a_f^3} \left(\frac{H_0}{H_f} \right)^2 f_{\text{PBH},0}(M).$$

Substituting H_0/H_f from Equation (4.6) and the resulting a_f from Equation (4.7), we find

$$\begin{aligned} \beta_f(M) &= \frac{1}{\sqrt{\gamma}} \frac{\Omega_{\text{CDM},0} H_0^{1/2}}{\sqrt{4\pi\Omega_{r,0}^{3/4}}} \left(\frac{g_{*f}}{g_{*0}} \right)^{\frac{1}{4}} \sqrt{\frac{M_{\text{PBH}}}{M_{\text{Pl}}}} f_{\text{PBH},0}(M) \\ &\approx \frac{4}{\sqrt{\gamma}} \times 10^{-9} \left(\frac{g_{*f}}{g_{*0}} \right)^{\frac{1}{4}} \sqrt{\frac{M_{\text{PBH}}}{M_{\odot}}} f_{\text{PBH},0}(M), \end{aligned} \quad (4.10)$$

where $M = M_{\text{PBH}}$ is the mass of the PBHs. See also the enlightening alternative derivation of this result by Motohashi & Hu [97].

⁶ $\Omega_{\text{CDM},0} \approx 0.26$ as given in Table 2.2 on page 16

* * *

We can now equate the result (4.10) to $\beta_f(M)$ of Equation (4.4): this will allow us to determine the necessary enhancement of the curvature power spectrum $\mathcal{P}_{\mathcal{R}}$ that an inflationary model must predict in order to allow for mass- M PBHs to account for a fraction $f_{\text{PBH},0}(M)$ of the total Dark Matter content of today's universe. In particular, setting $f_{\text{PBH},0}(M) = 1$ gives the condition that all of the universe's Dark Matter be in the form of PBHs (of a single mass M).

We set the collapse efficiency factor $\gamma = 1$ and consider only the relativistic degrees of freedom of the Standard Model of particle physics, such that $g_{*0} = 3.36$ and $g_{*f} = 106.75$ [101]. Setting also $\mathcal{R}_c = 1$ in Equation (4.4) by considering Equation (4.5) with $\delta_c = 0.45$, we get for $f_{\text{PBH},0}(M) = 1$ that

$$\Delta_{\mathcal{R}} e^{-1/2\Delta_{\mathcal{R}}^2} \approx \sqrt{2\pi} 10^{-8} \sqrt{\frac{M}{M_{\odot}}} . \quad (4.11)$$

As an example, for a PBH mass $M = 10^{-15} M_{\odot}$ we find that $\Delta_{\mathcal{R}} \approx 0.12$, in agreement with [101], and therefore $\mathcal{P}_{\mathcal{R}} \sim 10^{-2}$, which is approximately 10^7 times larger than the normalised spectrum $A_s \sim 10^{-9}$. In other words, in order to have all of DM be made of PBHs of mass $10^{-15} M_{\odot}$, we need an inflationary model that produces a local enhancement of $\mathcal{P}_{\mathcal{R}}$ by $\mathcal{O}(10^7)$. We point out that choosing a lower γ slightly increases the required $\mathcal{P}_{\mathcal{R}}$, while using a lower \mathcal{R}_c greatly decreases it (using $\mathcal{R}_c = 0.1$, we find that $\Delta_{\mathcal{R}}$ decreases by an order of magnitude, meaning the required power spectrum enhancement would now “only” need to be $\mathcal{O}(10^5)$).

While in our discussion we have considered a mass function tightly peaked around $M = M_{\text{PBH}}$, that is generally not the case, and contributions from various masses should be considered. This is explained in detail *e.g.* by Sasaki *et al.* [102]. The total fraction of PBHs against CDM is then given by

$$f_{\text{PBH}}^{\text{tot}} \equiv \frac{\Omega_{\text{PBH}}}{\Omega_{\text{CDM}}} = \int df_{\text{PBH}}(M) = \int \frac{df_{\text{PBH}}(M)}{d \ln M} d \ln M ,$$

where $df_{\text{PBH}}(M)$ is the fraction of PBH with masses $M \leq M_{\text{PBH}} \leq M + d \ln M$, and

$$\frac{df_{\text{PBH}}(M)}{d \ln M} = \nu(M)^2 \left| \frac{d \ln \nu(M)}{d \ln M} \right| f_{\text{PBH}}(M) ,$$

$f_{\text{PBH}}(M)$ being given by Equation (4.10) and $\nu(M) = \mathcal{R}/\Delta_{\mathcal{R}}$.

* * *

Another important quantity is the number of inflationary e -foldings over which the enhancement takes place, ΔN_e . Looking back at Figure 2.3 on page 19, it is evident that the aH values when a perturbation exits and re-enters the horizon are equal (the mode has a constant k). Considering H to be constant at a value H_i during inflation, we get for the CMB modes⁷ that $a_{\text{CMB}} H_i = a_0 H_0 \equiv k_*$, while for the PBH perturbations

⁷The modes that re-enter the horizon at present time are called CMB modes because that is the largest-scale fluctuation we can currently observe; they are not produced (neither exit/re-enter the horizon) at the time of CMB production.

$a_{\text{exit}}H_i = a_f H_f$. Manipulating this with the previous results, we find an upper bound for ΔN_e by calculating the number of e -folds between CMB scales and those of PBH production [97, 101]:

$$\begin{aligned} N_e^{\text{PBH}} &\equiv \ln\left(\frac{a_{\text{exit}}}{a_{\text{CMB}}}\right) = \ln\left(\frac{a_f H_f}{k_*}\right) \\ &= 18.4 - \frac{1}{12} \ln\left(\frac{g_{*f}}{g_{*0}}\right) + \frac{1}{2} \ln \gamma - \frac{1}{2} \ln\left(\frac{M}{M_\odot}\right) . \end{aligned} \quad (4.12)$$

This is such that $\Delta N_e \leq N_e^{\text{PBH}}$.

To find the maximum value that N_e^{PBH} can take, Motohashi & Hu [97] make the following considerations regarding PBH evaporation. As first discovered by Hawking [91], Black Holes radiate thermally and eventually evaporate⁸ over a timescale

$$t_{\text{ev}} = \frac{5120\pi G_{\text{N}}^2 M^3}{\hbar c^4} = 6.6 \times 10^{74} \left(\frac{M}{M_\odot}\right)^3 \text{ s} .$$

The smallest PBHs that can contribute to Dark Matter will be those that survive until the time of matter-radiation equality, which can be found from Equation (4.6). Finally, the minimum mass that a PBH needs to have is found to be [97]

$$M_{\text{min}} = 1.5 \times 10^{-21} \left(\frac{\Omega_{\text{m},0} h^2}{0.14}\right)^{-2/3} M_\odot ,$$

which, for the value of $\Omega_{\text{m},0}$ given in Table 2.2⁹ and those for g_* mentioned above, gives a maximum value for N_e^{PBH} being

$$N_e^{\text{PBH,max}} = 42 + \frac{1}{2} \ln \gamma .$$

What we have just calculated is actually the first of the constraints that are set on PBH masses and abundance, the discussion of which will be the topic of the next Section.

4.3 Constraints

There exist a number of theoretical and observational constraints on the possible abundance of PBHs for determined mass ranges. These are constantly updated, and some disagreement on a few constraints exists in the literature. Following the recent reviews by Carr & Kühnel [51, 103], Carr *et al.* (CKSY) [104], and Inomata *et al.* [105], we briefly introduce some of the most stringent bounds, which are shown in Figure 4.1.

The current bounds leave a few mass windows of interest, for which PBHs could account for a significant fraction of Dark Matter. For our considerations, as can be seen from Figure 4.1, these are around $M \sim 10^{-15} M_\odot$, $M \sim 10^{-12} M_\odot$, and to some extent around $M \sim 10^{-6} M_\odot$.

⁸The quantum properties of BHs make it so that they emit radiation with a temperature proportional to the BH's surface gravity. This emission decreases the BH's mass, thus increasing its surface gravity and reinforcing the thermal radiation. Eventually, BHs will therefore evaporate [91].

⁹Although Motohashi & Hu [97] refer to values that have since been refined, the result is not varied.

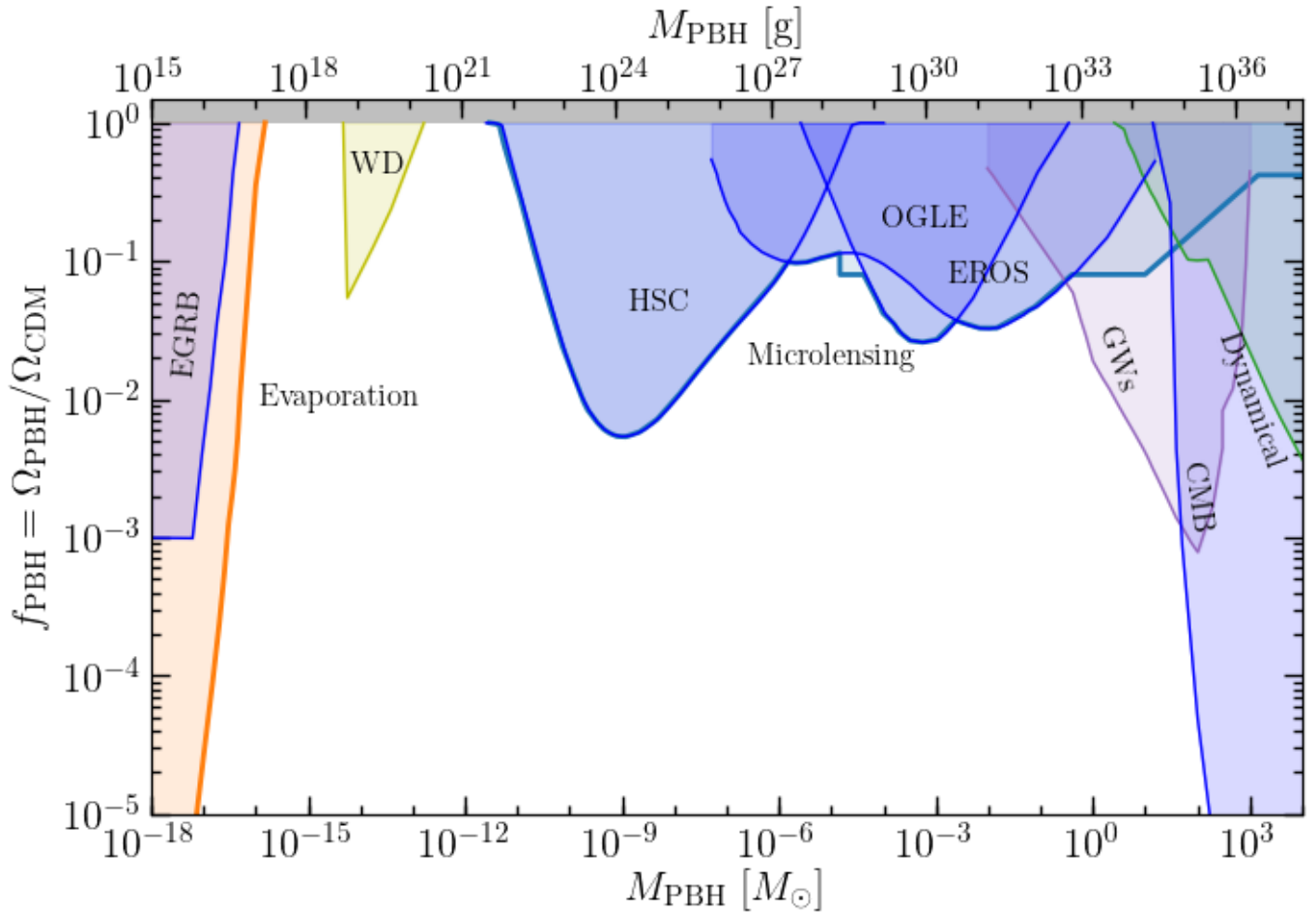


Figure 4.1: Constraints on PBH abundance as a function of PBH mass, $f_{\text{PBH}}(M_{\text{PBH}})$. The *Evaporation*, *Microlensing*, *GWs*, and *Dynamical* bounds comprise a number of separate observations; a few noteworthy ones are shown explicitly as well. The neutron stars and femtolensing constraints (which would appear in the empty mass ranges around $10^{-15} M_{\odot}$ and $10^{-12} M_{\odot}$) are not shown, since they are contested in the literature. Labels are described in the main texts, and further discussion can be found in [51, 103–105] and references therein. Image created using Kavanagh’s PBHBounds python code [94, 106].

CHAPTER 4. PRIMORDIAL BLACK HOLES

Evaporation. We saw at the end of the previous Section that PBHs radiate and eventually evaporate. It was calculated that the minimum mass a PBH needs to have in order to contribute to the present DM content is around $M \sim 10^{-19}M_\odot$. Slightly heavier PBHs in the range $10^{-19}M_\odot \lesssim M \lesssim 10^{-17}M_\odot$ could still exist, but are radiating strongly; this leaves an imprint in the extragalactic radiation background, observations of which set bounds on this mass range. These are shown on the left-hand side of Figure 4.1, labelled as *EGRB*. Other related observations exist, such as those coming from the 511 keV annihilation seen towards the centre of our galaxy. These are included within the orange *Evaporation* bound in Figure 4.1.

Gravitational Lensing. Observations (or rather, the non-observation) of gravitational lensing – the distortion of light coming from known background sources, due to transiting compact object – on various scales set constraints over a wide range of PBH masses. Femtolensing of γ -ray bursts would cover the range $10^{-17}M_\odot \lesssim M \lesssim 10^{-13}M_\odot$, but these have been contested in the literature. On the other hand, microlensing from galactic sources (OGLE), from M31 (Subaru Hyper Suprime-Cam HSC), and from the Magellanic clouds (EROS) stringently constrain f_{PBH} in the range $10^{-10}M_\odot \lesssim M \lesssim 10M_\odot$: see the overall *Microlensing* bounds in Figure 4.1.

Dynamical and Accretion Constraints. Dynamical interactions (collisions) of PBHs with astrophysical objects could be detected by observing the latter; in particular, the objects could be destroyed by transiting PBHs. This is the case for white dwarf stars (WD in the Figure) for the mass range $10^{-15}M_\odot \lesssim M \lesssim 10^3M_\odot$, although these have been disputed by the results of hydrodynamical simulations. On higher mass scales, bounds come from ultra-faint dwarf galaxies, from wide binaries in the galaxy, and from globular clusters. Overall, these cover the high-mass range $10M_\odot \lesssim M \lesssim 10^9M_\odot$, and are labelled as *Dynamical* in Figure 4.1. Accretion of background gases on PBHs could lead to increased luminosity at early times. This can be probed through X-ray and radio observations, and also applies to the high-mass range $M \gtrsim 10M_\odot$; the bounds are not shown in our Figure as they would overlap with Dynamical and CMB constraints, hindering the readability.

CMB. In the simplest PBH formation scenario discussed in the previous Sections, these form from the high-density tail of a Gaussian distribution. Silk damping could dissipate these density fluctuations at later times, leading to a distortion in the observed CMB spectrum; this sets constraints in the range $10^3M_\odot \lesssim M \lesssim 10^{12}M_\odot$. The bound is shown on the right-hand side of Figure 4.1 with the label *CMB*. Small non-Gaussianities could “free” the mass window $10^6M_\odot \lesssim M \lesssim 10^{10}M_\odot$, not considered in our Figure, and assuming PBHs formed at $M \lesssim 10^6M_\odot$ to then accrete mass would avoid these constraints.

Gravitational Waves. As calculated above, PBH formation at horizon re-entry of the perturbations requires a significant enhancement of the curvature power spectrum at horizon exit. As briefly introduced in §3.3.7, this would also induce a production of second-order Gravitational Waves. Furthermore, PBHs could coalesce at later times, producing additional GW events. (Non-)observation of these signals therefore strongly constrains f_{PBH} in the range $10^{-1}M_\odot \lesssim M \lesssim 10^2M_\odot$, as shown by the *GWs* bounds in Figure 4.1.

CHAPTER 4. PRIMORDIAL BLACK HOLES

From the discussion of the previous Sections, the reasoning is now two-fold: either we insert the mass values for the range of interest in the equations for $\beta_f(M)$ and determine the required value of the power spectrum, as was done below Equation (4.11), or we calculate the mass of the formed PBHs in terms of a comoving scale of interest, k . The second approach was taken by Inomata *et al.* [105], as well as by Braglia *et al.* [7]: from the relations of §4.2, they find that

$$\frac{M(k)}{M_\odot} = 30 \left(\frac{\gamma}{0.2} \right) \left(\frac{g_{*,f}}{10.75} \right)^{-1/6} \left(\frac{k}{2.9 \times 10^5 \text{Mpc}^{-1}} \right)^{-2}. \quad (4.13)$$

Braglia *et al.* then proceed to use the k values corresponding to the peak of their previously-found curvature power spectra [7, Figure 2], finding PBH masses in the allowed windows; for the $M \sim 10^{-12} M_\odot$ and $M \sim 10^{-15} M_\odot$ cases they calculate $f_{\text{PBH}} = 1$.

Alternatively, for the model-building approach, one calculates the necessary $\mathcal{P}_{\mathcal{R}}(k)$ enhancement from Equation (4.11) and the number of e -fold over which it needs to take place from Equation (4.12), and then searches for a model that accommodates such values. This is the method we will follow in the next Chapter. To this aim, we calculate here the necessary enhancement and duration for the three mass windows we individuated: we find that $(\mathcal{P}_{\mathcal{R}}, \Delta N_e)$ vary between $(1.5 \times 10^{-2}, 35)$ for $M \sim 10^{-12} M_\odot$ and $(2.0 \times 10^{-2}, 25)$ for $M \sim 10^{-6} M_\odot$, where in the last case we accounted for the fact that f_{PBH} can reach a maximum of ~ 0.1 . To the purpose of our subsequent analysis, we can approximate these results to an enhancement of $\mathcal{O}(10^7)$ with respect to A_s , with a duration of $\lesssim 30$ e -folds.

Chapter 5

PBHs from 2-Field Inflation

The enhancement of the curvature power spectrum required for Primordial Black Holes formation can in principle be attained in single-field inflation models with a rich enough structure. This requires an inflaton potential that remains sufficiently flat for some time during its evolution. Such models have been studied extensively in the literature, see *e.g.* [51, 102] and references therein. One of the promising aspect of multi-field inflation is that, on top of the potential's shape, such an enhancement can also be due to turns in the field space.

Let us focus our attention on the case of 2-field inflation, for which the \mathcal{N} -field dynamics of Chapter 3 simplify. Three main models of 2-field inflation will be studied, setting particular focus on whether they could allow for PBH production. We will find that the canonical Double Quadratic model of Huston & Christopherson [4] and that of Achúcarro *et al.* [5] do not provide sufficient enhancement of the curvature power spectrum to sustain PBH formation. On the other hand, substantial production can occur for the model of Braglia *et al.* [6, 7].

5.1 Reducing to $\mathcal{N} = 2$ Fields

In the case $\mathcal{N} = 2$, only two field-space orientations exist: tangent and normal to the inflationary trajectory. The index I of Chapter 3 then takes the values N, T , or equivalently \perp, \parallel . The vielbeins e_I^a are simply e_\perp^a, e_\parallel^a and, substituting the result $\Omega = H\eta_\perp$ (found from Equation (3.25)) in Equation (3.17), one obtains

$$\mathcal{D}_t e_\parallel^a = -H\eta_\perp e_\perp^a \quad , \quad (5.1)$$

which can be coupled to the corresponding

$$\mathcal{D}_t e_\perp^a = -H\eta_\perp e_\parallel^a \quad , \quad (5.2)$$

where the latter result has an additional term proportional to the projector tensor P_{ab} in the \mathcal{N} -field case (see [5, Appendix A]), which vanishes in the 2-field case. The basis vectors then take the explicit form

$$\begin{aligned} e_{\parallel}^a &= \frac{1}{\dot{\phi}} (\dot{\varphi}, \dot{\chi}) \quad , \\ e_{\perp}^a &= \frac{1}{\dot{\phi}\sqrt{\gamma}} (-\gamma_{12}\dot{\varphi} - \gamma_{22}\dot{\chi}, \gamma_{11}\dot{\varphi} + \gamma_{21}\dot{\chi}) \quad , \end{aligned} \quad (5.3)$$

where, in order to simplify the notation (in particular to avoid double indexing), we started denoting our two fields

$$(\phi^1, \phi^2) = (\varphi, \chi) \quad .$$

The perturbations will either be parallel or orthogonal to the background trajectory, $(I, J) = (N, T) \equiv (\perp, \parallel)$, and we find that $Y_{IJ} = H\eta_{\perp}$. The Equations of Motion for the perturbation, Equation (3.64), then reduce to the coupled system

$$\begin{aligned} \frac{d^2 v_{\alpha}^T}{d\tau^2} + 2\zeta \frac{dv_{\alpha}^N}{d\tau} - \zeta^2 v_{\alpha}^T + \frac{d\zeta}{d\tau} v_{\alpha}^N + \Omega_{TN} v_{\alpha}^N + (\Omega_{TT} + k^2) v_{\alpha}^T &= 0 \quad , \\ \frac{d^2 v_{\alpha}^N}{d\tau^2} - 2\zeta \frac{dv_{\alpha}^T}{d\tau} - \zeta^2 v_{\alpha}^N - \frac{d\zeta}{d\tau} v_{\alpha}^T + \Omega_{NT} v_{\alpha}^T + (\Omega_{NN} + k^2) v_{\alpha}^N &= 0 \quad , \end{aligned} \quad (5.4)$$

which are actually four coupled equations (two for $\alpha = 1$ and two for $\alpha = 2$). Here $\zeta = aH\eta_{\perp}$ and we decomposed $v^I = aQ^I = \sum_{\alpha} v_{\alpha}^I(k, \tau_i)$. The symmetric mass matrix Ω_{IJ} of Equation (3.59) is now given by

$$\begin{aligned} \Omega_{TT} &= -a^2 H^2 (2 + 2\epsilon - 3\eta_{\parallel} + \eta_{\parallel}\xi_{\parallel} - 4\epsilon\eta_{\parallel} + 2\epsilon^2 - \eta_{\perp}^2) \quad , \\ \Omega_{NN} &= -a^2 H^2 (2 - \epsilon) + a^2 M^2 \quad , \\ \Omega_{TN} &= a^2 H^2 \eta_{\perp} (3 + \epsilon - 2\eta_{\parallel} - \xi_{\perp}) = \Omega_{NT} \quad , \end{aligned} \quad (5.5)$$

with $M^2 \equiv V_{NN} + H^2\epsilon\mathbb{R}$ the effective squared mass of the v^N -mode and the Slow-Roll parameters being defined in §3.2.

We point out the important role of η_{\perp} as the coupling between the two perturbations v^T and v^N , which are respectively proportional to the curvature and isocurvature modes \mathcal{R} and \mathcal{S} . Setting η_{\perp} to zero in Equations (5.4) and (5.5), we can clearly see that the two perturbations decouple.

For consistency with our numerical approach, the EoM (5.4) are rewritten in terms of derivatives with respect to the number of e -foldings:

$$\begin{aligned} v_{\alpha}^{T''} + (1 - \epsilon)v_{\alpha}^{T'} + 2\eta_{\perp}v_{\alpha}^{N'} + [\tilde{\Omega}_{TN} + ((1 - \epsilon)\eta_{\perp} + \eta'_{\perp})]v_{\alpha}^N + \omega_{TT}v_{\alpha}^T &= 0 \quad , \\ v_{\alpha}^{N''} + (1 - \epsilon)v_{\alpha}^{N'} - 2\eta_{\perp}v_{\alpha}^{T'} + [\tilde{\Omega}_{NT} - ((1 - \epsilon)\eta_{\perp} + \eta'_{\perp})]v_{\alpha}^T + \omega_{NN}v_{\alpha}^N &= 0 \quad , \end{aligned} \quad (5.6)$$

where we temporarily introduced the shorthand $\omega_{IJ} = \tilde{\Omega}_{IJ} - \eta_{\perp}^2 + k^2/a^2 H^2$, and rescaled the mass matrix as $\tilde{\Omega}_{IJ} \equiv \Omega_{IJ}/a^2 H^2$.

We supplement these equations by imposing the Bunch–Davies initial conditions (3.65) and (3.66).

* * *

Recalling the definition of the comoving scalar perturbation (3.55), in this case we will have

$$\mathcal{R} = \frac{H}{\dot{\phi}_0} Q^T \quad , \quad (5.7)$$

$$\mathcal{S} = \frac{H}{\dot{\phi}_0} Q^N \quad , \quad (5.8)$$

where we have correspondingly defined the isocurvature perturbation through the normal direction vector. Following Equation (3.67), the power spectra for \mathcal{R} and \mathcal{S} then take the form

$$\mathcal{P}_{\mathcal{R}}(k, N_e) = \frac{H^2}{\dot{\phi}_0^2} \mathcal{P}_Q^{TT}(k, N_e) = \frac{k^3}{4\pi^2 a^2 M_{\text{Pl}}^2 \epsilon} \sum_{\alpha=1,2} v_{\alpha}^T(k, N_e) v_{\alpha}^{T*}(k, N_e) \quad , \quad (5.9)$$

$$\mathcal{P}_{\mathcal{S}}(k, N_e) = \frac{H^2}{\dot{\phi}_0^2} \mathcal{P}_Q^{NN}(k, N_e) = \frac{k^3}{4\pi^2 a^2 M_{\text{Pl}}^2 \epsilon} \sum_{\alpha=1,2} v_{\alpha}^N(k, N_e) v_{\alpha}^{N*}(k, N_e) \quad , \quad (5.10)$$

$$\mathcal{P}_{\mathcal{RS}}(k, N_e) = \frac{H^2}{\dot{\phi}_0^2} \mathcal{P}_Q^{TN}(k, N_e) = \frac{k^3}{4\pi^2 a^2 M_{\text{Pl}}^2 \epsilon} \sum_{\alpha=1,2} v_{\alpha}^T(k, N_e) v_{\alpha}^{N*}(k, N_e) \quad . \quad (5.11)$$

In the last line, we have also defined the cross-correlation spectrum. Calculating these quantities at the end of inflation, $N_e = N_e^{\text{end}}$, the total curvature, isocurvature, and cross-correlation spectra are determined:

$$\mathcal{P}_{\mathcal{R}}(k) \equiv \mathcal{P}_{\mathcal{R}}(k, N_e^{\text{end}}) \quad , \quad (5.12)$$

$$\mathcal{P}_{\mathcal{S}}(k) \equiv \mathcal{P}_{\mathcal{S}}(k, N_e^{\text{end}}) \quad , \quad (5.13)$$

$$\mathcal{P}_{\mathcal{RS}}(k) \equiv \mathcal{P}_{\mathcal{RS}}(k, N_e^{\text{end}}) \quad . \quad (5.14)$$

We are mainly interested in calculating the former, in order to determine if it can be enhanced enough as to allow for PBH production from the consideration of the previous Chapter.

With this knowledge, let us now analyse a few concrete models of 2-field inflation.

5.2 Double Quadratic model

In the simplest model of 2-field (or *double*) inflation, the massive scalar fields do not interact and are minimally coupled [107]. This means that no coupling is inserted in the field-space metric,

$$\gamma_{ab} = \mathbb{1}_2 \quad , \quad (5.15)$$

and the kinetic term of the fields' Lagrangian is canonical.

The potential – shown in Figure 5.1 – is quadratic (such as that of Equation (2.41)) in each field, giving

$$V(\phi) = \frac{1}{2} m_{\varphi}^2 \varphi^2 + \frac{1}{2} m_{\chi}^2 \chi^2 \quad . \quad (5.16)$$

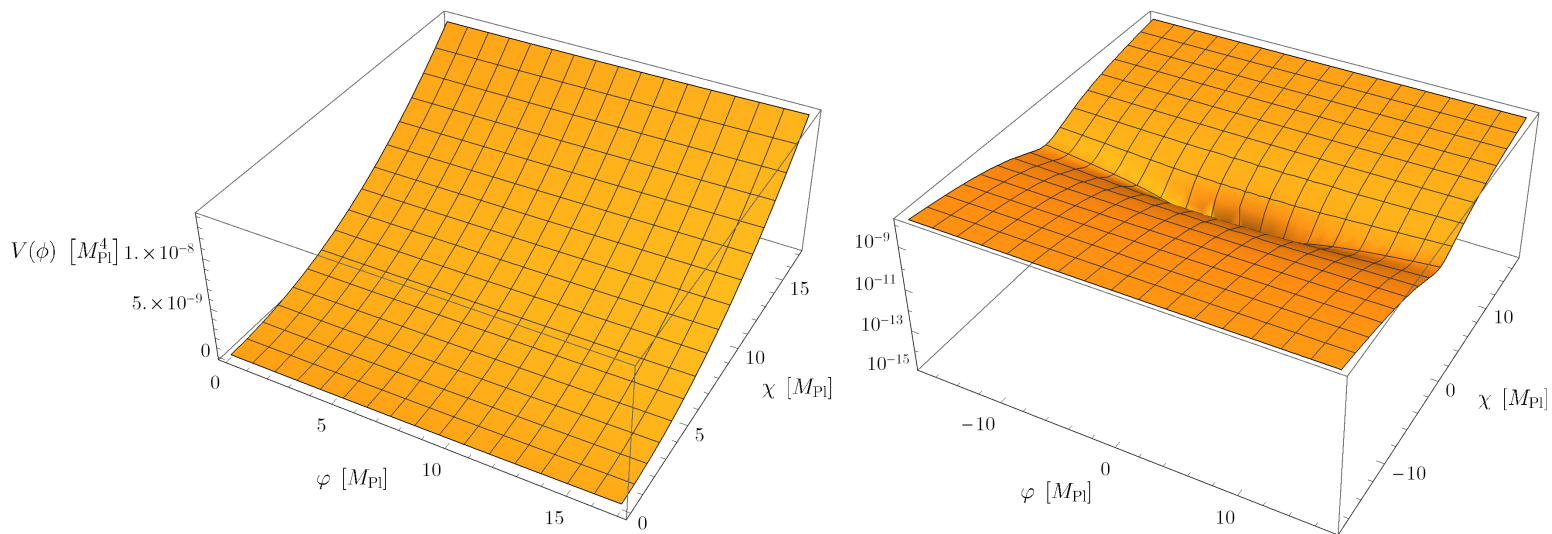


Figure 5.1: Double Quadratic potential for the two field φ and χ , as given in Equation (5.16). The fields satisfy the mass hierarchy $m_\chi = 7m_\varphi$ with $m_\varphi = 1.395 \times 10^{-6} M_{\text{Pl}}$ [4]. *Left panel:* Potential in linear scale, as usually visualised. *Right panel:* Potential in logarithmic scale, extending to non-physical negative field values. This is to highlight the shape of the potential in the φ -direction (i.e. that of the light field), and the potential’s minimum at $(\varphi, \chi) = (0, 0)$.

The fields satisfy a mass hierarchy, χ being the heavier one. We follow the definitions of Huston & Christopherson [4] here, setting $m_\chi = 7m_\varphi$ and $m_\varphi = 1.395 \times 10^{-6} M_{\text{Pl}}$.

Lastly, initial conditions on the field values and their derivatives need to be given; we have $\phi_i^a \equiv \phi_0^a(N_e^i) = (12, 12) M_{\text{Pl}}$ and $\pi_i^a \equiv \phi_0^{\prime a}(N_e^i) = (0.1, 0.1) M_{\text{Pl}}$.

With these ingredients, we were able to solve the Equations of Motion for the background, i.e. Equation (3.9). Code-wise, we used Mathematica’s numerical differential solution method `NDSolve`, with the condition $\epsilon - 1 = 0$ as an end point. Note that all the derivatives that appear in the quantities defined in §3.2 were differentiated analytically, rather than numerically, for better accuracy: comparing the two methods, significant discrepancies were in fact found.

* * *

Let us consider the right panel of Figure 5.1. The system of fields will start in the top right corner of the plot to then roll down the potential’s slope in the χ -direction until $\chi = 0$: this corresponds to a first inflation stage driven by the heavy field. At this point, the fields’ trajectory will turn and the system will roll down the potential in the φ -direction, all the way to $(\varphi, \chi) = (0, 0)$: this is a second inflation stage driven by the light field.

The evolution of the fields we just described can be seen in the first panel of Figure 5.2 on page 56. That figure also shows the temporal evolution of the Hubble parameter and of the Slow-Roll parameters ϵ and $\eta_{\parallel}, \eta_{\perp}$. The main takeaway is that the transition between the two stages of inflation – the first one driven by the heavy field χ and the second by the light field φ – generates a temporary enhancement of the SR parameters. Due to η_{\perp} being the coupling between the curvature and isocurvature perturbations, this *feature*, as

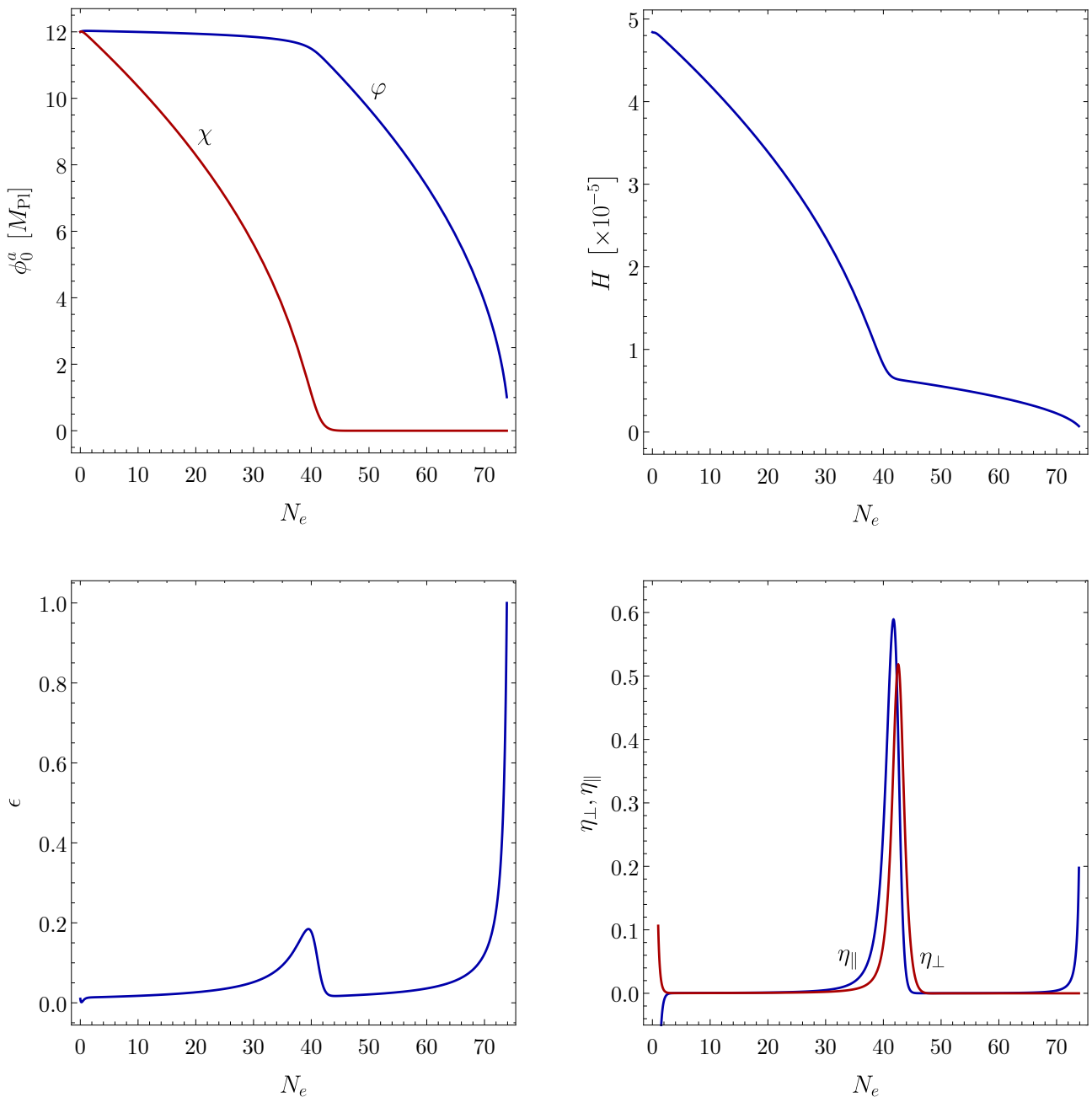


Figure 5.2: Temporal evolution of the background quantities ϕ_0^a , H , ϵ , and $\eta_{\parallel}, \eta_{\perp}$ for the Double Quadratic model [4]. *Top Left panel:* Evolution of the background fields φ and χ : the heavy field χ decays first, driving a first stage of inflation; when it reaches its minimum at $\chi = 0$, the light field also decays, driving a second stage of inflation. *Top Right panel:* Evolution of the Hubble parameter H : its amplitude varies very little, as expected, but we do notice a “dip” at the N_e value corresponding to the transition between the φ - and χ -driven inflation stages. We note that, when plotting the quantity aH in log scale, the same increasing behaviour as in Figure 2.2 can be observed, with a faint saddle point when the transition takes place. *Bottom Left panel:* Evolution of the first Slow-Roll parameter ϵ : this evolves from ~ 0 (i.e. satisfying SR) to $\epsilon(N_e^{\text{end}}) = 1$ which signals the end of inflation; the *feature* at the transition between inflation stages is quite noticeable here. *Bottom Right panel:* Evolution of the parallel and perpendicular components of the second Slow-Roll parameter η_{\parallel} and η_{\perp} : these satisfy $\eta \ll 1$ throughout, except for the feature noticed previously.

CHAPTER 5. PBHS FROM 2-FIELD INFLATION

we shall call it in what follows, will cause an enhancement of the scalar power spectra. We will later refer to the time at which this feature takes place as N_e^f . We point out the fact that the results for ϵ and $\eta_{\parallel}, \eta_{\perp}$ precisely match those of Avgoustidis *et al.* [108, Figure 3], who study this same model.

* * *

Having calculated the background quantities, we were now ready to solve the EoM for the perturbations (5.6), with the appropriate Bunch-Davies initial conditions (3.65)–(3.66), which we imposed at a time $N_e^{\text{BD}}(k) \equiv N_e^{\text{HX}}(k) - 5$.

This was the most computationally challenging aspect of our numerical code, since it required a high number of calculations. We in fact solved (using again the numerical differential solver `NDSolve`) the EoM for $\mathcal{O}(10^3)$ different k -modes, which were defined from their horizon-crossing time N_e^{HX} .

Having solved the EoM for the perturbations, it was finally possible to calculate the scalar power spectra $\mathcal{P}_{\mathcal{R}}(k, N_e)$ and $\mathcal{P}_{\mathcal{S}}(k, N_e)$ for each k -mode, as well as the overall spectra $\mathcal{P}_{\mathcal{R}}(k)$ and $\mathcal{P}_{\mathcal{S}}(k)$. As discussed previously, we are mostly interested in the curvature power spectrum in this work.

* * *

The $\mathcal{P}_{\mathcal{R}}(k, N_e)$ and $\mathcal{P}_{\mathcal{S}}(k, N_e)$ are shown in Figure 5.3 on page 58 for four different k -modes: one exiting the horizon *before* the feature takes place, $N_e^{\text{HX}} < N_e^f$, two which exit the horizon *during* the feature, $N_e^{\text{HX}} \sim N_e^f$, and a last one which exits the horizon *after* the feature, $N_e^{\text{HX}} > N_e^f$. The pseudo-single-field behaviour (see Equation (3.68)),

$$\mathcal{P}_{\mathcal{R}}^{\text{1-field}}(k, N_e = N_e^{\text{HX}}) = \frac{H^2(N_e^{\text{HX}})}{8\pi^2\epsilon(N_e^{\text{HX}})} \quad ,$$

is also shown; by “pseudo” we mean that this was calculated with the H and ϵ quantities of the 2-field model which, as we saw in Figure 5.11, do depart from the single-field behaviour.

The impact of the multi-field behaviour is explicit in this Figure. Consider the first panel: apart from the initial decaying behaviour, due to the initial conditions that were imposed, the curvature spectrum $\mathcal{P}_{\mathcal{R}}$ stabilises onto the single-field behaviour from the moment of horizon exit, around $N_e^{\text{HX}} \approx 10$ in this case, up until $N_e \approx N_e^f$. At this point, while the single-field spectrum remains constant (the mode is frozen [61]), the multi-field one is enhanced by the isocurvature perturbation. In the meantime, in fact, the isocurvature spectrum decays slowly for $N_e^{\text{HX}} < N_e < N_e^f$, increases abruptly around N_e^f , and eventually decays slowly, having transferred its energy to the curvature perturbation. At lower $\mathcal{P}_{\mathcal{S}}$ values, numerical errors begin to appear – the decaying trend is nevertheless maintained. We point out the fact that these results precisely match those of Huston & Christopherson [4, Figure 1] (our $\mathcal{P}_{\mathcal{S}}$ is their $\mathcal{P}_{\mathcal{S}^{\sim}}$) as well as those of Avgoustidis *et al.* [108, Figure 3], who study this same model. This comparison was one of the main reasons for considering this model in the first place: the fact that our results matched those of the literature – computed with different methods, such as `Pyflation` in the case of Huston & Christopherson – showed us that our numerical code gave the expected predictions.

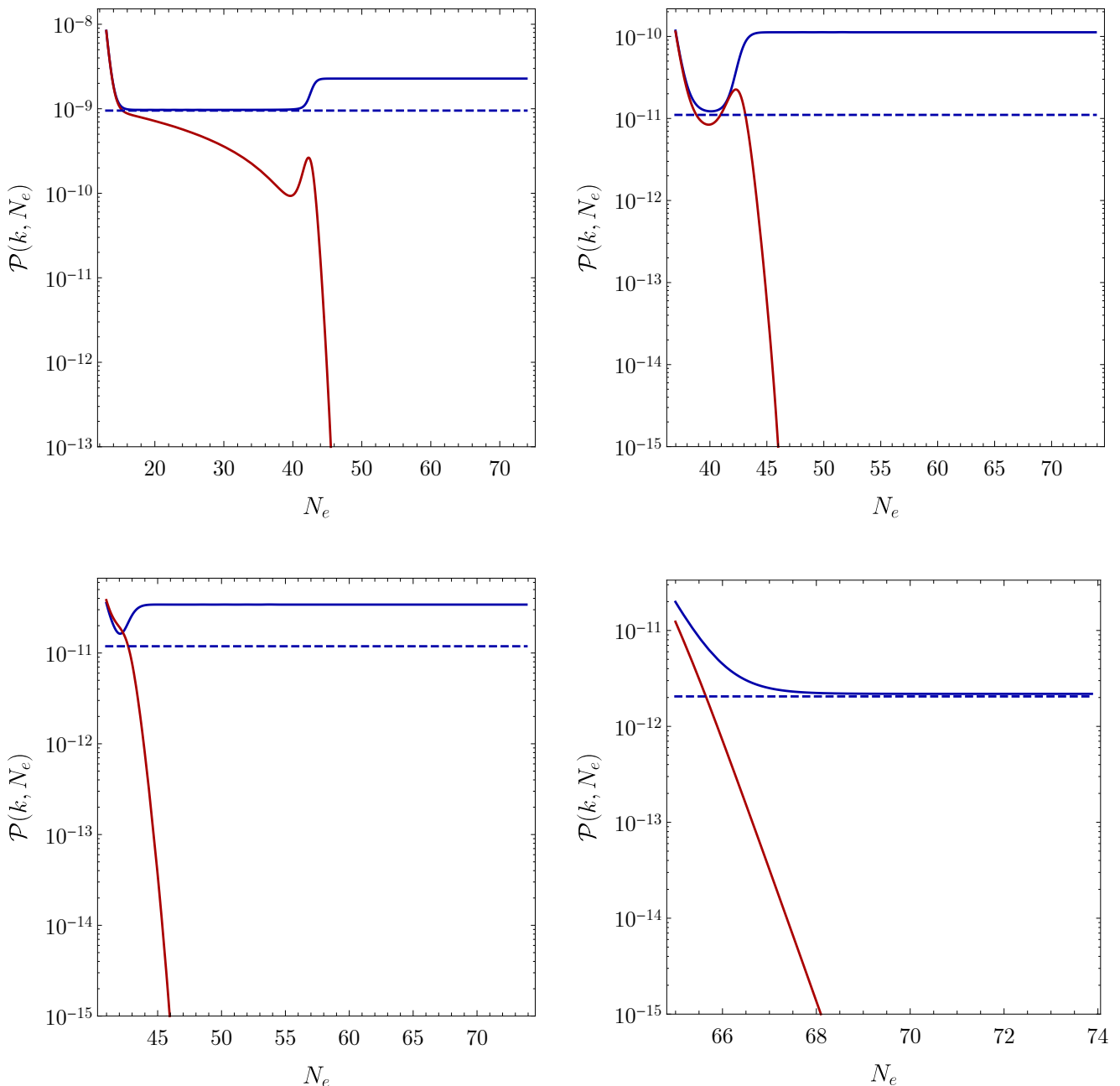


Figure 5.3: Temporal evolution of the curvature (in blue) and isocurvature (in red) power spectra, $\mathcal{P}_{\mathcal{R}}(k, N_e)$ and $\mathcal{P}_{\mathcal{S}}(k, N_e)$, for the Double Quadratic model [4]. The pseudo-single field value of the former, $\mathcal{P}_{\mathcal{R}}^{1\text{-field}}(k, N_e)$, is also shown (dashed blue lines). *Top Left panel:* k -mode exiting the horizon before the feature takes place. The enhancement of the curvature power spectrum at N_e^f with respect to its single-field limit can be seen, in correspondence with the abrupt enhancement and consecutive decay of the isocurvature spectrum. *Top Right panel:* k -mode exiting the horizon when the feature begins ($N_e^{\text{HX}} \lesssim N_e^f$). The behaviour of the spectra is similar to the previous case, albeit more accentuated. *Bottom Left panel:* k -mode exiting the horizon while the feature takes place. With respect to the previous panels, the curvature power spectrum never reaches the single-field limit and the isocurvature spectrum shows no sudden increase, decaying rapidly since the beginning. *Bottom Right panel:* k -mode exiting the horizon after the feature takes place. While the isocurvature spectrum decays quickly, the curvature spectrum tends to its single-field limit.

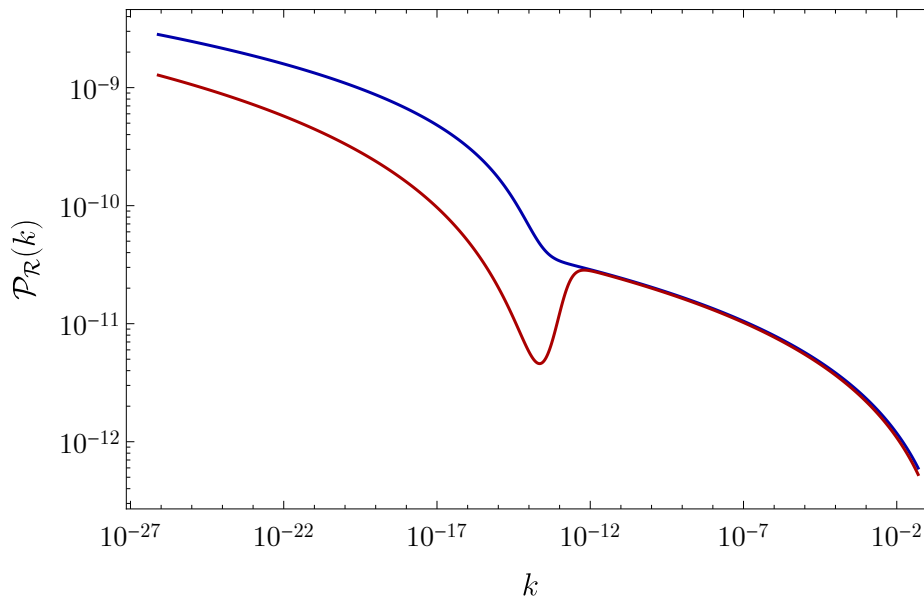


Figure 5.4: Curvature power spectrum $\mathcal{P}_{\mathcal{R}}(k)$ for the Double Quadratic model [4]. An enhancement with respect to the single-field behaviour for k -modes leaving the horizon before the feature takes place can be seen at low k scales. Notice that the pseudo-single field spectrum exhibits a decrease around N_e^f that would not appear in a real single-field spectrum.

For the k -modes exiting the horizon (roughly) during the feature (top right and bottom left panels of 5.7), the same behaviour can be observed. In the bottom left panel, the curvature spectrum is enhanced from the beginning, not even reaching the single-field limit. The isocurvature spectrum decays faster each time, not showing the enhancement around N_e^f in the bottom panels. In the last panel, we see that for k -modes exiting the horizon after the feature, the curvature spectrum goes back to its single-field limit: the isocurvature perturbation has in fact already decayed. This can be understood by thinking that, in the second stage of inflation, the heavy field has already decayed and cannot influence the dynamics in any way.

Finally, the overall curvature power spectrum $\mathcal{P}_{\mathcal{R}}(k) = \mathcal{P}_{\mathcal{R}}(k, N_e^{\text{end}})$ is shown in Figure 5.4. Here, the pseudo-single field spectrum is shown for completeness, but differs significantly from the real single-field behaviour by the “dip” at the scales $k(N_e^{\text{HX}} \approx N_e^f)$ (due to the increase in ϵ in the denominator). The point of this plot is to notice the additional contribution to the curvature power spectrum for scales exiting the horizon before (and especially around) the feature (i.e. the enhancement seen for $N_e > N_e^f$ in the first three panels of Figure 5.3). When plotted together with $\mathcal{P}_{\mathcal{S}}(k)$, the spectra exhibit a similar shape, albeit separated by ~ 40 orders of magnitude: see *e.g.* Huston & Christopherson’s [4, Figure 2], (or think of the results in Figure 5.9 without the oscillatory behaviour). Overall, the enhancement in $\mathcal{P}_{\mathcal{R}}(k)$ due to the multi-field behaviour is only of $\mathcal{O}(1)$; this is not nearly enough to generate Primordial Black Holes, as we saw at the end of Chapter 4.

This concludes the discussion of the Double Quadratic model of 2-field inflation. Moving on to the models of Achúcarro *et al.* [5] and Braglia *et al.* [6, 7], the methods described

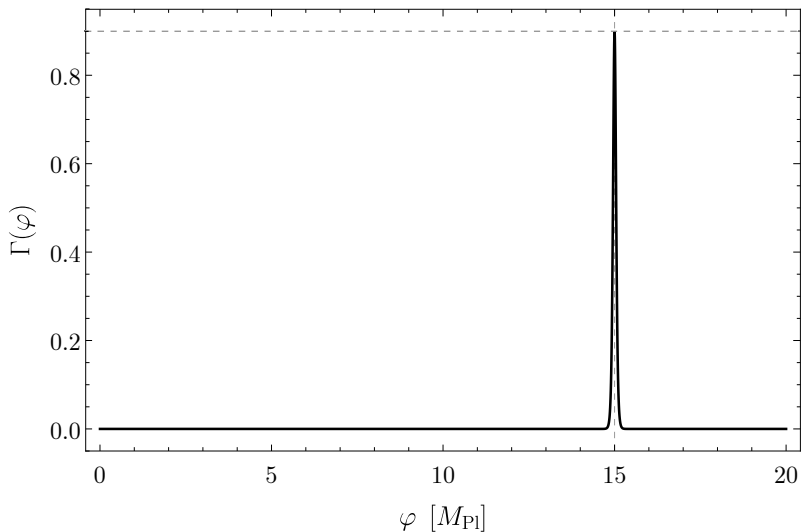


Figure 5.5: Coupling parameter $\Gamma(\varphi)$ for the Achúcarro model [5], as defined in Equation (5.18). The peak value is given by $\Gamma(\varphi_i = 15) = \Gamma_{\max} = 0.9$, and the coupling lasts for $\Delta\varphi = 0.12 M_{\text{Pl}}$. The horizontal dashed line corresponds to Γ_{\max} , and the vertical one to φ_i .

above will be the same and will thus not be repeated.

5.3 Achúcarro's model

The following model was introduced by Achúcarro *et al.* [5]. A coupling between the fields is inserted in the field-space metric,

$$\gamma_{ab} = \begin{pmatrix} 1 & \Gamma(\varphi) \\ \Gamma(\varphi) & 1 \end{pmatrix}, \quad (5.17)$$

through the dimensionless φ -dependent parameter $\Gamma(\varphi)$, which needs to satisfy $\Gamma^2(\varphi) \ll 1$. The explicit choice

$$\Gamma(\varphi) = \frac{\Gamma_{\max}}{\cosh^2[2(\varphi - \varphi_i)/\Delta\varphi]} \quad (5.18)$$

is considered, where $\Gamma_{\max} = 0.9$ is the maximum value that $\Gamma(\varphi)$ can reach, at $\varphi = \varphi_i$, and $\Delta\varphi$ is the field-space distance over which the coupling takes place. The field-dependence of the parameter $\Gamma(\varphi)$ is shown in Figure 5.5, and a more detailed discussion on its physical meaning can be found in [5].

The potential is instead given by

$$V(\phi) = V_0(\varphi) + \frac{1}{2}m_\chi^2\chi^2, \quad (5.19)$$

where $V_0(\varphi)$ was not explicitly specified in the original paper [5]. Considering the conditions that V_0 needs to satisfy, a parameter study of plausible quadratic and quartic potentials was performed. We eventually identified in the following model the most promising

candidate, in that it produced a significant enhancement of the SR parameters at N_e^f , which as we saw previously is related to the enhancement of the curvature power spectrum. We therefore chose to use $V_0(\varphi) = \frac{1}{2}m_\varphi^2\varphi^2$, such that the potential (5.19) reduces to the double quadratic one of Equation (5.16). The mass hierarchy in this case is given by $m_\varphi = \frac{1}{20}m_\chi$, with the latter satisfying $m_\chi^2 = 300H^2 = 3 \times 10^{-8} M_{\text{Pl}}^2$, using the standard result $H = 10^{-5} M_{\text{Pl}}$ [5]. While the numerical scale of $V(\phi)$ for the Achúcarro model will be different from that of the Double Quadratic model of §5.2, their shapes are approximately equal: we therefore refer the reader to Figure 5.1 for a visualisation of the fields potential.

The initial conditions were chosen to be $\phi_i^a = (15, 15) M_{\text{Pl}}$ and $\pi_i^a = (0.1, 0.1) M_{\text{Pl}}$.

* * *

Analogously to the Double Quadratic case, the evolution of the background quantities is shown in Figure 5.6 on page 62. Starting from the top left panel, we see the mechanism by which the heavy field, χ , decays first while the light one, φ , only evolves after that; as noted before, these decays drive two separate stages of inflation. At the transition between them, we now observe a (small but significant) oscillation of the fields. While H (top right panel) behaves very similarly to the previous case, the oscillatory behaviour is seen in the Slow-Roll parameters η (bottom left panel) and $\eta_{\parallel}, \eta_{\perp}$ (bottom right panel) as well. This is highlighted in the respective insets.

The magnitude of the feature in the SR parameters is also much greater than in the Double Quadratic case (compare this Figure to the bottom panels of Figure 5.2). Focusing on the last panel, we point out that the results for η_{\parallel} and η_{\perp} are quite similar to those found by the original authors [5, Figure 6], the discrepancy being due to the possibly different forms of $V_0(\varphi)$ that were considered.

* * *

The scalar power spectra $\mathcal{P}_{\mathcal{R}}(k, N_e)$ and $\mathcal{P}_{\mathcal{S}}(k, N_e)$ are again shown in Figure 5.7 for four k -modes leaving the horizon before, during, and after the feature. Their evolution is similar to the one discussed previously, if not for the oscillatory behaviour around N_e^f that comes from the background quantities analysed above. In the first three panels of this Figure, the numerical errors in $\mathcal{P}_{\mathcal{S}}(k, N_e)$ can be appreciated: the curve's overall trend is nevertheless unaffected.

The overall spectrum $\mathcal{P}_{\mathcal{R}}(k)$ is instead shown in Figure 5.8. As previously, we notice how the low- k modes are enhanced with respect to the (pseudo-)single-field limit, while high- k modes match this behaviour. Furthermore, the oscillatory behaviour of k -modes exiting the horizon at $N_e^{\text{HX}} \approx N_e^f$, which is typical of this model, is translated to the overall power spectrum as well. These results in fact resemble those of the original authors: see [5, Figures 5 and 6]. The discrepancy is most likely due to the possibly different models considered for $V_0(\varphi)$.

We also show the comparison between the curvature, $\mathcal{P}_{\mathcal{R}}(k)$, and isocurvature, $\mathcal{P}_{\mathcal{S}}(k)$, spectra in Figure 5.9, together with the correlation spectrum $\mathcal{P}_{\mathcal{RS}}(k)$. As anticipated at the end of §5.2, these all exhibit the same behaviour, albeit separated by many orders of magnitude. The oscillation observed in Figure 5.8 therefore appears here as well.

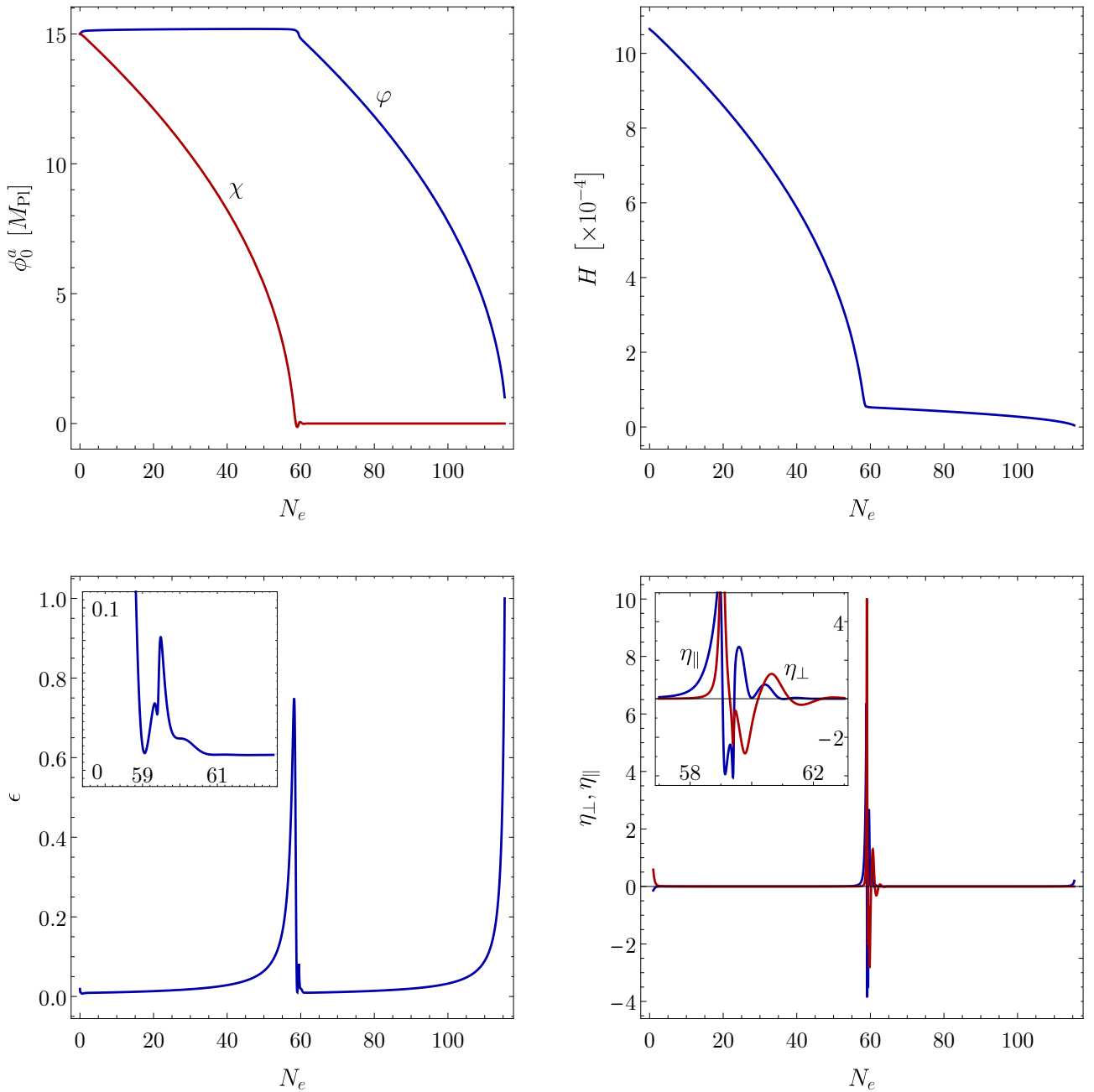


Figure 5.6: Temporal evolution of the background quantities ϕ_0^a (top left panel), H (top right panel), ϵ (bottom left panel), and $\eta_{\parallel}, \eta_{\perp}$ (bottom right panel) for Achúcarro’s model [5]. The behaviour of these quantities is as explained in Figure 5.2 for the Double Quadratic case, albeit more accentuated. Notice in particular the oscillatory behaviour exhibited by ϕ_0^a , ϵ , and the η components when the feature takes place. The cut-outs in the bottom panels show a magnification of this feature; the one in the η plot also clarifies how the two curves overlap.

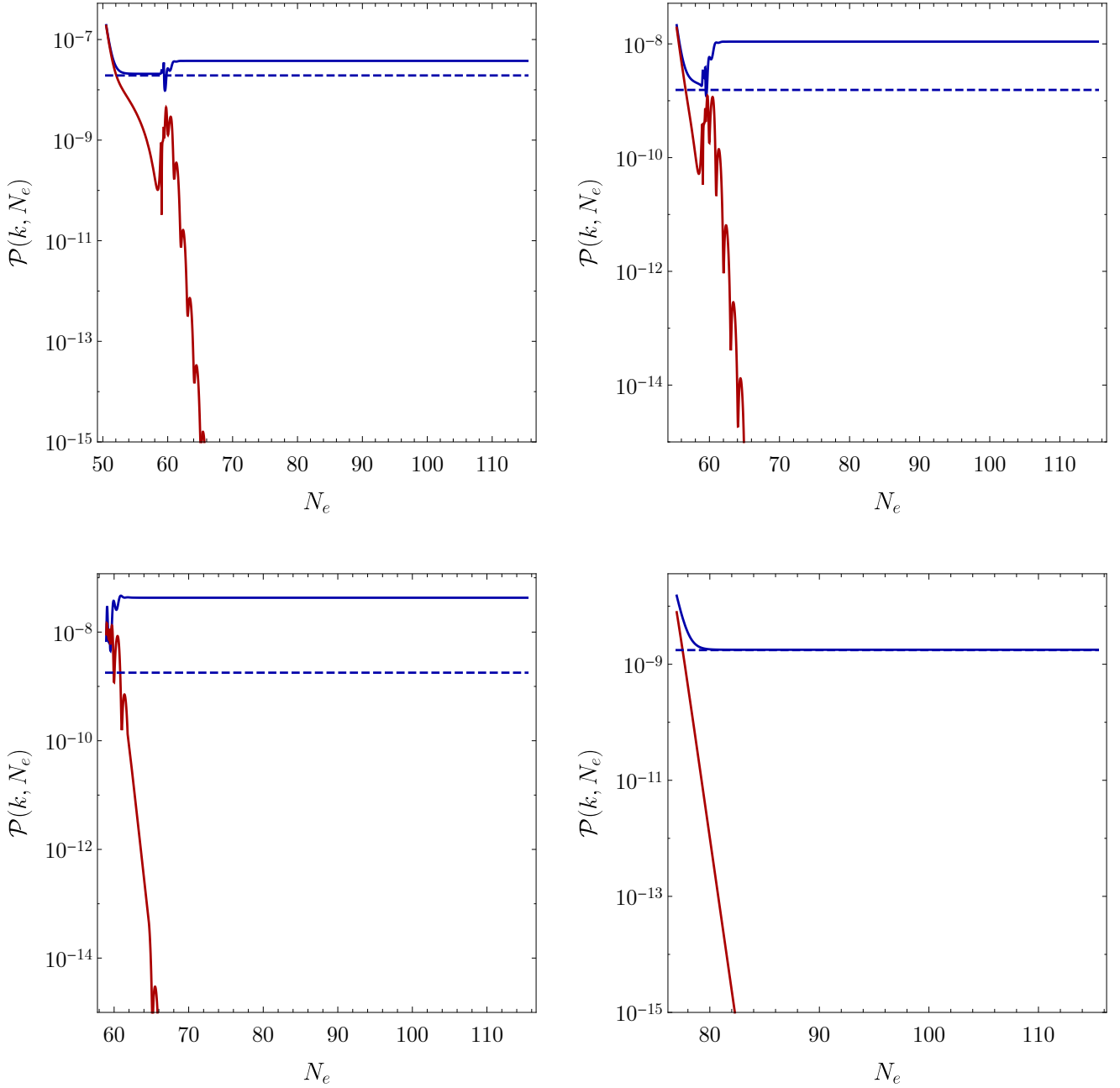


Figure 5.7: Temporal evolution of the curvature (in blue) and isocurvature (in red) power spectra, $\mathcal{P}_{\mathcal{R}}(k, N_e)$ and $\mathcal{P}_{\mathcal{S}}(k, N_e)$, for Achúcarro's model [5]. The pseudo-single field value of the former, $\mathcal{P}_{\mathcal{R}}^{1\text{-field}}(k, N_e)$, is also shown (dashed blue lines). As for the case of Figure 5.3, we illustrate k -modes exiting the horizon before, during, and after the feature takes place. The behaviour is as discussed in that Figure, except for the fact that the curvature spectrum exhibits some oscillatory behaviour at N_e^f . The above-mentioned numerical errors in the isocurvature spectra can be seen here; they nevertheless do not modify the overall evolution of $\mathcal{P}_{\mathcal{S}}$.

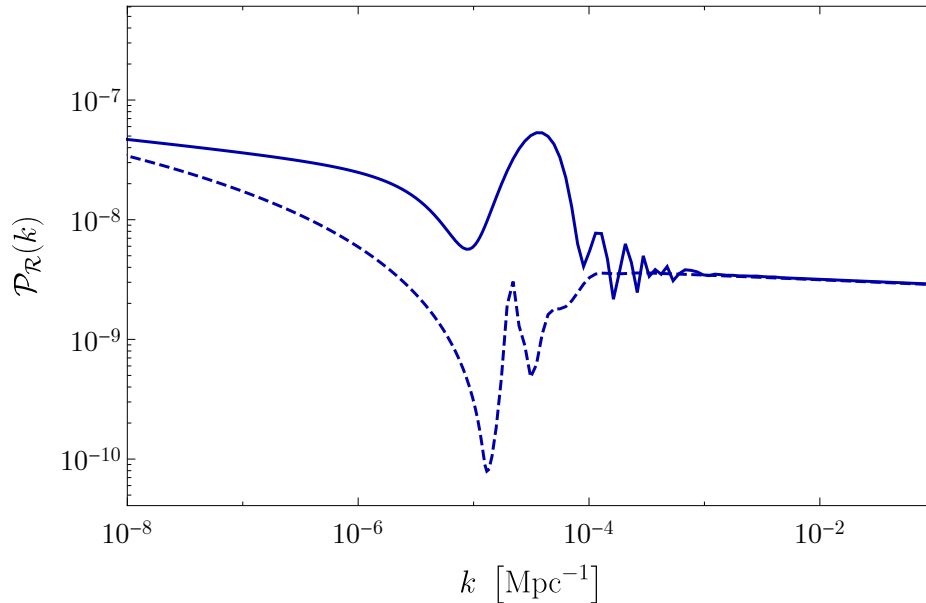


Figure 5.8: Curvature power spectrum $\mathcal{P}_{\mathcal{R}}(k)$ for Achúcarro’s model [5]. An enhancement with respect to the single-field behaviour for k -modes leaving the horizon before the feature takes place can be seen at low k scales. Notice that the pseudo-single field spectrum exhibits a decrease around N_e^f that would not appear in a real single-field spectrum. Furthermore, notice the additional oscillatory behaviour with respect to Figure 5.4.

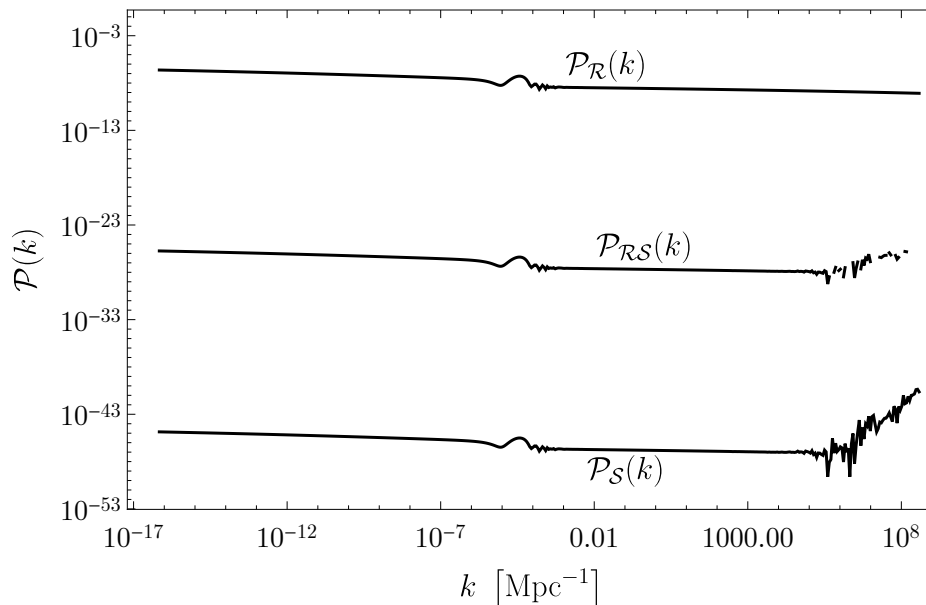


Figure 5.9: Comparison between the curvature, isocurvature, and correlation power spectra $\mathcal{P}_{\mathcal{R}}(k)$, $\mathcal{P}_{\mathcal{S}}(k)$, and $\mathcal{P}_{\mathcal{RS}}(k)$ for Achúcarro’s model [5].

Numerical errors can be seen to appear on the right-hand side of the plot for the latter two spectra.

In this model, the enhancement of $\mathcal{P}_{\mathcal{R}}(k)$ with respect to its single-field limit is almost of order $\mathcal{O}(10^2)$, thus more significant than the simple Double Quadratic case found in Figure 5.4. This is nevertheless still not sufficient to cause the generation of Primordial Black Holes (this model was in fact not designed to this purpose by the authors [5]).

5.4 Braglia's model

Lastly, we introduce the model of Braglia *et al.* [6, 7]. In this case, the coupling between the fields is a φ -dependent parameter in the $\chi - \chi$ matrix element of the metric:

$$\gamma_{ab} = \begin{pmatrix} 1 & 0 \\ 0 & f(\varphi) \end{pmatrix} . \quad (5.20)$$

Two forms of the coupling function are considered in [7], $f(\varphi) = e^{2b_1\varphi}$ and $f(\varphi) = e^{2b_2\varphi^2}$, with b_1 and b_2 being parameters of dimensions M_{Pl}^{-1} and M_{Pl}^{-2} respectively. While both cases were analysed, no drastic differences were found in our study; the remainder of this discussion will therefore focus on the former case, $f(\varphi) = e^{2b_1\varphi}$, and we invite the reader to refer to [6, 7] for a complete analysis. A range of values was considered for the b_1 parameter: $6.4 \leq b_1 \leq 8.4$. For this choice of the metric γ_{ab} , the field space exhibits a constant and negative curvature given by the Ricci scalar $\mathbb{R} = -b_1^2$.

The potential takes the form discussed in Reference [109] (i.e. the potential of [110, Equation (5.319)] with $p = 5$) for the heavy field φ , and a simple quadratic form for the light field χ :

$$V(\phi) = V_0 \frac{\varphi^2}{\varphi_0^2 + \varphi^2} + \frac{m_\chi^2}{2} \chi^2 . \quad (5.21)$$

The values $V_0 = 1$, $\varphi_0 = \sqrt{6} M_{\text{Pl}}$, $m_\chi = \sqrt{V_0/500}$ were taken, and the potential is shown in Figure 5.10. Notice how the light and heavy fields are exchanged with respect to the Double Quadratic (§5.2) and Achúcarro (§5.3) models.

In this model, the initial conditions are $\phi_i^a = (7, 7.31) M_{\text{Pl}}$ and $\pi_i^a = (0, 0) M_{\text{Pl}}$.

A parameter study in the 8-dimensional space spanned by $(b_1, V_0, \varphi_0, m_\chi, \phi_i^a, \pi_i^a)$ was performed: the above-mentioned values gave the clearest results, by which we mean the strongest enhancement of the SR parameters and eventually of the power spectrum.

* * *

Figure 5.11 shows the evolution of the background quantities for six values of the model parameter b_1 , its values being given in the colorbar. The parameter $\eta_{(\text{B})}$ of Equation (3.28) is considered, rather than the pair $\eta_{\parallel}, \eta_{\perp}$; this both allows for easy comparison with the authors' results, and improves the readability, which would be highly hindered by the overlapping sets of colours.

Similarly to the previous cases (Figures 5.2 and 5.6), a feature – i.e. a temporary increase in magnitude – appears in the Slow-Roll parameters in correspondence of the

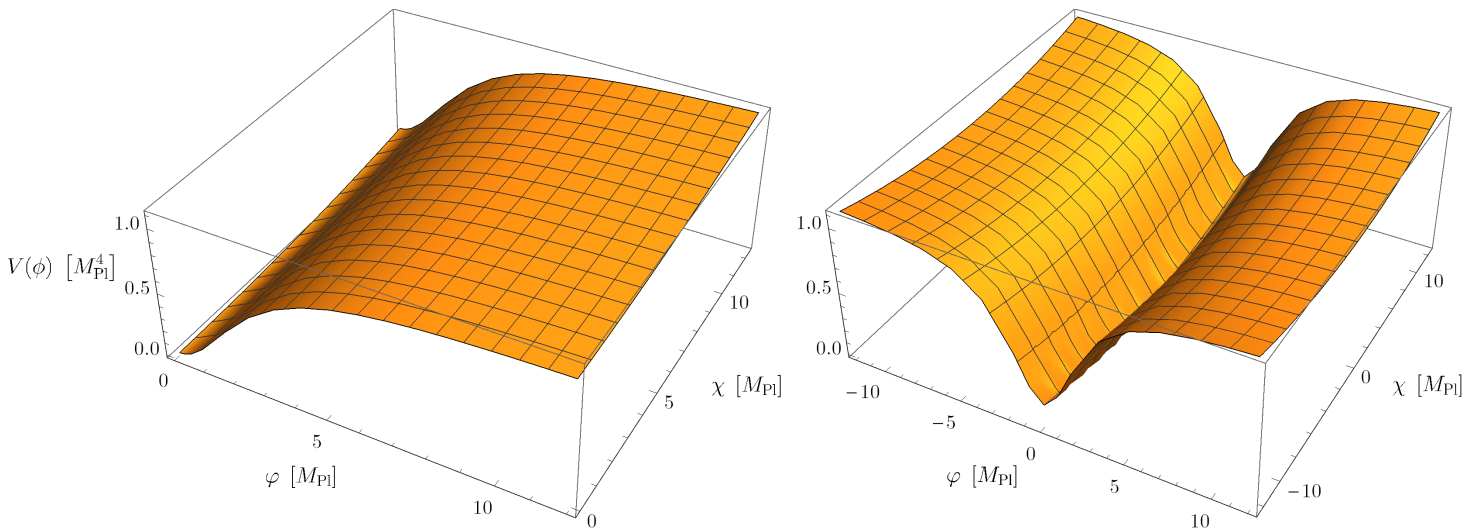


Figure 5.10: Braglia *et al.*'s potential for the two fields φ and χ , as given in Equation (5.21). *Left panel:* Potential in linear scale, as usually visualised. *Right panel:* Potential in logarithmic scale, extending to non-physical negative field values. This is to highlight the shape of the potential in the χ -direction (i.e. that of the light field), and the potential's minimum at $(\varphi, \chi) = (0, 0)$.

transition between the first (driven by the heavy field, φ in this case) and second stage (driven by the light field, χ here) of inflation. This feature is now much more accentuated, ϵ reaching values close to unity (and thus the end of inflation) at its peak. The oscillatory behaviour around the feature, which was noticed in Achúcarro's model, is present in this case as well, and magnified in the insets of each panel. These results correspond to those shown in [7, Figure 1].

* * *

It can be seen that inflation lasts longer for higher- b_1 curves. On the other hand, the oscillations do not seem to depend on b_1 in a clear way, and zooming in on the peak of ϵ one can observe that all curves overlap. What is very important, though, is that this is not the case for $\eta_{(B)}$: as shown in Figure 5.12, higher b_1 values lead to greater enhancement of $\eta_{(B)}$, and correspondingly of η_{\parallel} and η_{\perp} . Clearly, only the top of the feature is shown in the Figure for simplicity, but the same behaviour can be observed at the bottom.

As was noticed below Equation (5.4), the η parameters regulate the coupling between curvature and isocurvature perturbations: we therefore expect to see a significant interaction between the two modes. This can be thought of as a tachyonic instability¹ of the isocurvature perturbation [7]: its squared mass becomes in fact temporarily negative, and greatly enhanced, at the time of the feature. This can be seen in the top left and bottom right panels of Figure 5.13, which respectively illustrate the effective mass of the v^N perturbation, $M_{v^N}^2$, and its mass matrix element, Ω_{NN} . This instability feeds

¹Tachyonic particles were hypothesised as being superluminal, requiring them to have imaginary masses, or negative m^2 [111]. It is now common to use the term *tachyonic* to refer to the latter property.

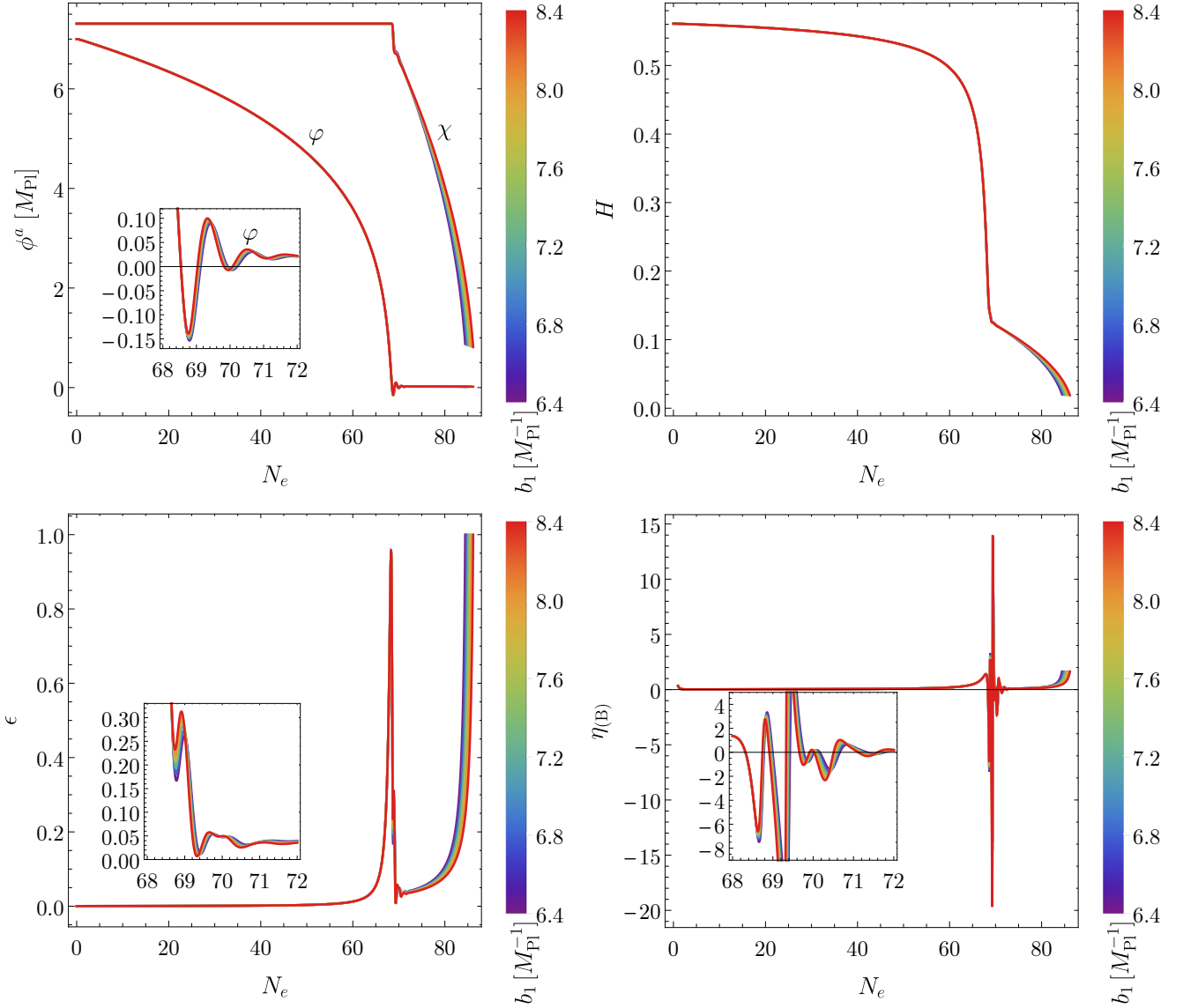


Figure 5.11: Temporal evolution of the background quantities ϕ_0^a (top left panel), H (top right panel), ϵ (bottom left panel), and $\eta_{(B)}$ (bottom right panel) for Braglia’s model [6, 7]. All the quantities are shown for different values of the parameter b_1 which characterises this model. Note that we are plotting $\eta_{(B)}$ here rather than the pair $\eta_{\parallel}, \eta_{\perp}$, both for best readability and to more easily compare this Figure to that of the authors, [7, Figure 1]; as explained in §2.2.2 and §3.2, the various η are related. The behaviour of these quantities is as explained in Figure 5.2 for the Double Quadratic case, albeit much more accentuated. Notice that the oscillatory behaviour encountered in the case of Achúcarro’s model appears here as well; this is highlighted in the insets which magnify the interested region of each panel.

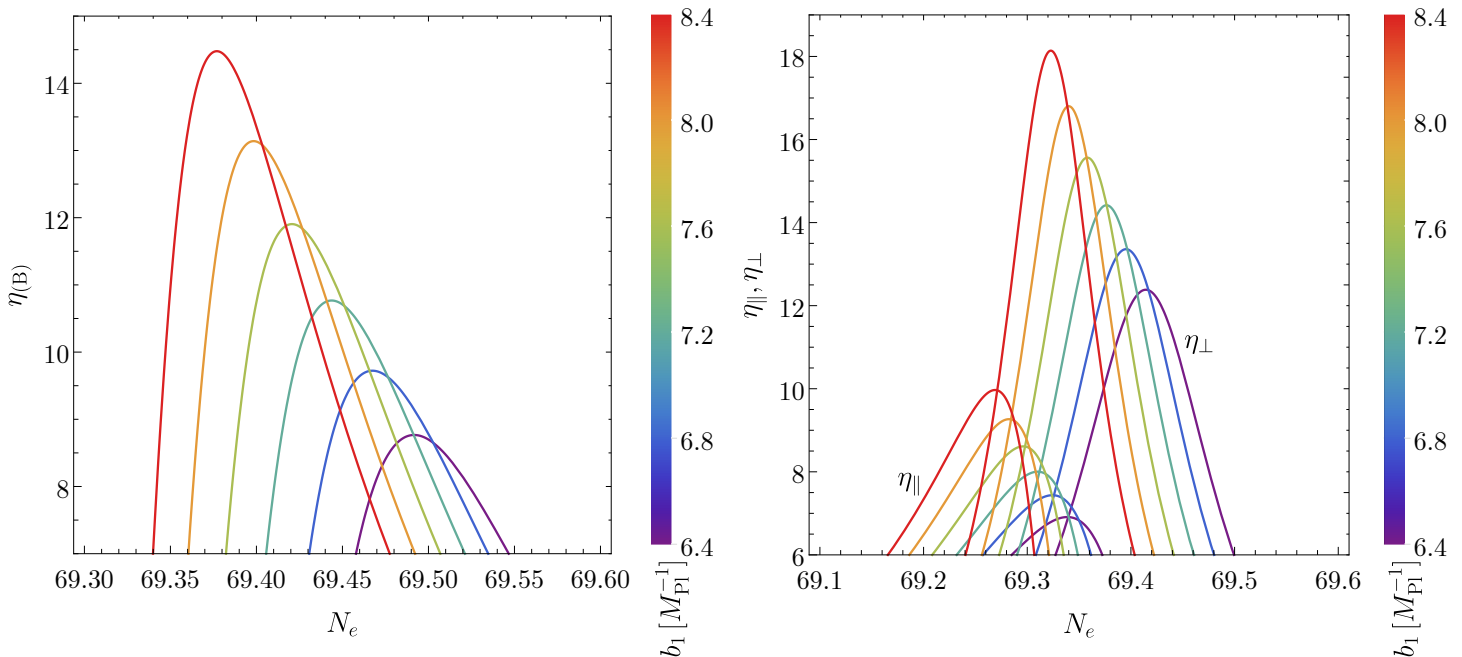


Figure 5.12: Top of the feature’s peak for the three η parameters ($\eta_{(B)}$ in the left panel, η_{\parallel} and η_{\perp} in the right one) in Braglia’s model [6, 7]. Varying the value of the parameter b_1 leads to variations in the local enhancement, and thus in the subsequent power spectrum.

on the curvature perturbation (see the increase in Ω_{TT}), and we thus expect to see an enhancement in its power spectrum $\mathcal{P}_{\mathcal{R}}$.

Furthermore, we see from Figure 5.13 that the higher the parameter b_1 is (i.e. the stronger the kinetic coupling between the scalar fields), the more violent the instability.

This enhancement of the curvature perturbation is indeed what we find in Figure 5.14 for the spectra of the single k -modes, $\mathcal{P}(k, N_e)$, and in Figure 5.15 for the overall curvature power spectrum, $\mathcal{P}_{\mathcal{R}}(k)$. The former follow the trend of the previous models, although they now depend strongly on the b_1 parameter; this is somewhat obfuscated by the considerable numerical errors in $\mathcal{P}_{\mathcal{S}}$.

The curvature power spectrum in Figure 5.15 is shown against the ratio of k to the *Planck* [19] normalisation $k_* = 0.005 \text{ Mpc}^{-1}$ and against the corresponding time of horizon exit, N_e^{HX} . It can be seen that, depending on the value of b_1 one chooses, the spectrum can be significantly enhanced with respect to the CMB value $A_s \sim 10^{-9}$. In particular, it can be enhanced by more than $\mathcal{O}(10^7)$.

The enhancement by $\mathcal{O}(10^7)$ is found for the curve with $b_1 = 7.6$. Higher values of the parameter give even stronger enhancement (up to $\sim \mathcal{O}(10^{10})$), which is more than required. We also see that the ΔN_e of the enhancement is well within the limit found at the end of Chapter 4. We can therefore conclude that this model is suitable for PBH production. We see in fact that the results shown in this Figure are consistent with those of the original authors: see [7, Figure 2].

* * *

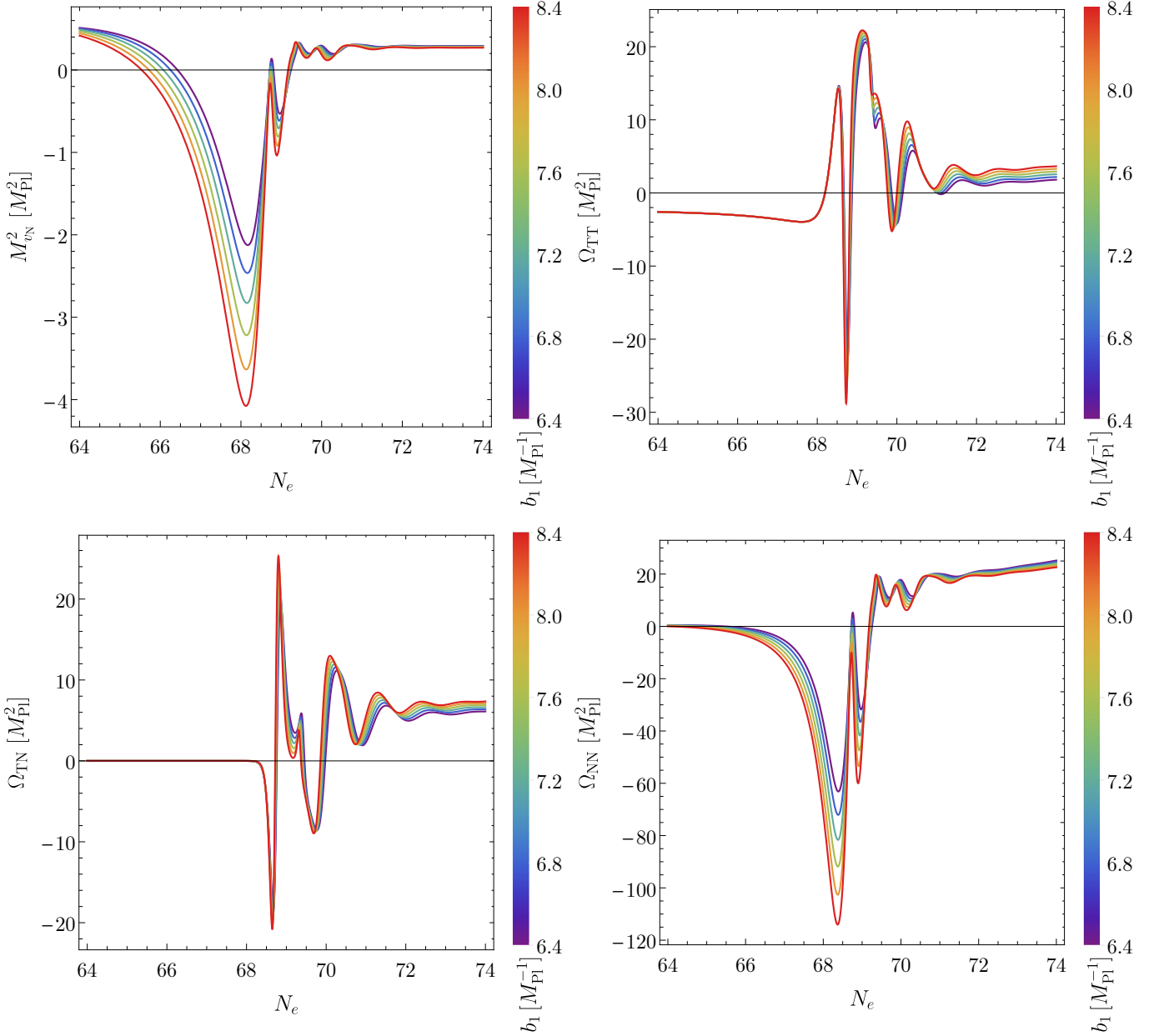


Figure 5.13: Temporal evolution of the mass matrix elements Ω_{IJ} , as well as the effective squared mass of the v^N -mode, $M_{v^N}^2$. All of these quantities exhibit a b_1 -dependent amplitude. *Top Left and Bottom Right panels:* The masses relating to the orthogonal mode v^N (itself proportional to the isocurvature perturbation) exhibit a transient tachyonic instability around the time of the feature, becoming negative and strongly enhanced.

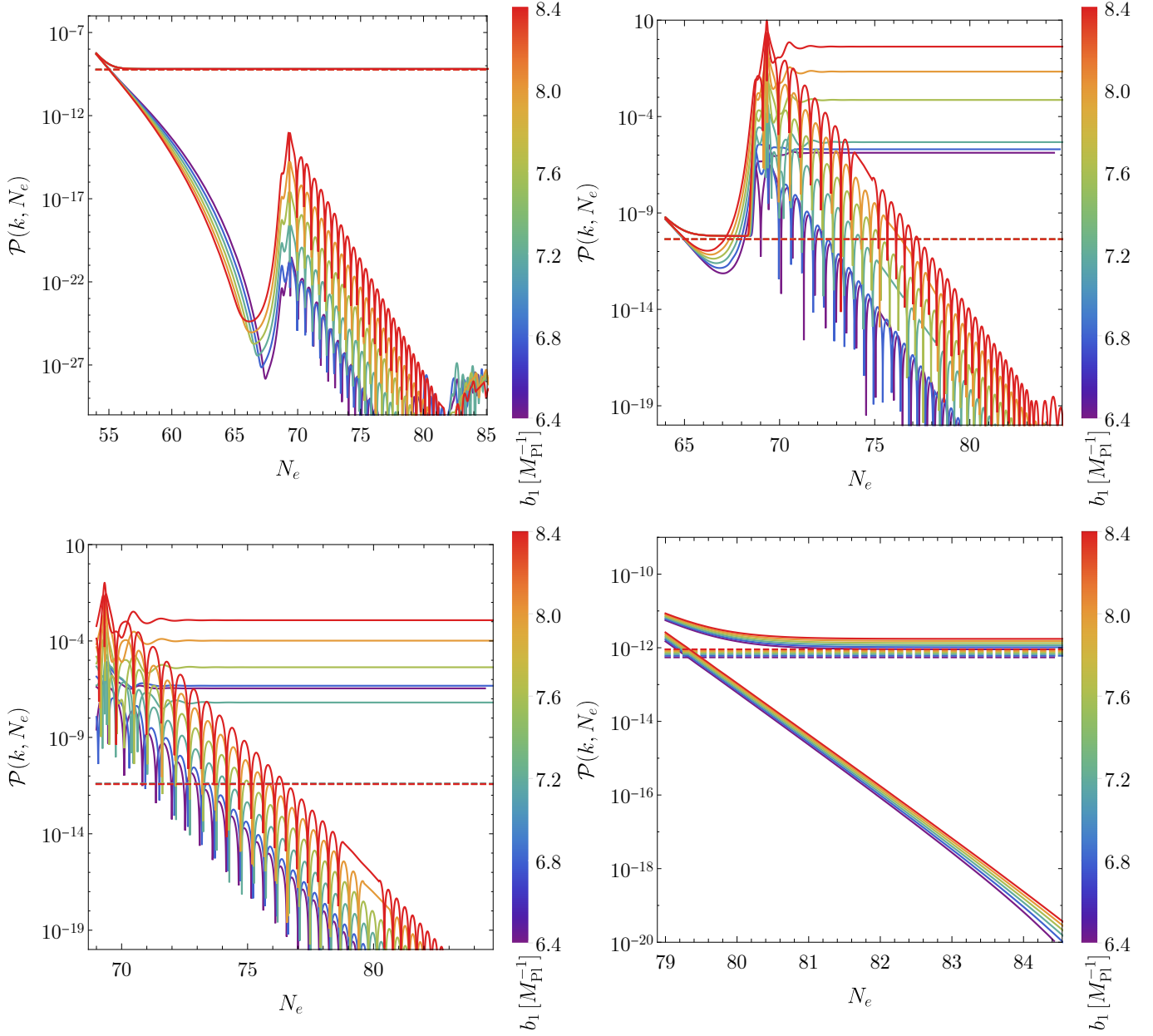


Figure 5.14: Temporal evolution of the curvature and isocurvature power spectra $\mathcal{P}_{\mathcal{R}}(k, N_e)$ and $\mathcal{P}_{\mathcal{S}}(k, N_e)$ for Braglia's model [6, 7]. The pseudo-single field value of the former, $\mathcal{P}_{\mathcal{R}}^{\text{1-field}}(k, N_e)$, is also shown (dashed lines). As for the case of Figure 5.3 and Figure 5.7, we illustrate k -modes exiting the horizon before, during, and after the feature takes place; the behaviour is as discussed in those Figures. It is evident here that higher- b_1 curves are more enhanced by the feature. The numerical errors on $\mathcal{P}_{\mathcal{S}}$ are quite large, but the general trend is visible.

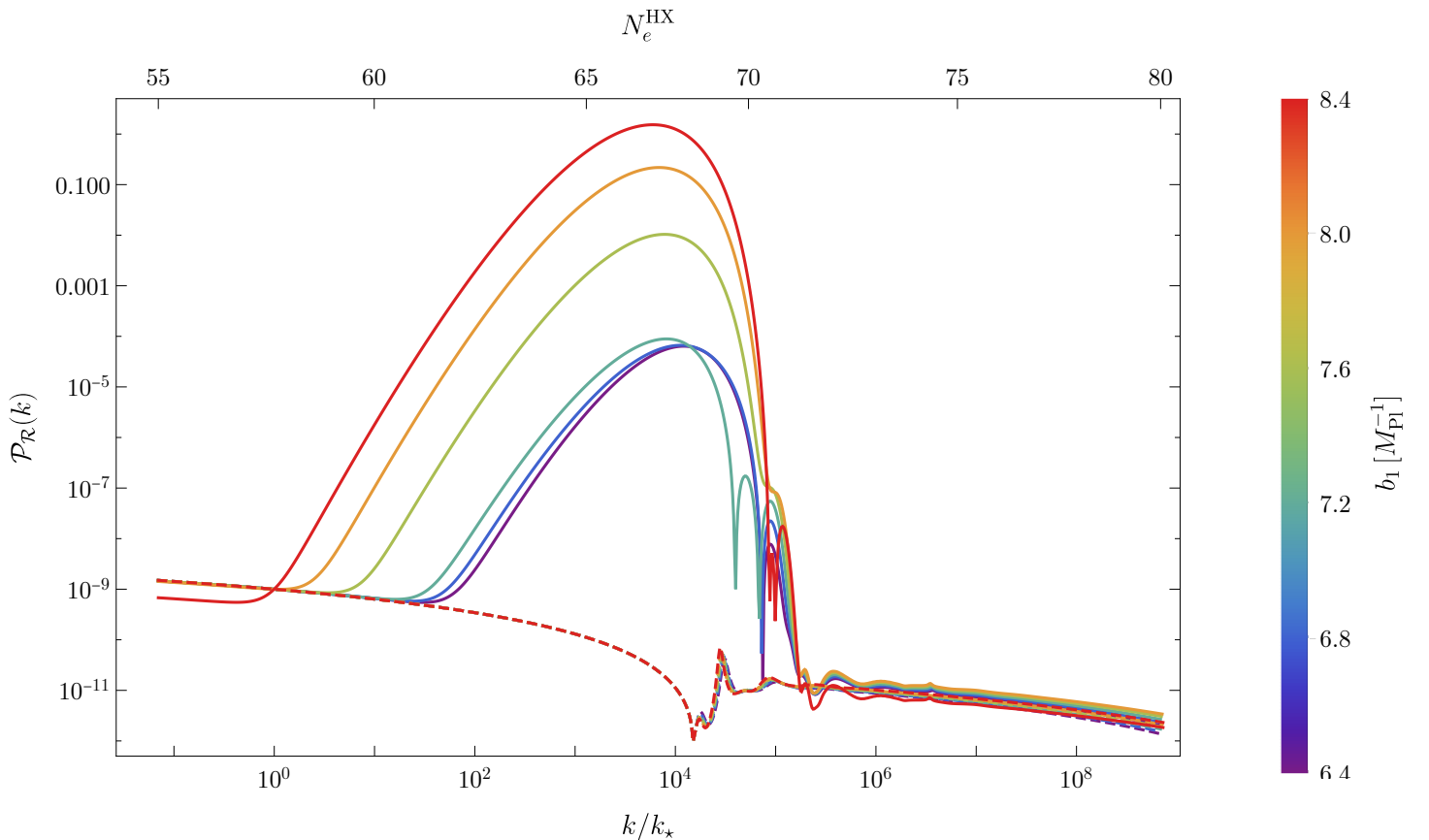


Figure 5.15: Curvature power spectrum $\mathcal{P}_{\mathcal{R}}(k)$ for Braglia’s model [6, 7]. The enhancement with respect to the single-field behaviour is evident, and strongly b_1 -dependent. Notice that the red line was not normalised correctly, and should be thought of as slightly shifted upwards.

Since this model has proven to be of phenomenological interest, a few additional remarks are in order. We first quote the value that the authors obtain for the spectral index of this power spectrum, that is $n_s = 0.9537$: this is in slight tension with *Planck*’s results [19]. This model is also used to calculate the induced GWs from PBH formation, suggesting they could be within the range of sensitivity of upcoming experiments. A modification of the model with the coupling $f(\varphi) = e^{2b_2\varphi^2}$ is also considered, finding similar results to ours and improving the tension on n_s .

Lastly, Kallosh & Linde [112] recently argued that such a model could be formulated in terms of α attractors, and interpreted as having a hyperbolic geometry. They then related the PBH masses and GW frequencies to the curvature of the Kähler geometry, which is simply given by $-b_1^2$, and develop a supergravity extension of the model. One interesting consequence of this study is a physical explanation for the sudden “drop” of the light field’s value at the time of tachyonic instability (see top left panel of 5.11); this would be due to a protection of the light (axion) field’s initial position caused by the Kähler curvature.

Chapter 6

Closing Remarks

6.1 Summary

Over the course of the year-long study that led to the writing of this thesis, we carefully analysed the theoretical framework of non-canonical \mathcal{N} -field inflation, as well as the production mechanisms for Primordial Black Holes. A numerical code (written in Mathematica) was then developed to compute the power spectra of curvature and isocurvature perturbations in models with $\mathcal{N} = 2$ scalar fields minimally coupled to gravity. This code is highly adaptable, allowing the user to define virtually any 2-field model they see fit (i.e. giving a potential, a field-space metric, and initial conditions on the fields' position and velocity). This was tested using known models, and was shown to be consistent with literature results.

* * *

In the first Chapter of this thesis, we gave a general introduction to the topic, providing a historical background of the field and highlighting the importance of our study. We discussed in an informal way the Standard Model of cosmology, its shortcomings, and inflation as a possible solution; the idea that Primordial Black Holes could explain the nature of the elusive Dark Matter was also introduced. This Chapter was aimed at as general a public as possible, allowing curious readers to get a sense of the topic with virtually no a-priori knowledge.

Chapter 2 then formalised our discussion, deriving cosmology's key dynamical equations to explain how our universe is composed and how it has evolved. This led us to the study of inflation in its standard single-field formalism, for which we reviewed the dynamics of the classical background fields, the Slow-Roll approximation, and briefly considered a simple concrete model.

The previous discussion was generalised in Chapter 3 to the case of \mathcal{N} interacting scalar fields driving inflation. Having extended our understanding of the background evolution to the multi-field framework, we proceeded to study the theory of cosmological

perturbations. Reviewing many important results, we wrote the linearised Einstein equations and eventually arrived to the Equations of Motion for the perturbations of the scalar fields about their background values. We then proceeded to quantise them, obtaining the main inflationary observables, that is the curvature and isocurvature power spectra.

Chapter 4 focused instead on Primordial Black Holes: we explained how they are formed from inflationary perturbations and in what way they could account for the Dark Matter content of the universe. We then summarised some of the most important observational constraints on PBHs' mass and abundance.

Finally, in Chapter 5, we focused on the most immediate $\mathcal{N} = 2$ case of multi-field inflation, showing how the dynamics simplify. Three particular models were then introduced: these are the ones we studied numerically with the code we developed. The evolution of the background quantities, the power spectra, and their implications for PBH production were analysed in each instance.

6.2 Conclusions

It was found that two-field models can exhibit a significant enhancement of the curvature power spectrum, mainly caused by a kinetic coupling in the field-space metric. The kinetic coupling is in fact reflected in a transient feature in the Slow-Roll parameters at the time of transition between two stages of inflation – the first one driven by the heavy field, and the second by the light field. The second SR parameter, η_{\perp} , represents the coupling between the evolution of curvature and isocurvature perturbations, and is greatly amplified in the presence of sharp turns in the inflationary trajectory. The above-mentioned feature causes a temporary tachyonic amplification of the isocurvature mode, and produces feedback on the curvature one. Finally, this leads to an enhancement of the primordial curvature power spectrum.

If the kinetic coupling is large enough, the resulting enhancement of the power spectrum can be compatible with the production of PBHs. In particular, these could be formed in one of the allowed mass ranges to be Dark Matter candidates, i.e. around masses of $M \sim 10^{-15} M_{\odot}$, $M \sim 10^{-12} M_{\odot}$, and to some extent $M \sim 10^{-6} M_{\odot}$. This fact could have important implications for our understanding of the universe.

6.3 Future Outlook

Continuing from this study, future work could focus on different 2-field models: using the same code and applying the same analysis, the search for PBHs could continue in slightly different directions. A discussion on additional models of interest was started, the criterion being to have a strong kinetic coupling between the fields. Additional potentials were briefly investigated as well. From the literature, the following models seemed to be promising candidates [113–115]; the goal would nevertheless be to develop a novel model.

CHAPTER 6. CLOSING REMARKS

Aside from its linear continuation, an extension of this work could be centred on analysing the related second-order production of Gravitational Waves (as done *e.g.* in [6]). Analysing departures from Gaussianity, such as by calculating their bispectrum [116], would also be important. Lastly, it would be interesting to consider a top-down approach, i.e. finding inflation models motivated by theoretical considerations rather than by phenomenology; this is often the case in models of Supersymmetry and string inflation such as [101, 117].

* * *

Multi-field inflation and the search for Primordial Black Holes are topics of great scientific interest, and a plethora of studies exists and continues growing. See for example the paper by Geller *et al.* [118] that just appeared on the arXiv, where the focus is set on fields non-minimally coupled to gravity.

Even if these inflationary theories were to be refuted by tighter future observational constraints, studying them would nevertheless have proven useful. For example, Cicoli *et al.* [119] recently postulated a model of late-time cosmology based on the same multi-field framework considered in this work. In a similar fashion, were PBHs to be ruled out as being the entirety of the universe's Dark Matter content, their study would still be important for astrophysical and cosmological processes, or for models of DM such as those considering a mixture of PBHs and WIMPs [51].

==== Acknowledgements ====

I am extremely thankful for all the people who I have had the chance of meeting over these years, whom I have grown up with, learned with, and thanks to whom I eventually became the person I am today. Thank you for your help, for reminding me to aim higher, and for – in some way or another – eventually making it possible for me to write this thesis.

First and foremost, I am grateful for Prof. Francisco Pedro for his supervision; for his valuable and always-on-point guidance and feedback, for his ever-present availability, and for his patience in bearing with me through these particularly challenging times.

A warm thank you goes to my parents for their ever-present support and understanding. It is thanks to them, as well as to all of my dear friends between Bologna, Brussels, and Manchester, that I have managed to get to where I am today. I am indeed standing on the shoulders of giants. I hope every single one of you know how much you matter to me.

Lastly, but surely not “leastly”, I want to thank all the people, both Professors and friends, with whom I have had the pleasure of exchanging ideas and discussing fascinating topics. This is what helps me remind myself of the reason I am studying theoretical physics when I start doubting myself, and what makes me go back to looking at the greater picture when I restrict my horizons to a very specific problem I may be faced with. In particular, I would like to thank Prof. Scott Kay and Dr. Simona Toscano, with whom I have really started understanding how scientific research works, and why it is what I aspire to keep working on.

Bibliography

- [1] A. H. Guth, “Inflationary universe: A possible solution to the horizon and flatness problems,” *Phys. Rev. D*, vol. 23, no. 2, p. 347, 1981, [DOI:10.1103/PhysRevD.23.347](https://doi.org/10.1103/PhysRevD.23.347).
- [2] G. F. Chapline, “Cosmological effects of primordial black holes,” *Nature*, vol. 253, no. 5489, pp. 251–252, 1975, [DOI:10.1038/253251a0](https://doi.org/10.1038/253251a0).
- [3] P. Ivanov, P. Naselsky, and I. Novikov, “Inflation and primordial black holes as dark matter,” *Phys. Rev. D*, vol. 50, no. 12, p. 7173, 1994, [DOI:10.1103/PhysRevD.50.7173](https://doi.org/10.1103/PhysRevD.50.7173).
- [4] I. Huston and A. J. Christopherson, “Calculating Non-adiabatic Pressure Perturbations during Multi-field Inflation,” *Phys. Rev. D*, vol. 85, no. 6, p. 063507, 2012, [arXiv:1111.6919](https://arxiv.org/abs/1111.6919).
- [5] A. Achúcarro, J.-O. Gong, S. Hardeman, G. A. Palma, and S. P. Patil, “Features of heavy physics in the CMB power spectrum,” *JCAP*, vol. 2011, no. 01, p. 030, 2011, [arXiv:1010.3693](https://arxiv.org/abs/1010.3693).
- [6] M. Braglia, D. K. Hazra, L. Sriramkumar, and F. Finelli, “Generating primordial features at large scales in two field models of inflation,” *JCAP*, vol. 2020, no. 08, p. 025, 2020, [arXiv:2004.00672](https://arxiv.org/abs/2004.00672).
- [7] M. Braglia, D. K. Hazra, F. Finelli, G. F. Smoot, L. Sriramkumar, and A. A. Starobinsky, “Generating PBHs and small-scale GWs in two-field models of inflation,” *JCAP*, vol. 2020, no. 08, p. 001, 2020, [arXiv:2005.02895](https://arxiv.org/abs/2005.02895).
- [8] A. Liddle, *An Introduction to Modern Cosmology*. John Wiley & Sons, 2015.
- [9] D. S. Gorbunov and V. A. Rubakov, *Introduction to the Theory of the Early Universe I: Hot Big Bang Theory*. World Scientific, 2011.
- [10] K. N. Abazajian, J. K. Adelman-McCarthy, M. A. Agüeros, S. S. Allam, C. A. Prieto, D. An, K. S. Anderson, S. F. Anderson, J. Annis, N. A. Bahcall, *et al.*, “The Seventh Data Release of the Sloan Digital Sky Survey ,” *ApJS*, vol. 182, no. 2, p. 543, 2009, [arXiv:0812.0649](https://arxiv.org/abs/0812.0649).

BIBLIOGRAPHY

- [11] A. Einstein, “Die Grundlage der allgemeinen Relativitätstheorie,” *Ann. Phys.*, vol. 354, no. 7, pp. 769–822, 1916, [DOI:10.1002/andp.19163540702](https://doi.org/10.1002/andp.19163540702).
- [12] A. Einstein, “Kosmologische Betrachtungen zur allgemeinen Relativitätstheorie,” *Sitzungsb. Königl. Preuss. Akad.*, pp. 142–152, 1917, [DOI:10.1002/3527608958.ch10](https://doi.org/10.1002/3527608958.ch10).
- [13] A. Friedman, “Über die Krümmung des Raumes,” *Z. Physik*, vol. 10, no. 1, pp. 377–386, 1922, [DOI:10.1007/BF01332580](https://doi.org/10.1007/BF01332580).
- [14] E. Hubble, “Extra-Galactic Nebulae,” *Contrib. Mount Wilson Obs. / Carnegie Inst. Washington*, vol. 324, pp. 1–49, 1926, [DOI:10.1086/143018](https://doi.org/10.1086/143018).
- [15] E. Hubble, “A relation between distance and radial velocity among extragalactic nebulae,” *Proc. Natl. Acad. Sci.*, vol. 15, no. 3, pp. 168–173, 1929, [DOI:10.1073/pnas.15.3.168](https://doi.org/10.1073/pnas.15.3.168).
- [16] M. Hamuy, M. Phillips, J. Maza, N. B. Suntzeff, R. Schommer, and R. Aviles, “A Hubble Diagram of Distant Type Ia Supernovae,” *AJ*, vol. 109, pp. 1–13, 1995, [DOI:10.1086/117251](https://doi.org/10.1086/117251).
- [17] A. R. Liddle and D. H. Lyth, *Cosmological Inflation and Large-Scale Structure*. Cambridge University Press, 2000.
- [18] G. Lemaître, “Un Univers homogène de masse constante et de rayon croissant rendant compte de la vitesse radiale des nébuleuses extra-galactiques,” vol. 47, pp. 49–59, 1927, [Bibcode:1927ASSB...47...49L](https://bibcode.org/1927ASSB...47...49L).
- [19] [Planck Collaboration], N. Aghanim, *et al.*, “Planck 2018 results. VI. Cosmological parameters,” *A&A*, vol. 641, p. A6, 2020, [arXiv:1807.06209](https://arxiv.org/abs/1807.06209).
- [20] A. G. Riess, W. Yuan, L. M. Macri, D. Scolnic, D. Brout, S. Casertano, D. O. Jones, Y. Murakami, L. Breuval, T. G. Brink, *et al.*, “A Comprehensive Measurement of the Local Value of the Hubble Constant with 1 km/s/Mpc Uncertainty from the Hubble Space Telescope and the SH0ES Team,” 2021, [arXiv:2112.04510](https://arxiv.org/abs/2112.04510).
- [21] E. Abdalla, G. F. Abellán, A. Aboubrahim, A. Agnello, Ö. Akarsu, Y. Akrami, G. Alestas, D. Aloni, L. Amendola, L. A. Anchordoqui, *et al.*, “Cosmology Intertwined: A Review of the Particle Physics, Astrophysics, and Cosmology Associated with the Cosmological Tensions and Anomalies,” *JHEP*, 2022, [arXiv:2203.06142](https://arxiv.org/abs/2203.06142).
- [22] A. Blanchard, J.-Y. Héloret, S. Ilić, B. Lamine, and I. Tutusaus, “ Λ CDM is alive and well,” 2022, [arXiv:2205.05017](https://arxiv.org/abs/2205.05017).
- [23] G. Lemaître, “The Beginning of the World from the Point of View of Quantum Theory,” *Nature*, vol. 127, no. 3210, pp. 706–706, 1931, [DOI:10.1038/127706b0](https://doi.org/10.1038/127706b0).
- [24] R. A. Alpher, H. Bethe, and G. Gamow, “The origin of chemical elements,” *Phys. Rev.*, vol. 73, no. 7, p. 803, 1948, [DOI:10.1103/PhysRev.73.803](https://doi.org/10.1103/PhysRev.73.803).
- [25] R. A. Alpher and R. C. Herman, “On the relative abundance of the elements,” *Phys. Rev.*, vol. 74, no. 12, p. 1737, 1948, [DOI:10.1103/PhysRev.74.1737](https://doi.org/10.1103/PhysRev.74.1737).

BIBLIOGRAPHY

- [26] A. A. Penzias and R. W. Wilson, “A measurement of excess antenna temperature at 4080 mc/s.,” *ApJ*, vol. 142, pp. 419–421, 1965, DOI:10.1086/148307.
- [27] V. C. Rubin, W. K. Ford Jr, and N. Thonnard, “Rotational properties of 21 SC galaxies with a large range of luminosities and radii, from NGC 4605 (R=4kpc) to UGC 2885 (R=122 kpc),” *ApJ*, vol. 238, pp. 471–487, 1980, DOI:10.1086/158003.
- [28] G. Bertone and D. Hooper, “History of Dark Matter,” *Rev. Mod. Phys.*, vol. 90, no. 4, p. 045002, 2018, arXiv:1605.04909.
- [29] A. G. Riess, A. V. Filippenko, P. Challis, A. Clocchiatti, A. Diercks, P. M. Garnavich, R. L. Gilliland, C. J. Hogan, S. Jha, R. P. Kirshner, *et al.*, “Observational Evidence from Supernovae for an Accelerating Universe and a Cosmological Constant,” *ApJ*, vol. 116, no. 3, p. 1009, 1998, arXiv:astro-ph/9805201.
- [30] “Image: Timeline of the Universe,” NASA, available at map.gsfc.nasa.gov [last accessed January 2022].
- [31] D. S. Gorbunov and V. A. Rubakov, *Introduction to the Theory of the Early Universe II: Cosmological Perturbations and Inflationary Theory*. World Scientific, 2011.
- [32] V. Mukhanov, *Physical Foundations of Cosmology*. Cambridge University Press, 2005.
- [33] D. Fixsen, “The temperature of the cosmic microwave background,” *ApJ*, vol. 707, no. 2, p. 916, 2009, arXiv:0911.1955.
- [34] M. Dine and A. Kusenko, “The Origin of the Matter-Antimatter Asymmetry,” *Rev. Mod. Phys.*, vol. 76, no. 1, p. 1, 2003, arXiv:hep-ph/0303065.
- [35] A. De Felice and S. Tsujikawa, “ $f(R)$ Theories,” *Living Rev. Relativ.*, vol. 13, no. 1, pp. 1–161, 2010, arXiv:1002.4928.
- [36] M. Milgrom, “A modification of the Newtonian dynamics as a possible alternative to the hidden mass hypothesis,” *ApJ*, vol. 270, pp. 365–370, 1983, DOI:10.1086/161130.
- [37] S. Bahamonde, K. F. Dialektopoulos, C. Escamilla-Rivera, G. Farrugia, V. Gakis, M. Hendry, M. Hohmann, J. L. Said, J. Mifsud, and E. Di Valentino, “Teleparallel Gravity: from Theory to Cosmology,” 2021, arXiv:2106.13793.
- [38] A. Linde, *Particle Physics and Inflationary Cosmology*. CRC Press, 1990.
- [39] A. H. Guth, *The Inflationary Universe: the Quest for a New Theory of Cosmic Origins*. Vintage Books, 1998.
- [40] A. D. Linde, “A new inflationary universe scenario: A possible solution of the horizon, flatness, homogeneity, isotropy and primordial monopole problems,” *Phys. Lett.*, vol. 108B, no. 6, pp. 389–393, 1982, DOI:10.1016/0370-2693(82)91219-9.
- [41] A. Albrecht and P. J. Steinhardt, “Cosmology for Grand Unified Theories with Radiatively Induced Symmetry Breaking,” *Phys. Rev. Lett.*, vol. 48, no. 17, p. 1220, 1982, DOI:10.1103/PhysRevLett.48.1220.

BIBLIOGRAPHY

- [42] M. Alishahiha, E. Silverstein, and D. Tong, “DBI in the Sky: Non-Gaussianity from inflation with a speed limit,” *Phys. Rev. D*, vol. 70, no. 12, p. 123505, 2004, [arXiv:hep-th/0404084](#).
- [43] C. Armendariz-Picon, T. Damour, and V.-i. Mukhanov, “k-Inflation,” *Phys. Lett. B*, vol. 458, no. 2-3, pp. 209–218, 1999, [arXiv:hep-th/9904075](#).
- [44] A. D. Linde, “Chaotic inflation,” *Phys. Lett.*, vol. 129B, no. 3-4, pp. 177–181, 1983, [DOI:10.1016/0370-2693\(83\)90837-7](#).
- [45] K. Griest and M. Kamionkowski, “Supersymmetric Dark Matter,” *Phys. Rep.*, vol. 333, pp. 167–182, 2000, [arXiv:hep-ph/9506380](#).
- [46] [LIGO/Virgo Collaboration], B. P. Abbott, *et al.*, “Observation of Gravitational Waves from a Binary Black Hole Merger,” *Phys. Rev. Lett.*, vol. 116, no. 6, p. 061102, 2016, [arXiv:1602.03837](#).
- [47] Event Horizon Telescope Collaboration, K. Akiyama, *et al.*, “First M87 Event Horizon Telescope Results. I. The Shadow of the Supermassive Black Hole,” *ApJ Lett.*, vol. 875, no. L1, 2019, [arXiv:1906.11238](#).
- [48] Event Horizon Telescope Collaboration, K. Akiyama, *et al.*, “First Sagittarius A* Event Horizon Telescope Results. I. The Shadow of the Supermassive Black Hole in the Center of the Milky Way,” *ApJ Lett.*, vol. 930, no. L12, 2022, [DOI:10.3847/2041-8213/ac6674](#).
- [49] Ya. B. Zel’dovich and I. D. Novikov, “The Hypothesis of Cores Retarded during Expansion and the Hot Cosmological Model,” *Astronomicheskii Zhurnal*, vol. 43, p. 758, 1966, [DOI:1966AZh...43..758Z](#).
- [50] S. Hawking, “Gravitationally Collapsed Objects of Very Low Mass,” *MNRAS*, vol. 152, no. 1, pp. 75–78, 1971, [DOI:10.1093/mnras/152.1.75](#).
- [51] B. Carr and F. Kühnel, “Primordial Black Holes as Dark Matter Candidates,” *SciPost Physics Lecture Notes*, p. 048, 2021, [arXiv:2110.02821](#).
- [52] S. Dodelson, *Modern Cosmology*. Elsevier, 2003.
- [53] D. Baumann, “TASI Lectures on Inflation,” 2012, [arXiv:0907.5424](#).
- [54] S. Weinberg, *Cosmology*. Oxford University Press, 2008.
- [55] E. Kolb and M. Turner, *The Early Universe*. Addison–Wesley, 1988.
- [56] S. Weinberg, *Gravitation and Cosmology: principles and applications of the general theory of relativity*. John Wiley & Sons, 1972.
- [57] W. de Sitter, “On the relativity of inertia. Remarks concerning Einstein’s latest hypothesis,” *Proc. Kon. Ned. Acad. Wet.*, vol. 19, no. 2, pp. 1217–1225, 1917, [Bibcode:1917KNAB...19.1217D](#).

BIBLIOGRAPHY

- [58] E. Di Valentino, A. Melchiorri, and J. Silk, “Planck evidence for a closed Universe and a possible crisis for cosmology,” *Nat. Astron.*, pp. 1–8, 2019, [arXiv:1911.02087](#).
- [59] K. Lozanov, *Reheating After Inflation*. Springer, 2020.
- [60] R. Allahverdi, R. Brandenberger, F.-Y. Cyr-Racine, and A. Mazumdar, “Reheating in Inflationary Cosmology: Theory and Applications,” *Annu. Rev. Nucl. Part. Sci.*, vol. 60, pp. 27–51, 2010, [DOI:10.1146/annurev.nucl.012809.104511](#).
- [61] S. Weinberg, “Adiabatic Modes in Cosmology,” *Phys. Rev. D*, vol. 67, no. 12, p. 123504, 2003, [arXiv:astro-ph/030232](#).
- [62] D. Wands, K. A. Malik, D. H. Lyth, and A. R. Liddle, “New approach to the evolution of cosmological perturbations on large scales,” *Phys. Rev. D*, vol. 62, no. 4, p. 043527, 2000, [arXiv:astro-ph/0003278](#).
- [63] M. Lemoine, J. Martin, and P. Peter, *Inflationary Cosmology*, vol. 738. Springer, 2007.
- [64] J. M. Bardeen, “Gauge-invariant cosmological perturbations,” *Phys. Rev. D*, vol. 22, no. 8, p. 1882, 1980, [DOI:10.1103/PhysRevD.22.1882](#).
- [65] D. Baumann, “The Physics of Inflation,” *Lectures at the ICTP, Trieste, Italy*, 2011, available at [ictp.res.in](#) [last accessed March 2022].
- [66] S. Groot Nibbelink and B. J. W. van Tent, “Scalar perturbations during multiple-field slow-roll inflation,” *Class. Quantum Gravity*, vol. 19, no. 4, p. 613, 2002, [arXiv:hep-ph/0107272](#).
- [67] S. Groot Nibbelink and B. J. W. van Tent, “Density perturbations arising from multiple field slow-roll inflation,” 2000, [arXiv:hep-ph/0011325](#).
- [68] B. A. Bassett, S. Tsujikawa, and D. Wands, “Inflation Dynamics and Reheating,” *Rev. Mod. Phys.*, vol. 78, no. 2, p. 537, 2006, [arXiv:astro-ph/0507632](#).
- [69] A. R. Liddle and S. M. Leach, “How long before the end of inflation were observable perturbations produced?,” *Phys. Rev. D*, vol. 68, no. 10, p. 103503, 2003, [arXiv:astro-ph/0305263S](#).
- [70] A. A. Starobinsky, “Multicomponent de Sitter (inflationary) stages and the generation of perturbations,” *JETP Lett.*, vol. 42, no. 3, pp. 152–155, 1985, [Bibcode:1985JETPL..42..152S](#).
- [71] J. Silk and M. S. Turner, “Double inflation,” *Phys. Rev. D*, vol. 35, no. 2, p. 419, 1987, [DOI:10.1103/PhysRevD.35.419](#).
- [72] C. Gordon, D. Wands, B. A. Bassett, and R. Maartens, “Adiabatic and entropy perturbations from inflation,” *Phys. Rev. D*, vol. 63, no. 2, p. 023506, 2000, [arXiv:astro-ph/0009131](#).

BIBLIOGRAPHY

- [73] C. M. Peterson and M. Tegmark, “Testing Two-Field Inflation,” *Phys. Rev. D*, vol. 83, no. 2, p. 023522, 2011, [arXiv:1005.4056](#).
- [74] R. Bravo, G. A. Palma, and S. Riquelme, “A Tip for Landscape Riders: Multi-Field Inflation Can Fulfill the Swampland Distance Conjecture,” *JCAP*, vol. 2020, no. 02, p. 004, 2020, [arXiv:1906.05772](#).
- [75] F. Di Marco, F. Finelli, and R. Brandenberger, “Adiabatic and Isocurvature Perturbations for Multifield Generalized Einstein Models,” *Phys. Rev. D*, vol. 67, no. 6, p. 063512, 2003, [arXiv:astro-ph/0211276](#).
- [76] C. M. Peterson and M. Tegmark, “Testing Multi-Field Inflation: A Geometric Approach,” *Phys. Rev. D*, vol. 87, no. 10, p. 103507, 2013, [arXiv:1111.0927](#).
- [77] V. F. Mukhanov, H. A. Feldman, and R. H. Brandenberger, “Theory of cosmological perturbations,” *Phys. Rep.*, vol. 215, no. 5-6, pp. 203–333, 1992, [DOI:10.1016/0370-1573\(92\)90044-Z](#).
- [78] J. M. Stewart, “Perturbations of Friedmann–Robertson–Walker cosmological models,” *Class. Quantum Gravity*, vol. 7, no. 7, pp. 1169–1180, 1990, [DOI:10.1088/0264-9381/7/7/013](#).
- [79] V. F. Mukhanov, “Quantum theory of gauge-invariant cosmological perturbations,” *Sov. Phys. JETP*, vol. 94, no. 1, 1988, [Bibcode:1988JETP..67.1297M](#).
- [80] M. Sasaki, “Large Scale Quantum Fluctuations in the Inflationary Universe,” *Progr. Theor. Phys.*, vol. 76, no. 5, pp. 1036–1046, 1986, [DOI:10.1143/PTP.76.1036](#).
- [81] A. D. Linde, “Generation of isothermal density perturbations in the inflationary universe,” *Phys. Lett.*, vol. 158B, no. 5, pp. 375–380, 1985, [DOI:10.1016/0370-2693\(85\)90436-8](#).
- [82] H. Kodama and M. Sasaki, “Cosmological Perturbation Theory,” *Progr. Theor. Phys. Suppl.*, vol. 78, pp. 1–166, 1984, [DOI:10.1143/PTPS.78.1](#).
- [83] T. T. Nakamura and E. D. Stewart, “The spectrum of cosmological perturbations produced by a multi-component inflaton to second order in the slow-roll approximation,” *Phys. Lett. B*, vol. 381, no. 4, pp. 413–419, 1996, [arXiv:astro-ph/9604103](#).
- [84] M. Sasaki and E. D. Stewart, “A General Analytic Formula for the Spectral Index of the Density Perturbations produced during Inflation,” *Prog. Theor. Phys.*, vol. 95, no. 1, pp. 71–78, 1996, [arXiv:astro-ph/9507001](#).
- [85] R. Arnowitt, S. Deser, and C. W. Misner, “Republication of: The dynamics of general relativity,” *General Relativity and Gravitation*, vol. 40, no. 9, pp. 1997–2027, 2008, [DOI:10.1007/s10714-008-0661-1](#).
- [86] N. Bartolo, E. Komatsu, S. Matarrese, and A. Riotto, “Non-Gaussianity from inflation: Theory and observations,” *Phys. Rep.*, vol. 402, no. 3-4, pp. 103–266, 2004, [DOI:10.1016/j.physrep.2004.08.022](#).

BIBLIOGRAPHY

- [87] Y. Wang, “Inflation, Cosmic Perturbations and Non-Gaussianities,” *Commun. Theor. Phys.*, vol. 62, no. 1, p. 109, 2014, [DOI:10.1088/0253-6102/62/1/19](https://doi.org/10.1088/0253-6102/62/1/19).
- [88] [Planck Collaboration], Y. Akrami, *et al.*, “Planck 2018 results. IX. Constraints on primordial non-Gaussianity,” *A&A*, vol. 641, p. A10, 2020, [arXiv:1905.05697](https://arxiv.org/abs/1905.05697).
- [89] A. Achúcarro, M. Biagetti, M. Braglia, G. Cabass, E. Castorina, R. Caldwell, X. Chen, W. Coulton, R. Flauger, J. Fumagalli, *et al.*, “Inflation: Theory and Observations,” 2022, [arXiv:2203.08128](https://arxiv.org/abs/2203.08128).
- [90] N. Pedron, M. Cicoli, and F. G. Pedro, “Gravitational Waves from Primordial Black Holes in String Inflation,” Master’s thesis, Dipartimento di Fisica e Astronomia, Alma Mater Studiorum, Università degli Studi di Bologna, 2020, [available from amslaurea.unibo.it](https://amslaurea.unibo.it).
- [91] S. W. Hawking, “Black hole explosions?,” *Nature*, vol. 248, no. 5443, pp. 30–31, 1974, [DOI:10.1038/248030a0](https://doi.org/10.1038/248030a0).
- [92] I. Musco and J. C. Miller, “Primordial black hole formation in the early universe: critical behaviour and self-similarity,” *Class. Quantum Gravity*, vol. 30, no. 14, p. 145009, 2013, [DOI:10.1088/0264-9381/30/14/145009](https://doi.org/10.1088/0264-9381/30/14/145009).
- [93] T. Harada, C.-M. Yoo, and K. Kohri, “Threshold of primordial black hole formation,” *Phys. Rev. D*, vol. 88, no. 8, p. 084051, 2013, [arXiv:1309.4201](https://arxiv.org/abs/1309.4201).
- [94] A. M. Green and B. J. Kavanagh, “Primordial Black Holes as a dark matter candidate,” *J. Phys. G: Nucl. Part. Phys.*, vol. 48, no. 4, p. 043001, 2021, [arXiv:2007.10722](https://arxiv.org/abs/2007.10722).
- [95] W. H. Press and P. Schechter, “Formation of Galaxies and Clusters of Galaxies by Self-Similar Gravitational Condensation,” *ApJ*, vol. 187, pp. 425–438, 1974, [DOI:10.1086/152650](https://doi.org/10.1086/152650).
- [96] B. J. Carr, “The primordial black hole mass spectrum,” *ApJ*, vol. 201, pp. 1–19, 1975, [DOI:10.1086/153853](https://doi.org/10.1086/153853).
- [97] H. Motohashi and W. Hu, “Primordial Black Holes and Slow-Roll Violation,” *Phys. Rev. D*, vol. 96, no. 6, p. 063503, 2017, [arXiv:1706.06784](https://arxiv.org/abs/1706.06784).
- [98] K. Ando, K. Inomata, and M. Kawasaki, “Primordial black holes and uncertainties in the choice of the window function,” *Phys. Rev. D*, vol. 97, no. 10, p. 103528, 2018, [arXiv:1802.06393](https://arxiv.org/abs/1802.06393).
- [99] S. Young, C. T. Byrnes, and M. Sasaki, “Calculating the mass fraction of primordial black holes,” *JCAP*, vol. 2014, no. 07, p. 045, 2014, [arXiv:1405.7023](https://arxiv.org/abs/1405.7023).
- [100] C. Germani and T. Prokopec, “On primordial black holes from an inflection point,” *Phys. Dark Universe*, vol. 18, pp. 6–10, 2017, [arXiv:1706.04226](https://arxiv.org/abs/1706.04226).
- [101] M. Cicoli, V. A. Diaz, and F. G. Pedro, “Primordial Black Holes from String Inflation,” *JCAP*, vol. 2018, no. 06, p. 034, 2018, [arXiv:1803.02837](https://arxiv.org/abs/1803.02837).

BIBLIOGRAPHY

- [102] M. Sasaki, T. Suyama, T. Tanaka, and S. Yokoyama, “Primordial Black Holes – Perspectives in Gravitational Wave Astronomy,” *Class. Quantum Gravity*, vol. 35, no. 6, p. 063001, 2018, [arXiv:1801.05235](#).
- [103] B. Carr and F. Kühnel, “Primordial Black Holes as Dark Matter: Recent Developments,” *Ann. Rev. Nucl. Part. Sci.*, vol. 70, pp. 355–394, 2020, [arXiv:2006.02838](#).
- [104] B. Carr, K. Kohri, Y. Sendouda, and J. Yokoyama, “Constraints on primordial black holes,” *Phys. Rep.*, vol. 84, no. 11, p. 116902, 2021, [arXiv:2002.12778](#).
- [105] K. Inomata, M. Kawasaki, K. Mukaida, Y. Tada, and T. T. Yanagida, “Inflationary Primordial Black Holes as All Dark Matter,” *Phys. Rev. D*, vol. 96, no. 4, p. 043504, 2017, [arXiv:1701.02544](#).
- [106] B. J. Kavanagh, “PBHbounds: A collection of bounds on PBHs and code for plotting them,” Nov. 2019, [DOI:10.5281/zenodo.3538998](#).
- [107] D. Langlois, “Correlated adiabatic and isocurvature perturbations from double inflation,” *Phys. Rev. D*, vol. 59, no. 12, p. 123512, 1999, [arXiv:astro-ph/9906080](#).
- [108] A. Avgoustidis, S. Cremonini, A.-C. Davis, R. H. Ribeiro, K. Turzyński, and S. Watson, “The Importance of Slow-Roll Corrections during Multi-field Inflation,” *JCAP*, vol. 2012, no. 02, p. 038, 2012, [arXiv:1110.4081](#).
- [109] R. Kallosh, A. Linde, and Y. Yamada, “Planck 2018 and Brane Inflation Revisited,” *JHEP*, vol. 2019, no. 1, pp. 1–28, 2019, [arXiv:1811.01023](#).
- [110] J. Martin, C. Ringeval, and V. Vennin, “Encyclopædia Inflationaris,” *Phys. Dark Univ.*, vol. 5, pp. 75–235, 2014, [arXiv:1303.3787](#).
- [111] G. Feinberg, “Possibility of Faster-Than-Light Particles,” *Phys. Rev.*, vol. 159, no. 5, p. 1089, 1967, [DOI:10.1103/PhysRev.159.1089](#).
- [112] R. Kallosh and A. Linde, “Dilaton-Axion Inflation with PBHs and GWs,” 2022, [arXiv:2203.10437](#).
- [113] M. Cicoli, V. Guidetti, F. G. Pedro, and G. P. Vacca, “A geometrical instability for ultra-light fields during inflation?,” *JCAP*, vol. 2018, no. 12, p. 037, 2018, [arXiv:1807.03818](#).
- [114] A. Achúcarro, V. Atal, C. Germani, and G. A. Palma, “Cumulative effects in inflation with ultra-light entropy modes,” *JCAP*, vol. 2017, no. 02, p. 013, 2017, [arXiv:1607.08609](#).
- [115] P. Christodoulidis, D. Roest, and E. I. Sfakianakis, “Attractors, Bifurcations and Curvature in Multi-field Inflation,” *JCAP*, vol. 2020, no. 08, p. 006, 2020, [arXiv:1903.03513](#).
- [116] D. I. Kaiser, E. A. Mazenc, and E. I. Sfakianakis, “Primordial Bispectrum from Multifield Inflation with Nonminimal Couplings,” *Phys. Rev. D*, vol. 87, no. 6, p. 064004, 2013, [arXiv:1210.7487](#).

BIBLIOGRAPHY

- [117] F. G. Pedro and A. Westphal, “Flattened Axion Monodromy Beyond Two Derivatives,” *Phys. Rev. D*, vol. 101, no. 4, p. 043501, 2020, [arXiv:1909.08100](#).
- [118] S. Geller, W. Qin, E. McDonough, and D. I. Kaiser, “Primordial Black Holes from Multifield Inflation with Nonminimal Couplings,” 2022, [arXiv:2205.04471](#).
- [119] M. Cicoli, G. Dibitetto, and F. G. Pedro, “New accelerating solutions in late-time cosmology,” *Phys. Rev. D*, vol. 101, no. 10, p. 103524, 2020, [arXiv:2002.02695](#).

Appendix A

Key Elements of General Relativity

Some of the basic definitions and results of General Relativity, which were used throughout this work, are stated in the present Appendix. The aim is not to be thorough or self-contained, but rather to provide a very short summary of key equations. The reader is strongly encouraged to refer to General Relativity textbooks such as [56] for more detailed discussions.

A.1 Basic Definitions

Spacetime manifolds are endowed with a *metric* which describes its geometrical properties. For a line element ds , the metric tensor $g_{\mu\nu}$ satisfies

$$ds^2 \equiv g_{\mu\nu} dx^\mu dx^\nu . \quad (\text{A.1})$$

We only consider four-dimensional spacetimes in this work, and adopt the $(-+++)$ signature. The Einstein summation over repeated indices is implied. The metric tensor is symmetric, $g_{\mu\nu} = g_{\nu\mu}$, and its inverse, $g^{\mu\nu}$, satisfies

$$g^{\mu\nu} g_{\nu\lambda} = \delta_\lambda^\mu ,$$

where δ_ν^μ is the usual Kronecker delta ($\delta_\nu^\mu = 1$ if $\mu = \nu$, and 0 otherwise). The metric tensor and its inverse are used to raise and lower spacetime indices.

The simplest spacetime metric is the Minkowski one, which reads

$$ds^2 = -dt^2 + \delta_{ij} dx^i dx^j . \quad (\text{A.2})$$

The Minkowski metric tensor then corresponds to the diagonal matrix

$$g_{\mu\nu}^{(M)} = \text{diag}(-1, +1, +1, +1) .$$

APPENDIX A. KEY ELEMENTS OF GENERAL RELATIVITY

When studying cosmology, a metric that satisfies the cosmological principle (homogeneity and isotropy of the large-scale universe, see §1.1) is required. This is provided by the Friedmann–Lemaître–Robertson–Walker (FLRW) metric discussed in §2.1, that is

$$ds^2 = -dt^2 + a^2(t) \left[\frac{dr^2}{1 - kr^2} + r^2 d\Omega^2 \right] . \quad (\text{A.3})$$

For the case of a flat universe, i.e. $k = 0$, the FLRW metric tensor reduces to

$$g_{\mu\nu}^{(\text{FLRW}, k=0)} = \text{diag}(-1, +a^2, +a^2, +a^2) .$$

A plethora of metrics exist that categorise equivalently many spacetime manifolds, such as the Schwarzschild metric for ordinary non-rotating Black Holes. These are nevertheless beyond the scope of this work.

* * *

For a given metric $g_{\mu\nu}$, one can define the *Christoffel symbols* (or *affine connection*),

$$\Gamma_{\mu\nu}^{\lambda} = \frac{1}{2} g^{\lambda\sigma} (\partial_{\mu} g_{\nu\sigma} + \partial_{\nu} g_{\mu\sigma} - \partial_{\sigma} g_{\mu\nu}) , \quad (\text{A.4})$$

where the shorthand notation $\partial_{\mu} \equiv \partial/\partial x^{\mu}$ was used. Note that the Christoffel symbols are symmetric in their lower indices, $\Gamma_{\mu\nu}^{\lambda} = \Gamma_{\nu\mu}^{\lambda}$. An important property of the Christoffel symbols is that when contracting indices,

$$\Gamma_{\nu\mu}^{\mu} = \partial_{\nu} \ln \sqrt{-g} ,$$

with $g = \det g_{\mu\nu}$ the determinant of the metric tensor.

Building upon this, the *Riemann tensor* can be defined as

$$R^{\lambda}_{\mu\nu\sigma} = \partial_{\nu} \Gamma_{\mu\sigma}^{\lambda} - \partial_{\sigma} \Gamma_{\mu\nu}^{\lambda} + \Gamma_{\nu\alpha}^{\lambda} \Gamma_{\sigma\mu}^{\alpha} - \Gamma_{\sigma\alpha}^{\lambda} \Gamma_{\nu\mu}^{\alpha} . \quad (\text{A.5})$$

Contracting the Riemann tensor, one obtains the *Ricci tensor*, that is [31, Equation (A.41)]

$$R_{\mu\nu} = R^{\lambda}_{\mu\lambda\nu} = \partial_{\lambda} \Gamma_{\mu\nu}^{\lambda} - \partial_{\nu} \Gamma_{\mu\lambda}^{\lambda} + \Gamma_{\mu\nu}^{\lambda} \Gamma_{\lambda\sigma}^{\sigma} - \Gamma_{\mu\sigma}^{\lambda} \Gamma_{\lambda\nu}^{\sigma} . \quad (\text{A.6})$$

Contracting this again allows for the determination of the *Ricci (curvature) scalar*,

$$R = R^{\mu}_{\mu} = g^{\mu\nu} R_{\mu\nu} . \quad (\text{A.7})$$

* * *

Another important concept is that of the *geodesic equation*, where we remind that a geodesic is the shortest line between two spacetime points. For the four-velocity $u^{\mu} = dx^{\mu}/ds$ (where s is the proper time),

$$\frac{du^{\lambda}}{ds} + \Gamma_{\mu\nu}^{\lambda} u^{\mu} u^{\nu} = 0 . \quad (\text{A.8})$$

A.2 Deriving the Friedmann Equations

This Section provides a few additional details to the sketch of the derivation of the Friedmann equations of §2.1.1. In particular, we focus here on the left hand side of the Einstein equations,

$$R_{\mu\nu} - \frac{1}{2}R g_{\mu\nu} \equiv G_{\mu\nu} = 8\pi G_N T_{\mu\nu} \quad , \quad (\text{A.9})$$

i.e. the metric-dependent terms. The following discussion is based on [9, §I.3.1], [56, §15.1], and [52, §2.1].

For the FLRW metric (A.3), we have

$$g_{00} = -1 \quad , \quad g_{0i} = 0 \quad , \quad g_{ii} = a^2 \left(\frac{1}{1 - kr^2}, r^2, r^2 \sin^2 \theta \right) \equiv a^2 \tilde{g}_{ij} \quad , \quad g_{ij} = 0 \text{ for } i \neq j \quad ,$$

such that, from the first term, $\partial_\mu g_{00} = 0$. We introduced in the third term the time-independent metric tensor for the three-dimensional maximally-symmetric space, \tilde{g}_{ij} . The Christoffel symbols with upper index 0 reduce to (notice that $g^{00} = g_{00} = -1$)

$$\begin{aligned} \Gamma_{\mu\nu}^0 &= \frac{1}{2} g^{00} (\partial_\mu g_{\nu 0} + \partial_\nu g_{\mu 0} - \partial_0 g_{\mu\nu}) \\ &= \frac{1}{2} \partial_0 g_{\mu\nu} \quad . \end{aligned}$$

Clearly, $\Gamma_{00}^0 = \Gamma_{i0}^0 = 0$ while

$$\Gamma_{ij}^0 = \frac{1}{2} \partial_0 g_{ij} = a \dot{a} \tilde{g}_{ij} \quad .$$

Conversely, the Christoffel symbols with upper index i reduce to

$$\begin{aligned} \Gamma_{00}^i &= \frac{1}{2} g^{ii} (\partial_0 g_{0i} + \partial_0 g_{0i} - \partial_i g_{00}) \\ &= 0 \quad , \\ \Gamma_{0j}^i &= \frac{1}{2} g^{ii} (\partial_0 g_{ji} + \partial_j g_{0i} - \partial_i g_{0j}) \\ &= \frac{1}{2} g^{ii} 2a \dot{a} \tilde{g}_{ij} \\ &= a \dot{a} \delta_j^i \frac{1}{a^2} \\ &= \frac{\dot{a}}{a} \delta_j^i \quad , \\ \Gamma_{jk}^i &= \frac{1}{2} g^{il} (\partial_j g_{kl} + \partial_k g_{jl} - \partial_l g_{jk}) \\ &= \tilde{\Gamma}_{jk}^i \quad . \end{aligned}$$

In the last result, $\tilde{\Gamma}_{jk}^i$ are the Christoffel symbols for the metric \tilde{g}_{ij} .

APPENDIX A. KEY ELEMENTS OF GENERAL RELATIVITY

The Ricci tensor has components

$$\begin{aligned}
R_{00} &= \partial_\lambda \Gamma_{00}^\lambda - \partial_0 \Gamma_{0\lambda}^\lambda + \Gamma_{00}^\lambda \Gamma_{\lambda\sigma}^\sigma - \Gamma_{0\sigma}^\lambda \Gamma_{\lambda 0}^\sigma \\
&= -\partial_0 \left(\frac{\dot{a}}{a} \delta_i^i \right) - \frac{\dot{a}}{a} \delta_j^j \frac{\dot{a}}{a} \delta_i^i \\
&= -3 \left(\frac{\ddot{a}}{a} - \frac{\dot{a}^2}{a^2} \right) - 3 \frac{\dot{a}^2}{a^2} \\
&= -3 \frac{\ddot{a}}{a} , \\
R_{0i} &= \partial_\lambda \Gamma_{0i}^\lambda - \partial_0 \Gamma_{i\lambda}^\lambda + \Gamma_{0i}^\lambda \Gamma_{\lambda\sigma}^\sigma - \Gamma_{0\sigma}^\lambda \Gamma_{\lambda i}^\sigma \\
&= \partial_j \Gamma_{0i}^j - \partial_0 \Gamma_{ij}^j + \Gamma_{0i}^j \Gamma_{jk}^k - \Gamma_{0k}^j \Gamma_{ji}^k \\
&= 0 , \\
R_{ij} &= \partial_\lambda \Gamma_{ij}^\lambda - \partial_i \Gamma_{j\lambda}^\lambda + \Gamma_{ij}^\lambda \Gamma_{\lambda\sigma}^\sigma - \Gamma_{i\sigma}^\lambda \Gamma_{\lambda j}^\sigma \\
&= \left(\partial_0 \Gamma_{ij}^0 + \partial_k \Gamma_{ij}^k \right) - \partial_i \Gamma_{jk}^k + \left(\Gamma_{ij}^0 \Gamma_{0k}^k + \Gamma_{ij}^l \Gamma_{lk}^k \right) - \\
&\quad - \left(\Gamma_{ik}^0 \Gamma_{0j}^k + \Gamma_{i0}^l \Gamma_{lj}^0 + \Gamma_{ik}^l \Gamma_{lj}^k \right) \\
&= \tilde{R}_{ij} + \partial_0 (a \dot{a} \tilde{g}_{ij}) + (a \dot{a} \tilde{g}_{ij}) \left(\frac{\dot{a}}{a} \delta_k^k \right) - \\
&\quad - (a \dot{a} \tilde{g}_{ik}) \left(\frac{\dot{a}}{a} \delta_j^k \right) - \left(\frac{\dot{a}}{a} \delta_i^l \right) (a \dot{a} \tilde{g}_{lj}) \\
&= \tilde{R}_{ij} + \left(2\dot{a}^2 + a\ddot{a} \right) \tilde{g}_{ij} \\
&= \left(2\dot{a}^2 + a\ddot{a} + 2k \right) \tilde{g}_{ij} \\
&= \left(2 \frac{\dot{a}^2}{a^2} + \frac{\ddot{a}}{a} + 2 \frac{k}{a^2} \right) g_{ij} .
\end{aligned}$$

To understand that $R_{0i} = 0$, notice that Γ_{0j}^i does not depend on spatial coordinates, $\Gamma_{ji}^i = \tilde{\Gamma}_{ji}^i$ is time-independent, and that $\Gamma_{0j}^i \propto \delta_j^i$ so that the $\Gamma\Gamma$ terms cancel. For the more involved case of R_{ij} , we defined \tilde{R}_{ij} , the Ricci tensor for the metric \tilde{g}_{ij} of the maximally-symmetric 3-space, which needs to satisfy [56, Equations (13.2.4) and (13.2.7)]

$$\begin{aligned}
\tilde{R}_{ij} &= \frac{1}{3} \tilde{g}_{ij} \tilde{R}_k^k \\
&= \frac{1}{3} 6k \tilde{g}_{ij} ,
\end{aligned}$$

with $\tilde{R} = \tilde{R}_k^k$ the Ricci curvature scalar associated to \tilde{g}_{ij} .

The Ricci scalar R then becomes

$$\begin{aligned}
R &= g^{\mu\nu} R_{\mu\nu} \\
&= g^{00} R_{00} + g^{ij} R_{ij} \\
&= - \left(-3 \frac{\ddot{a}}{a} \right) + g^{ij} g_{ij} \left(2 \frac{\dot{a}^2}{a^2} + \frac{\ddot{a}}{a} + 2 \frac{k}{a^2} \right) \\
&= 6 \left(\frac{\ddot{a}}{a} + \frac{\dot{a}^2}{a^2} + \frac{k}{a^2} \right) .
\end{aligned}$$

APPENDIX A. KEY ELEMENTS OF GENERAL RELATIVITY

It is now straightforward to show that the (00) and (ii) components of the Einstein tensor $G_{\mu\nu}$ (i.e. the left hand side of the Einstein equations (A.9)) read

$$G_{00} = 3 \left(\frac{\dot{a}^2}{a^2} + \frac{k}{a^2} \right) ,$$

$$G_{ii} = - \left(2 \frac{\ddot{a}}{a} + \frac{\dot{a}^2}{a^2} + \frac{k}{a^2} \right) g_{ii} .$$

Finally, recalling that the right hand side of the equations is given by the perfect fluid Energy-Momentum tensor ($T_{00} = \rho$ and $T_{ii} = pg_{ii}$), we write the Friedmann and Raychaudhuri equations,

$$\frac{\dot{a}^2}{a^2} = \frac{8\pi G_{\text{N}}}{3} \rho - \frac{k}{a^2}$$

and

$$2 \frac{\ddot{a}}{a} + \frac{\dot{a}^2}{a^2} = -8\pi G_{\text{N}} p - \frac{k}{a^2} ,$$

as advertised in Equations (2.6) and (2.7).

Appendix B

\mathcal{N} -Field Equations of Motion

We derive here the Equations of Motion (3.5) for a generic \mathcal{N} -field system described by the action (3.1), repeated here for simplicity:

$$S = \int d^4x \sqrt{-g} \left[-\frac{1}{2} \gamma_{ab} g^{\mu\nu} \partial_\mu \phi^a \partial_\nu \phi^b - V(\phi) + \frac{M_{\text{Pl}}^2}{2} R \right] . \quad (\text{B.1})$$

This pedagogical discussion is deemed useful since the detailed derivation – which is less obvious than one may think – was not found anywhere in the literature. The references considered throughout this work give in fact only the initial action (B.1) and the resulting Equations of Motion (EoM) – see for example [5, 66].

We will begin our discussion by considering the simpler case of single-field inflation, in order to then generalise to the full \mathcal{N} -field scenario. In either case, we use the fact that the action is related to the Lagrangian density, \mathcal{L} , by $S = \int d^4x \mathcal{L}$, since we will work with the latter. We will furthermore only consider the part of \mathcal{L} that describes the field(s), denoted \mathcal{L}_ϕ , since we use the fact that the field-derivatives of the spacetime Ricci scalar are null, as well as its derivatives with respect to $\partial_\alpha \phi^{(c)}$. Using the shorthand notation $\phi^{(c)}$ to denote both single- and multi-field cases, this means:

$$\frac{\partial R}{\partial \phi^{(c)}} = \frac{\partial R}{\partial \partial_\alpha \phi^{(c)}} = 0 .$$

The same relations hold for the derivatives of the spacetime metric, $g_{\mu\nu}$, and of its modulus, g , with respect to the field(s) and the spacetime derivatives of the field(s):

$$\begin{aligned} \frac{\partial g^{\mu\nu}}{\partial \phi^{(c)}} &= \frac{\partial g^{\mu\nu}}{\partial \partial_\alpha \phi^{(c)}} = 0 , \\ \frac{\partial g}{\partial \phi^{(c)}} &= \frac{\partial g}{\partial \partial_\alpha \phi^{(c)}} = 0 . \end{aligned}$$

The above relations are important when considering that the derivation of the EoM is based on the use of the (generalised) Euler–Lagrange (EL) equations, that is

$$\partial_\alpha \frac{\partial \mathcal{L}_\phi}{\partial \partial_\alpha \phi^{(c)}} - \frac{\partial \mathcal{L}_\phi}{\partial \phi^{(c)}} = 0 . \quad (\text{B.2})$$

APPENDIX B. \mathcal{N} -FIELD EQUATIONS OF MOTION

We will furthermore calculate the system's energy-momentum tensor (EMt) [9, Appendix I.A.6],

$$T_\nu^\mu \equiv \frac{-1}{\sqrt{-g}} \left(\frac{\partial \mathcal{L}_\phi}{\partial \partial_\mu \phi^{(c)}} \partial_\nu \phi^{(c)} - \delta_\nu^\mu \mathcal{L}_\phi \right) , \quad (\text{B.3})$$

in either scenario.

From here onwards, the above shorthand notation is dropped. The field-derivatives will be denoted by $\partial_\phi = \partial/\partial\phi$ in the single-fields case, and by $\partial_c = \partial/\partial\phi^c$ when considering \mathcal{N} fields.

B.1 Single-Field Case

The field Lagrangian in the single-field case is given by

$$\mathcal{L}_\phi = \sqrt{-g} \left(-\frac{1}{2} g^{\mu\nu} \partial_\mu \phi \partial_\nu \phi - V(\phi) \right) . \quad (\text{B.4})$$

The second term of the EL equations (B.2) is calculated as, using $V = V(\phi)$,

$$\begin{aligned} \frac{\partial \mathcal{L}_\phi}{\partial \phi} &= \sqrt{-g} \left\{ -\frac{1}{2} g^{\mu\nu} [(\partial_\phi \partial_\mu \phi) \partial_\nu \phi + \partial_\mu \phi (\partial_\phi \partial_\nu \phi)] - \partial_\phi V \right\} \\ &= -\sqrt{-g} \partial_\phi V , \end{aligned} \quad (\text{B.5})$$

where we made use of the fact that $\partial_\phi \partial_\mu \phi = \partial_\mu \partial_\phi \phi = \partial_\mu 1 = 0$. The first term of the EL equations (B.2) is instead given by the ∂_α derivative of

$$\begin{aligned} \frac{\partial \mathcal{L}_\phi}{\partial \partial_\alpha \phi} &= \sqrt{-g} \left\{ -\frac{1}{2} g^{\mu\nu} \left[\frac{\partial(\partial_\mu \phi)}{\partial(\partial_\alpha \phi)} \partial_\nu \phi + \partial_\mu \phi \frac{\partial(\partial_\nu \phi)}{\partial(\partial_\alpha \phi)} \right] - \frac{\partial V}{\partial(\partial_\alpha \phi)} \right\} \\ &= -\frac{1}{2} \sqrt{-g} g^{\mu\nu} (\delta_\mu^\alpha \partial_\nu \phi + \partial_\mu \phi \delta_\nu^\alpha) \\ &= -\frac{1}{2} \sqrt{-g} (g^{\alpha\nu} \partial_\nu \phi + g^{\mu\alpha} \partial_\mu \phi) \\ &= -\sqrt{-g} \partial^\alpha \phi . \end{aligned} \quad (\text{B.6})$$

Here we noticed that the potential is defined as $V(\phi)$ and not as $V(\phi, \partial_\alpha \phi)$, i.e. it does not depend on the field's spacetime derivatives and thus the last term on the first row of the above equation is set to zero. We also used the relation $\partial(\partial_\mu \phi)/\partial(\partial_\alpha \phi) = \delta_\mu^\alpha$ with δ_μ^α being the Kronecker delta. To get to the last row, we noticed that both terms in the bracket contract to the same derivative.

To calculate the derivative of Equation (B.6), we need to make use of the relations for the variation of the modulus of the metric tensor

$$\delta g = g g^{\beta\sigma} \delta g_{\beta\sigma} \quad \Rightarrow \quad \delta \sqrt{-g} = \frac{1}{2} \sqrt{-g} g^{\beta\sigma} \delta g_{\beta\sigma} , \quad (\text{B.7})$$

APPENDIX B. \mathcal{N} -FIELD EQUATIONS OF MOTION

which can be derived using the properties of linear algebra, $\det(M + \delta M) = \det(M)[1 + \text{Tr}(M^{-1}\delta M) + \mathcal{O}(\delta M)]$ (see [9, §I.A.4]). In terms of ∂_α , this gives

$$\partial_\alpha \sqrt{-g} = \frac{\delta \sqrt{-g}}{\delta g_{\beta\sigma}} \partial_\alpha g_{\beta\sigma} = \frac{1}{2} \sqrt{-g} g^{\beta\sigma} \partial_\alpha g_{\beta\sigma} . \quad (\text{B.8})$$

Furthermore, reminding ourselves that the spacetime Christoffel symbols are defined as

$$\Gamma_{\alpha\beta}^\lambda = \frac{1}{2} g^{\lambda\sigma} (\partial_\alpha g_{\sigma\beta} + \partial_\beta g_{\alpha\sigma} - \partial_\sigma g_{\alpha\beta}) , \quad (\text{B.9})$$

it is evident (keeping in mind that the metric tensor needs be symmetric, $g_{\mu\nu} = g_{\nu\mu}$) that the contraction

$$\begin{aligned} \Gamma_{\alpha\beta}^\beta &= \frac{1}{2} (g^{\beta\sigma} \partial_\alpha g_{\beta\sigma} + \partial^\sigma g_{\alpha\sigma} - \partial^\beta g_{\alpha\beta}) \\ &= \frac{1}{2} g^{\beta\sigma} \partial_\alpha g_{\beta\sigma} , \end{aligned} \quad (\text{B.10})$$

where we noticed that the last two terms in the first row are equal and thus cancel. This is nonetheless than the right hand side of Equation (B.8).

Using these results, the first term of the EL equations becomes

$$\begin{aligned} \partial_\alpha \frac{\partial \mathcal{L}_\phi}{\partial \partial_\alpha \phi} &= - (\partial_\alpha \sqrt{-g}) \partial^\alpha \phi - \sqrt{-g} \partial_\alpha \partial^\alpha \phi \\ &= -\sqrt{-g} (\Gamma_{\beta\alpha}^\beta \partial^\alpha \phi + \partial_\alpha \partial^\alpha \phi) \\ &= -\sqrt{-g} (\Gamma_{\alpha\beta}^\alpha \partial^\beta \phi + \partial_\alpha \partial^\alpha \phi) , \end{aligned} \quad (\text{B.11})$$

where we switched the internal indices $\alpha \leftrightarrow \beta$ in the first term of the second row.

Substituting the two terms (B.5) and (B.11) into the EL equations (B.2), dividing by $\sqrt{-g}$, and changing signs, we finally get that

$$\Gamma_{\alpha\beta}^\alpha \partial^\beta \phi + \partial_\alpha \partial^\alpha \phi = V_{,\phi} ,$$

where we adopt – for this derivation only – the notation $V_{,\phi} \equiv \partial_\phi V$. Defining the covariant spacetime derivative,

$$D_\mu A^\nu \equiv \partial_\mu A^\nu + \Gamma_{\mu\lambda}^\nu A^\lambda , \quad (\text{B.12})$$

as well as the covariant spacetime d'Alembert (or *box*) operator acting on a scalar field,

$$\square \phi \equiv D_\mu \partial^\mu \phi , \quad (\text{B.13})$$

it is then easy to cleanly rewrite the Equations of Motion of the single-field system described by the Lagrangian density (B.4) as

$$\boxed{\square \phi = V_{,\phi}} . \quad (\text{B.14})$$

This equation is the same as that of [67, Equation (12)], as we expected.

Using the result (B.6), we can furthermore write the system's EMt from Equation (B.3):

$$\boxed{T_\nu^\mu = \partial^\mu \phi \partial_\nu \phi - \delta_\nu^\mu \left(\frac{1}{2} \partial^\alpha \phi \partial_\alpha \phi + V(\phi) \right)} . \quad (\text{B.15})$$

B.2 Multi-Field Case

The fields Lagrangian in the multi-field case is instead given by

$$\mathcal{L}_\phi = \sqrt{-g} \left(-\frac{1}{2} \gamma_{ab} g^{\mu\nu} \partial_\mu \phi^a \partial_\nu \phi^b - V(\phi) \right) , \quad (\text{B.16})$$

where now $\phi = (\phi^a, \dots, \phi^N)$ denotes the set of all fields. We will again use $V = V(\phi)$.

The $\partial\mathcal{L}/\partial\phi^c$ term of the EL equations (B.2) is found using the same considerations as in Equation (B.5), except for an additional term $\partial_c\gamma_{ab}$ dependent on the multi-field geometry:

$$\frac{\partial\mathcal{L}_\phi}{\partial\phi^c} = -\sqrt{-g} \left[\frac{1}{2} (\partial_c\gamma_{ab}) g^{\mu\nu} \partial_\mu \phi^a \partial_\nu \phi^b + \partial_c V \right] . \quad (\text{B.17})$$

The term $\partial\mathcal{L}/\partial\partial_\alpha\phi^c$ is instead

$$\begin{aligned} \frac{\partial\mathcal{L}_\phi}{\partial\partial_\alpha\phi^c} &= \sqrt{-g} \left\{ -\frac{1}{2} \left(\frac{\partial\gamma_{ab}}{\partial\partial_\alpha\phi^c} \right) g^{\mu\nu} \partial_\mu \phi^a \partial_\nu \phi^b - \frac{1}{2} \gamma_{ab} g^{\mu\nu} \left[\frac{\partial(\partial_\mu\phi^a)}{\partial(\partial_\alpha\phi^c)} \partial_\nu \phi^b + \partial_\mu \phi^a \frac{\partial(\partial_\nu\phi^b)}{\partial(\partial_\alpha\phi^c)} \right] - \right. \\ &\quad \left. - \frac{\partial V}{\partial(\partial_\alpha\phi)} \right\} \\ &= -\frac{1}{2} \sqrt{-g} \gamma_{ab} g^{\mu\nu} \left(\delta_\mu^\alpha \delta_c^a \partial_\nu \phi^b + \partial_\mu \phi^a \delta_\nu^\alpha \delta_c^b \right) \\ &= -\frac{1}{2} \sqrt{-g} \left(\gamma_{bc} \partial^\alpha \phi^b + \gamma_{ac} \partial^\alpha \phi^a \right) . \end{aligned} \quad (\text{B.18})$$

Similar considerations to the corresponding single-field case were again employed, notably that $\partial V/\partial\partial_\alpha\phi^c = 0$ and that $\partial(\partial_\mu\phi^a)/\partial(\partial_\alpha\phi^c) = \delta_\mu^\alpha \delta_c^a$. We furthermore considered that γ_{ab} depends only on the fields and not on their spacetime derivatives, meaning the first term of the first row vanishes.

Taking the ∂_α derivative of the above, the first term will again be given by the relations (B.8) and (B.10), while we will make use of the chain rule $\partial_\alpha\gamma_{ac} = (\partial_d\gamma_{ac})\partial_\alpha\phi^d$ for the second:

$$\begin{aligned} \partial_\alpha \frac{\partial\mathcal{L}_\phi}{\partial\partial_\alpha\phi^c} &= -\frac{1}{2} (\partial_\alpha\sqrt{-g}) \left(\gamma_{bc} \partial^\alpha \phi^b + \gamma_{ac} \partial^\alpha \phi^a \right) - \frac{1}{2} \sqrt{-g} \left[(\partial_\alpha\gamma_{bc}) \partial^\alpha \phi^b + (\partial_\alpha\gamma_{ac}) \partial^\alpha \phi^a \right] - \\ &\quad - \frac{1}{2} \sqrt{-g} \left[\gamma_{bc} \partial_\alpha \partial^\alpha \phi^b + \gamma_{ac} \partial_\alpha \partial^\alpha \phi^a \right] \\ &= -\frac{1}{2} \sqrt{-g} \left[\overbrace{\Gamma_{\beta\alpha}^\beta \left(\gamma_{bc} \partial^\alpha \phi^b + \gamma_{ac} \partial^\alpha \phi^a \right)}^{(1)} + \overbrace{(\partial_d\gamma_{bc}) \partial_\alpha \phi^d \partial^\alpha \phi^b}^{(2)} + \overbrace{(\partial_d\gamma_{ac}) \partial_\alpha \phi^d \partial^\alpha \phi^a}^{(3)} + \right. \\ &\quad \left. + \overbrace{\gamma_{bc} \partial_\alpha \partial^\alpha \phi^b + \gamma_{ac} \partial_\alpha \partial^\alpha \phi^a}^{(4)} \right] . \end{aligned}$$

APPENDIX B. \mathcal{N} -FIELD EQUATIONS OF MOTION

We then identify the terms (1) and (4) as the covariant derivatives (B.12), by switching the internal indices $\alpha \leftrightarrow \beta$ in the former. We also rename the indices $d \rightarrow a$ and $d \rightarrow b$ in terms (2) and (3), respectively:

$$= -\frac{1}{2}\sqrt{-g} \left[\overbrace{\gamma_{bc}D_\alpha\partial^\alpha\phi^b}^{(1)} + \overbrace{\gamma_{ac}D_\alpha\partial^\alpha\phi^a}^{(2)} + \overbrace{(\partial_a\gamma_{bc})\partial_\alpha\phi^a\partial^\alpha\phi^b}^{(3)} + \overbrace{(\partial_b\gamma_{ac})\partial_\alpha\phi^b\partial^\alpha\phi^a}^{(4)} \right].$$

Finally, we rename the internal index $b \rightarrow a$ in term (1) such that it equals term (2), and we identify $D_\alpha\partial^\alpha\phi^a = \square\phi^a$ from Equation (B.12). We use $\partial^\alpha = g^{\alpha\beta}\partial_\beta$ in the last two terms, where we redefine $(\alpha, \beta) \rightarrow (\mu, \nu)$ in (3) and $(\alpha, \beta) \rightarrow (\nu, \mu)$ in (4):

$$= -\sqrt{-g} \left[\gamma_{ac}\square\phi^a + \frac{1}{2}(\partial_a\gamma_{bc} + \partial_b\gamma_{ac})g^{\mu\nu}\partial_\mu\phi^a\partial_\nu\phi^b \right]. \quad (\text{B.19})$$

Substituting the results (B.17) and (B.19) in the EL equations (B.2) we get that, dividing by $\sqrt{-g}$ and changing signs,

$$\gamma_{ac}\square\phi^a + \frac{1}{2}(\partial_a\gamma_{bc} + \partial_b\gamma_{ac} - \partial_c\gamma_{ab})g^{\mu\nu}\partial_\mu\phi^a\partial_\nu\phi^b = \partial_c V.$$

We now contract this equation with γ^{dc} . Using the definition of inverse metric $\gamma^{dc}\gamma_{ac} = \delta_a^d$, the box term reduces to $\square\phi^d$, while we define $V^{,d} \equiv \gamma^{dc}\partial_c V$ on the right hand side. The remaining term is easily identified with the field-space Christoffel symbol Γ_{ab}^d by looking at Equation (3.2).

Lastly, we rotate the indices $(a, b, c, d) \rightarrow (b, c, d, a)$ to find

$$\boxed{\square\phi^a + \Gamma_{bc}^a g^{\mu\nu}\partial_\mu\phi^b\partial_\nu\phi^c = V^{,a}}. \quad (\text{B.20})$$

This is the expected result (3.5) (see [5, Equation (2.4)] or [66, Equation (4)], where a different notation is used) and thus concludes our derivation. Notice the similarity with Equation (B.14), with the addition of the field-space-dependent Γ_{bc}^a -term which provides a further coupling between the different fields, on top of the one included in $V(\phi)$.

Using the result (B.18) – where we rename the internal index $b \rightarrow a$ in the first term to sum it to the second –, it is also possible to write the \mathcal{N} -field EMt (3.6):

$$\boxed{T_\nu^\mu = \gamma_{ac}\partial^\mu\phi^a\partial_\nu\phi^c - \delta_\nu^\mu \left(\frac{1}{2}\gamma_{ac}\partial^\alpha\phi^a\partial_\alpha\phi^c + V(\phi) \right)}. \quad (\text{B.21})$$

Notice there are no additional terms with respect to the single-field EMt (B.3). This is the expected result (see [66, Equation (5)], which uses a different notation), and is given in the text as Equation (3.6).